Drift waves and transport

W. Horton

Institute for Fusion Studies, The University of Texas, Austin, Texas 78712

Drift waves occur universally in magnetized plasmas producing the dominant mechanism for the transport of particles, energy and momentum across magnetic field lines. A wealth of information obtained from quasistationary laboratory experiments for plasma confinement is reviewed for drift waves driven unstable by density gradients, temperature gradients and trapped particle effects. The modern understanding of Bohm transport and the role of sheared flows and magnetic shear in reducing the transport to the gyro-Bohm rate are explained and illustrated with large scale computer simulations. The types of mixed wave and vortex turbulence spontaneously generated in nonuniform plasmas are derived with reduced magnetized fluid descriptions. The types of theoretical descriptions reviewed include weak turbulence theory, Kolmogorov anisotropic spectral indices, and the mixing length. A number of standard turbulent diffusivity formulas are given for the various space-time scales of the drift-wave turbulent mixing. [S0034-6861(99)00803-X]

CONTENTS

I. INTRODUCTION

The past decade of research in plasma confinement has shown that plasma transport across the magnetic field is largely controlled by low-frequency drift-wave fluctuations. The purpose of this review is to describe the current understanding of the drift-wave transport phenomenon. This area of research is rich with many theoretical and computational tools and laboratory experiments developed over the past several decades in the magnetic fusion energy research programs throughout the world. The present review necessarily selects a small fraction of the information currently available about the role of low-frequency drift-wave fluctuations and the associated plasma transport in magnetized plasmas.

Transport in high-temperature ionized gases called plasmas is dominated by the long-range collective electric-field $\mathbf{E}_{\mathbf{k}\omega}$ part of the Coulomb interactions between the charged particles. Here the subscripts $\mathbf{k}\omega$ specify the vector wave-number $\mathbf{k}$ and the angular frequency ω of the electric-field fluctuation $\mathbf{E}_{\mathbf{k}\omega}$. For a plasma of density n and temperature T the single-particle Coulomb electric field falls off exponentially beyond the Debye shielding length $\lambda_D=(k_BT/4\pi ne^2)^{1/2}$ where k_B is the Boltzmann constant. Thus we characterize the electric-field fluctuations at $\mathbf{k}\omega$ as collective self-consistent field interactions for $k\lambda_D\ll 1$ and collisional binary interactions for $k\lambda_D\gtrsim 1$. For plasmas with a large number of particles in the Debye sphere $N_D=(4\pi/3)n\lambda_D^3\gg 1$ the collective electric fields dominate the plasma dynamics through the collective modes. For unmagnetized plasma the collective modes are the high-frequency electron plasma oscillations $\omega_{pe}=(4\pi ne^2/m_e)^{1/2}$ and the low-frequency ion acoustic waves $\omega=\pm k(k_BT_e/m_i)^{1/2}$ with these low-frequency oscillations determining the plasma transport properties of resistivity and thermal conductivity when driven unstable by substantial plasma currents and temperature gradients. For magnetized plasmas there are many collective modes, but again the lowest frequency modes ($\omega\ll eB/m_ic\equiv\omega_{ci}$) dominate the transport. At these low frequencies the ion acoustic oscillations are determined

by the parallel component $k_\parallel$ of the wave vector, and the electric field associated with the perpendicular component $\mathbf{k}_\perp$ produces the $\mathbf{E}\times\mathbf{B}$ drift of the particle guiding centers across the magnetic field. We will assume that the reader is familiar with the drift motions of the guiding centers of charged particles in slow space-time varying electric and magnetic fields (Schmidt, 1979, Chap. 2).

Density and temperature gradients in magnetized plasma give rise to electron and ion diamagnetic currents $\mathbf{j}_a$ across the magnetic field $\mathbf{B}$ that provide force balance through $\mathbf{j}\times\mathbf{B}/c=\nabla(p_e+p_i)$ in the equilibrium. Here we use the subscript a to label the species of the charged particles in the plasma. The Boltzmann constant is suppressed in the partial pressures $p_a=n_aT_a$ by using energy units for the temperature T_a. The drift velocities $v_{da}=(1/e_an_aB)(\partial p_a/\partial r)=j_a/e_an_a$ associated with these currents give rise to collective oscillations called drift waves. The details of how these convective waves arise and propagate is the first subject addressed in detail in Sec. II.A. In Sec. II.B we discuss the laboratory observations of the electron drift-wave fluctuations associated with $\omega_{*e}=\mathbf{k}\cdot\mathbf{v}_{\rm de}$ and the ion drift waves associated with $\omega_{*e}=\mathbf{k}\cdot\mathbf{v}_{\rm di}$. In Secs. III and IV we focus on the coupling of the ion acoustic motion with ion temperature gradient-driven drift wave and the associated convective transport of ion thermal energy. In Sec. V we describe the turbulence associated with the electron drift wave $\omega_{*e}=\mathbf{k}\cdot\mathbf{v}_{\rm de}$ which is perhaps the more ubiquitous form of drift-wave turbulence. As a preliminary to the study of the drift waves we conclude this introduction with an explanation of the relationship between the classical one-fluid magnetohydrodynamics description and the two-component description of plasma dynamics with the drift-wave dynamics.

A. Separation of the ion and electron dynamics

The most common mathematical paradigm for describing the dynamics of a plasma is given by the ideal magnetohydrodynamics (MHD) equations. Built into this set of equations is the use of Ohm's law of a moving fluid with zero resistivity, which has the form

$$\mathbf{E}+\frac{1}{c}\mathbf{v}_F\times\mathbf{B}=0, \tag{1}$$

where $\mathbf{E}$ is an electric field, $\mathbf{B}$ the magnetic field, $\mathbf{v}_F$ the velocity of the fluid, and c the velocity of light. When combined with Faraday's induction equation of electromagnetism, $\partial\mathbf{B}/\partial t=-c\nabla\times\mathbf{E}$, the following equation results:

$$\frac{\partial\mathbf{B}}{\partial t}=\nabla\times(\mathbf{v}_F\times\mathbf{B}). \tag{2}$$

The magnetic flux $\Delta\Phi_M$ through an area ΔA is $\Delta\Phi_M=\int_{\Delta A}\mathbf{B}\cdot d\mathbf{A}$ and is constant when ΔA moves with the fluid velocity. Equation (2) leads to the conclusion (Chandresekhar, 1961, p. 84) that plasma particles can move along the magnetic flux tube Φ_M, but they are constrained to remain in the tube of magnetic flux as the tube moves. If the tube is insulated from the confining walls, then so are the particles constituting the plasma. The magnetic-field lines are said to be *frozen* into the plasma.

The physical consequences that are based on the ideal MHD equations correctly predict many important plasma characteristics, such as plasma equilibrium, gross plasma stability, plasma flow phenomena and the spectrum of Alfvén waves. However, these equations do not have the property of describing separate motion for electrons and ions which lead to additional extremely important plasma phenomena. In particular a different set of waves, not described in MHD theory, is established: the so-called drift waves whose frequency is typically lower than the frequencies associated with MHD waves. The additional degree of freedom for separate ion and electron motion also introduces a new destabilization source into the problem, the universal instability drive. The universality of this drive arises because there is always the potential for instability when there is a spatial gradient in the particles' distribution function. This instability mechanism can spontaneously convert particle thermal energy into wave energy, and the electromagnetic fields from the waves in turn can cause stochastic motion of the constituent plasma particles. This motion leads to so-called anomalous transport, which results in the escape of particles and energy in an otherwise magnetically confined system. Heat and particle loss observed in most plasma confinement experiments are attributed to this drift-wave mechanism of plasma turbulence.

Let us first examine from a particle point of view why ions and electrons should "stick" to magnetic-field lines. We will then discuss various mechanisms that allow this sticking to break down.

The motion of a charged particle in an electromagnetic field, $[\mathbf{E}(\mathbf{r})$ and $\mathbf{B}(\mathbf{r})]$, takes the form

$$m_j\frac{d\mathbf{v}_j}{dt}=q_j\left(\mathbf{E}(\mathbf{r}_j)+\frac{1}{c}\mathbf{v}_j\times\mathbf{B}(\mathbf{r}_j)\right), \tag{3}$$

where $\mathbf{v}_j$, q_j, and m_j are the velocity, charge, and mass of the charged particle of species j. Let us further assume that $\mathbf{E}\cdot\mathbf{B}=0$, which must be the case when the ideal Ohm's law, Eq. (1), applies. When the electric and magnetic fields are constant, the particle motion can be described as a spiral about a guiding center position:

$$\mathbf{R}_j=\mathbf{r}_j-\frac{\mathbf{b}\times\mathbf{u}_j}{\omega_{cj}}+\int_0^t\mathbf{v}_E(t')dt'$$

with $\mathbf{b}=\mathbf{B}/|\mathbf{B}|$ the direction of the magnetic field, $\mathbf{u}_j=\mathbf{v}_j-\mathbf{v}_E$, $\mathbf{v}_E=c\mathbf{E}\times\mathbf{b}/|\mathbf{B}|$, and $\omega_{cj}=q_j|\mathbf{B}|/m_jc$.

Note that the guiding center $\mathbf{R}_j$ moves along the magnetic-field direction and transverse to the magnetic-field direction at the "electric-field drift velocity" $\mathbf{v}_E=c\mathbf{E}\times\mathbf{B}/B^2$. Note that $\mathbf{v}_E$ is independent of charge and mass of the particle, and this velocity can also be attributed to the field line. From this point of view the particles and magnetic lines move together, and the velocity that appears in Ohm's law can be attributed to the motion of the electrons, ions, or the magnetic-field line.

This result continues to be valid if (1) the electric field is nearly perpendicular to the magnetic field, (2) the time rate of change of the electromagnetic field $1/T$ is slow compared to the ion cyclotron frequency ($1/\omega_{ci}T \ll 1$; i for ion, below we use e for electron), and (3) the spatial scale of the electromagnetic field L_{em} is large compared to an ion gyroradius ($L_{em}/\rho_i \gg 1$, with $\rho_i = |\mathbf{u}_i \times \mathbf{b}|/\omega_{ci}$).

Let us now examine the consequences of breaking these constraints.

B. Breaking the $E_\parallel = 0$ constraint (defrosting the magnetic field lines)

The essence of the nonideal Ohm's law is captured by replacing it with the equation of motion of electrons treated as a separate fluid. Then Ohm's law can be written as

$$\mathbf{E} + \frac{1}{c}\mathbf{v}_e \times \mathbf{B} = \frac{1}{e}\mathbf{F}_d - \frac{\nabla p_e}{n_e e} - \frac{m_e}{e}\frac{d\mathbf{v}_e}{dt}. \tag{4}$$

Here $\mathbf{F}_d$, in the first term on the right-hand side, is the drag force on the electrons moving relative to the ions. This force is proportional to the difference of the velocity between the electrons and the ions, and can be written as $\mathbf{F}_d = -m_e \nu_e (\mathbf{v}_e - \mathbf{v}_i) \equiv (\nu_e m_e / n_e e)\mathbf{j}$ where ν_e is the momentum relaxation rate of the electron, and $\mathbf{j}$ is the current density. If we neglect the other terms on the right-hand side of Eq. (4), we obtain the most commonly used form of Ohm's law:

$$\mathbf{E} + \frac{1}{c}\mathbf{v}_e \times \mathbf{B} = \eta \mathbf{j},$$

where η is the resistivity $\eta = \nu_e m_e / n_e e^2$. Using this form of Ohm's law to eliminate $\mathbf{E}$ from the Faraday induction equation using Ampere's law and $\nabla \cdot \mathbf{B} = 0$ yields the magnetic diffusion equation

$$\frac{\partial \mathbf{B}}{\partial t} = \nabla \times (\mathbf{v}_e \times \mathbf{B}) + \frac{\eta c^2}{4\pi}\nabla^2 \mathbf{B}. \tag{5}$$

In deriving Eq. (5) the displacement current is dropped, which is valid for space-time scales (L,T) such that $L/T \ll c$ the speed of light.

This equation describes the diffusion between the magnetic-field lines and the plasma motion. We can use dimensional analysis to estimate when significant diffusion arises. The time scale $T(\partial B/\partial t \sim B/T)$ on the left-hand side balances the resistive diffusion when

$$T > 4\pi \frac{L_{em}^2}{\eta c^2}.$$

Hence we expect that a wave with an angular frequency $\omega \sim 1/T$ and perpendicular wave number $k_\perp \sim 1/L_{em}$ will not necessarily have $\mathbf{E} \perp \mathbf{B}$ when

$$\frac{\omega}{\nu_e}\frac{\omega_{\rm pe}^2}{k_\perp^2 c^2} < 1. \tag{6}$$

Instead, there can be an electric field component along the field line. In the extreme, we can have an electrostatic wave, where $\mathbf{E} = -\nabla\Phi$ and Φ varies along the field line.

Additional conditions for obtaining an electrostatic wave can be obtained when the other terms in the electron force equation are significant. For example, the electron inertia term is approximately given by

$$\left| m_e \frac{d\mathbf{v}_e}{dt} \right| = \omega m_e \mathbf{v}_e,$$

and if $\omega \gtrsim \nu_e$ (and $\mathbf{v}_e \gg \mathbf{v}_i$, which is readily satisfied for motion along field lines) we can roughly replace ν_e by $(\nu_e^2 + \omega^2)^{1/2}$ in the diffusion term of Eq. (5), and the condition for the failure of the constraint that accounts for both finite ν_e and ω becomes

$$\frac{\omega_{\rm pe}^2}{k_\perp^2 c^2}\frac{\omega}{(\omega^2 + \nu_e^2)^{1/2}} < 1. \tag{7}$$

Drift waves associated with scale length $\delta = c/\omega_{\rm pe}$ are considered in Sec. V.I. We can also solve the force balance equation for electrons (4) and relate the parallel electron pressure gradient to the parallel electron flow velocity and thus the perturbed electric fields. When this electron flow velocity is related to the plasma current and similar dimensional arguments are applied, we obtain the following condition for the failure of the frozen field line assumption which allows electrostatic fields to arise:

$$\frac{\omega_{\rm pe}^2}{k_\perp^2 c^2}\frac{|\omega - \omega_{*e}|}{[\omega^2 + \nu_e^2 + k_\parallel^2 v_{\rm the}^2]^{1/2}} < 1, \tag{8}$$

where $v_{\rm the}$ is the thermal speed for electrons and $k_\parallel$ the parallel wave number. We will see that this condition is readily satisfied in low-beta plasmas (beta is the ratio of plasma pressure to magnetic-field pressure) where many confinement experiments in tokamaks and other magnetic confinement configurations operate. We will see that the important electrostatic wave that can now be excited is the drift wave.

II. DRIFT-WAVE MECHANISM

A. Plasma convection in quasineutral disturbances

Consider the $\mathbf{E} \times \mathbf{B}$ convection of plasma around a local excess of positive-ion density δn_i as shown in Fig. 1.

The direction of the background density gradient is x, and the depth of the disturbance is δx; the symmetry direction is y, and the length of the disturbance is δy. The confining magnetic field is in the z direction. For slow dynamics the electrons neutralize the excess ion charge by flowing along the magnetic field to establish the local Boltzmann density distribution $n_e = N \exp(e\phi/k_B T_e)$ where ϕ is the electrostatic potential created by the charge imbalance and $N(x)$ the ambient density in the absence of the perturbation ($\phi = 0$). Here k_B is the Boltzmann constant and T_e the electron temperature.

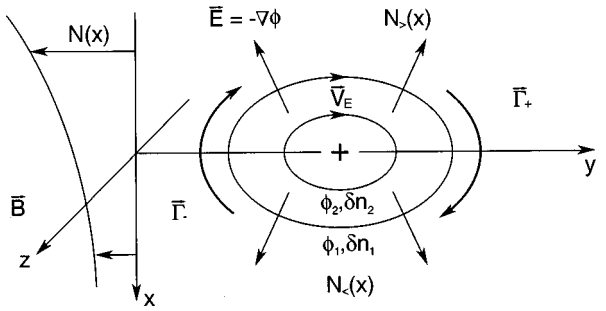

FIG. 1. Drift-wave mechanism showing $\mathbf{E}\times\mathbf{B}$ convection in a nonuniform, magnetized plasma.

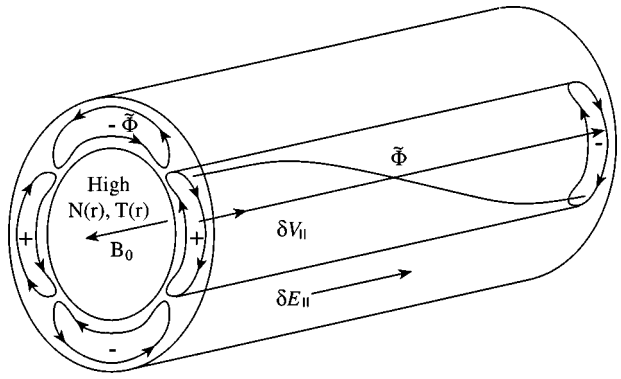

FIG. 2. Three-dimensional configuration of the drift-wave fields in a cylinder.

In general the perturbed potential is determined by Poisson's equation

$$\nabla^2\phi = -4\pi e(\delta n_i - \delta n_e). \tag{9}$$

In this self-consistent field problem $\delta n_a = \delta n_a(\mathbf{x}, \phi(\mathbf{x},t))$. For structures that are large compared to the electron Debye length $\lambda_{\mathrm{De}} = (k_B T_e/4\pi N e^2)^{1/2}$; however, the fractional charge separation allowed by the Poisson equation is small. From Eq. (9) the fractional deviation of electron and ion density is

$$\frac{(\delta n_i - \delta n_e)}{N} = \left(\frac{-k_B T_e}{4\pi e^2 N}\right)\nabla^2\left(\frac{e\phi}{k_B T_e}\right) \lesssim \left(\frac{\lambda_{\mathrm{De}}^2}{\delta x^2}\right)\left(\frac{e\phi}{k_B T_e}\right) \ll 1. \tag{10}$$

Thus the *principle of quasineutrality* applies. In the quasineutral regime the plasma potential adjusts its value to make $n_i(\phi) = n_e(\phi)$ to the first order in $\lambda_{\mathrm{De}}^2/\delta x^2$. The resulting small fractional charge separation is computed from Poisson's equation using the potential rather than vice versa. All the drift-wave dynamics discussed in this review are in the regime of quasineutrality where $\tilde{\rho}_Q = \Sigma_a q_a \tilde{n}_a = 0$ determines the evolution of the electrostatic potential and the plasma eigenmodes. Here a is the species index for particles of charge q_a and density n_a. In terms of the particle currents $\mathbf{j}_a$ the quasineutral dynamics is given by $\Sigma_a \nabla\cdot\mathbf{j}_a = 0$. In plasma physics it is conventional to measure temperature in energy units $k_B T_e \to T_e$ leaving free the k symbol for a wave number $\mathbf{k}$ associated with the fluctuations. The discussion regarding Fig. 1 applies equally well to each cell of a wave with $\delta x \simeq \pi/k$. Figure 2 shows the three-dimensional structure of the drift wave as observed, for example, in either a Q machine or the Columbia Linear Machine (see Sec. II.B), with the $m=2$ mode dominant. We return to analyze the convection in Figs. 1 and 2 in Sec. C after discussing the general features of the fluctuations.

The condition for the electrons to establish the Boltzmann distribution in the drift-wave–ion acoustic wave disturbances follows from the parallel electron force balance equation. For fluctuations with the parallel variation $k_{\|} = 2\pi/\lambda_{\|}$ sufficiently strong so that electrons with thermal velocity $v_e = (T_e/m_e)^{1/2}$ move rapidly along $k_{\|}$ compared with time rate of change of the fields ($\omega < k_{\|} v_e$) the dominant terms in the electron fluid force balance equation

$$m_e n_e\left(\frac{du_{\|}^e}{dt}\right) = -e n_e E_{\|} - \nabla_{\|} p_e + \frac{\nu_e m_e j_{\|}}{e} \tag{11}$$

are the electric field $E_{\|} = -\nabla_{\|}\phi$ and the isothermal pressure gradient $\nabla_{\|} p_e = T_e \nabla_{\|} n_e$. The temperature gradient is small compared with density gradient due to the fast electron thermal flow associated with $k_{\|} v_e > \omega$. Thus much of the low-frequency drift-wave dynamics falls in the regime where the Boltzmann description of the electron response

$$\delta n_e = N\left[\exp\left(\frac{e\phi}{T_e}\right) - 1\right]$$

applies in the form

$$\delta n_e \cong \frac{N e\phi}{T_e}. \tag{12}$$

Here in the last step it is convenient to adopt an equality in the sense of defining the linear, adiabatic electron model. The model requires that $e\phi/T_e \ll 1$ and $k_{\|} v_e \gg (\nu_e^2 + \omega^2)^{1/2}$. For example, both the Hasegawa-Mima equation and the ideal ion temperature gradient (ITG) model rely on the adiabatic electron model defined by Eq. (12). For the simple drift-wave instability, however, the adiabatic electron response defined by Eq. (12) is broken by dissipation as we now discuss.

After dropping the electron inertia ($m_e \to 0$) the parallel electron force balance becomes

$$E_{\|} + \frac{\nabla_{\|} p_e}{e n_e} + \frac{\hat{\mathbf{b}}\cdot(\nabla\cdot\boldsymbol{\pi}_e)}{e n_e} = \eta \mathbf{j}_{\|},$$

where $\boldsymbol{\pi}_e$ is the traceless momentum stress tensor that includes the electron viscosity and η is the electrical resistivity. Using collisional or neoclassical transport theory, the nonadiabatic contributions to Eq. (12) can be computed. For the collisional regime $\nu_e > k_{\|} v_e$ the electron temperature fluctuations $\delta T_e/T_e \sim (\omega\nu_e/k_{\|}^2 v_e^2)(\delta n_e/n_e)$ and the resistivity contribution to δn_e are of the same order, both giving rise to a δn_e-ϕ

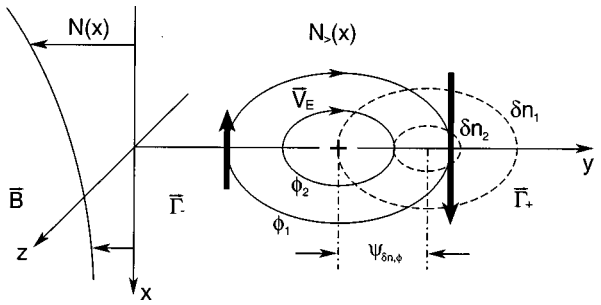

FIG. 3. A segment of a drift-wave fluctuation showing the variation of the electrostatic potential perpendicular to the magnetic field at a given instant of time. The contours of φ = const in the plane perpendicular to $B\hat{\mathbf{z}}$ are the stream lines of the $\mathbf{E}\times\mathbf{B}$ particle motion. A segment of the correlated but phase shifted density variation δn. The potential and density variation are out of phase by $\psi_{\delta n,\varphi}$ with the density fluctuation leading the potential fluctuation for propagation along the positive $\hat{y}$ axis.

phase difference of order $\delta_k \simeq (\omega \nu_e / k_\parallel^2 v_e^2)$ compared to unity. For the collisionless regime the electron parallel viscosity $\mu_\parallel^e$ and the parallel thermal flux $\nabla\cdot\mathbf{q}_\parallel^e \simeq 2(2/\pi)^{1/2}|k_\parallel| v_e \delta p_e$ dominate the deviation $\delta_{k\omega}$ from the Boltzmann distribution. These collisionless closures of the fluid equations are given in Hammett and Perkins, 1990; Chang and Callen, 1992; Dorland and Hammett, 1993; Beer and Hummett, 1996; and Waltz *et al.*, 1997.

There are many calculations for the nonadiabatic electron response based on the truncated chain of electron hydrodynamic equations (Braginskii, 1965; Horton and Varma, 1972) and on the kinetic equations (Tang, 1978; Kadomtsev and Pogutse, 1979; Horton, 1990). The general results are complicated by the distinction between the trapped and passing electron orbits and the collisionally broadened resonances of the electron guiding center drift orbits with the wave. For the purpose of the review we note that once the collisionality and geometry are specified (e.g., collisional, collisionless, trapped electron in toroidal or mirror geometry) the nonadiabatic behavior is given by

$$\delta n_{e,\mathbf{k}} = \frac{N e \phi_{\mathbf{k}}}{T_e}(1 - i\delta_{\mathbf{k}}), \tag{13}$$

where the $\mathbf{k}$ dependence of $\delta_{\mathbf{k}}$ is $\delta_{-\mathbf{k}} = -\delta_{\mathbf{k}}$. Thus $i\delta_{\mathbf{k}}$ corresponds to an anti-Hermitian spatial operator describing the electron *dissipation* from transport coefficients in the collisional regime and from the resonant electron-wave interactions in the collisionless regime. The phase shift given by $i\delta_{\mathbf{k}}$ will cause the density maxima to lead the potential maxima, which produces an exponential growth $e^{\gamma_k t}$ with $\gamma_k/\omega_k \propto \delta_k$. Clearly the growth works both in the collisionless and collisional regime but turns into a decay for the opposite direction of the phase shift $\delta_k < 0$. The origin of the exponential growth is shown in Fig. 3 where we see that the phase shift of the density maximum produces an imbalance in the right and left convective fluxes across the x = const surface. The initial density perturbation is reinforced in proportion to itself and the $N_> - N_<$ density gradient for $\psi_{\delta n,\phi} > 0$. With a positive phase shift there is a net transport of plasma down the density gradient across the confining magnetic field. This transport is a universal feature for the many varieties of drift waves in different regimes of plasma collisionality and different confinement geometries.

B. Drift waves in the laboratory

The collisional drift waves with $i\delta_{\mathbf{k}}$ determined by resistivity and thermal diffusivity were the first drift waves to be discovered and thoroughly investigated. The identification was made in low-temperature steady-state plasmas produced by thermal (contact) ionization of Alkali elements (principally cesium and potassium) in long cylindrical devices called Q machines. Here the Q is for the *quiescent* plasmas produced in this system. Detailed correlations between the observed potential-density waves with the properties predicted by the linear dispersion relation and the single-wave finite amplitude formulas were used by Hendel *et al.* (1968) to establish that the localized, 10 kHz rotating wave structures were the drift waves. The drift-wave phase shift $\delta_k > 0$ in Eq. (13) is measured in the Q machine. The density $\tilde{n}/n$ and potential $e\tilde{\phi}/T_e$ waves are approximately equal in amplitude with $\tilde{n}$ leading $\tilde{\phi}$ by 30° to 45° for the Hendel *et al.* (1968) experiment. Vortex dynamics has also been observed in the plasmas produced in Q machines. In the experiments of Pécseli *et al.* (1984, 1985), externally excited vortices of like signs were shown to coalesce into one vortex. Vortices of opposite signs were reported to interact with each other but no claim was made about the formation of a dipole vortex pair. The presence of vortices in a spectrum of waves changes the wave number spectrum making energy spectrum decay as $k_\perp^{-m}$ with the spectral decay index appreciably larger than the value of $m = 3$ derived in Sec. V.C for drift-wave turbulence.

A variety of drift-type instabilities relevant to toroidal magnetic fusion devices, including the trapped electron modes by Prager, Sen, and Marshall (1974), the trapped ion instability by Slough, Navratil, and Sen (1982), the collisionless curvature-driven trapped particle mode by Scarmozzino, Sen, and Navratil (1986), have been produced and identified in the Columbia Linear Machine.

The drift wave driven by the radial ion temperature gradient in a collisionless cylindrical plasma was demonstrated in the modified Columbia Linear Machine by Sen, Chen, and Mauel (1991) by using biased wire screens to create a $T_{i\perp}(r)$ gradient sufficient to excite a new $m = 2$,10 kHz (in the plasma frame) drift-wave oscillation. The toroidal ion temperature gradient mode driven by the magnetic curvature was also produced and identified by Chen and Sen (1995) in the same machine. In all these experiments the plasma is in a steady state like the Q-machine experiments except that the plasma temperatures are an order of magnitude higher ($T_i \gtrsim T_e \sim 8$ eV), the density is lower ($N \sim 10^9\,\mathrm{cm}^{-3}$), as required for low collisionality ($\nu < \omega_k$), and the working gas is hydrogen. There are approximately ten ion gyroradii in the plasma radius.

Drift waves were found in the transient plasmas produced in the multipole confinement devices that were both linear and toroidal devices with strongly varying **B** fields from parallel conductors carrying large currents. The multipole plasmas of hydrogen, helium, and argon were produced by microwave frequency heating. The theory for the drift waves in the multipole took into account the localization of the unstable oscillations to regions of unfavorable gradient B and curvature particle drifts and the shear in the helical $\mathbf{B}(\mathbf{x})$ field (Ohkawa and Yoshikawa, 1967). These experiments provided further evidence for the universal appearance of drift waves in confinement geometries. The correlation of drift-wave theory with the multipole and spherator experiments are described in Sec. 3.3 of the Horton (1990) review article. The main result to be noted here is that the experiments by Okabayashi and Arunasalam (1977) showed that increasing the magnetic shear reduced fluctuation amplitudes. The multipole devices are unique in being able to continuously vary the magnetic shear parameter $S=L_n/L_s$ from zero to order of unity. Here L_n is the density gradient scale length, and L_s is the scale length for rotation of the **B** vector through angle of order one radian. Even with the strongest magnetic shear, however, the fluctuations were not eliminated.

The magnetic shear plays a central role in the linear and nonlinear theory of the drift waves consistent with the role of shear on the fluctuations measured in these experiments. In recent theory and experiments for tokamak confinement devices the combined roles of $\mathbf{E}_r\times\mathbf{B}$ sheared flows and magnetic shear are known to produce enhanced confinement regimes (Synakowski *et al.*, 1997; Burrell, 1997). The improved confinement occurs over narrow radial regions giving rise to new confinement regimes with internal transport barriers (Koide *et al.*, 1994; Levinton *et al.*, 1995; Strait *et al.*, 1995). The principal tools available for understanding these changes in transport are the dependence of drift-wave turbulence on the system parameters especially the magnetic shear in $\mathbf{B}(\mathbf{x})$ and mass flow shear in the hydrodynamic flow velocity $\mathbf{u}(\mathbf{x})$.

In tokamaks the first convincing identification of drift waves in the core plasma came from the microwave scattering experiments (Mazzucato, 1976) and infrared CO_2 laser scattering experiments (Surko and Slusher, 1976, 1978). These experimental results for the fluctuations were explained in the context of drift waves existing at the mixing-length level of saturation (Horton, 1976) with a nonadiabatic electron response due to the trapped electron-wave dissipation. Subsequently, many experiments around the world have observed the universal appearance of a broadband of drift-wave fluctuations with $\omega/2\pi\simeq 50-500\,\mathrm{kHz}$ at $k_\perp=1-15\,\mathrm{cm}^{-1}$ in toroidal confinement devices for both the tokamak and helical-stellarator systems. Many fluctuation and transport studies at facilities including TFTR, Alcator, TEXT, ATF, Heliotron, JFT2M, and ASDEX were undertaken in the 1980s and 1990s after these initial findings of drift-wave turbulence.

An exhaustive basic physics research program on plasma fluctuations and anomalous transport was carried out from 1982–1994 in the TEXT tokamak at The University of Texas at Austin. This experiment provided the most complete correlated data sets of core fluctuations from five $k_\perp$ values (2, 4.5, 7, 9, 12 cm^{-1}) from far infrared (IR) laser scattering, complex probe arrays for edge turbulence, the heavy-ion (HI) beam probe for measurements of the radial electric field E_r and the space-time localized fluctuating potential $\tilde{\phi}$ in addition to the usual complement of spectrometers, interferometers, bolometers, and magnetic coils for determining the state of the plasma. A review of the far IR and HI beam probe data, as well as other diagnostics, leading to the conclusion that the drift waves are present and responsible for the transport is given in Bravenec *et al.* (1992). A review of the diagnostics on TEXT and other tokamaks is given by Gentle *et al.* (1995). The task of correlating the wealth of fluctuation and transport data with theory turned out to be difficult—leading to numerous controversies over the details of the identification of driving terms and the collisionality regimes of the unstable modes. There is substantial supporting evidence in the high-level edge fluctuations data for resistive ballooning, parallel shear flow, impurity drift modes and recombination ionization modes. (The order given corresponds to the author's view of the relative importance of the effects on the edge plasma turbulence for the TEXT experiments.) In the core plasma the dissipative trapped electron mode dominates in TEXT (Bravenec *et al.*, 1992). In contrast to this Ohmic heated tokamak, for auxiliary heated plasmas where the Ohmic heating is a fraction of the total input power the ion temperature gradient-driven drift wave is the dominant driving mechanism for the drift-wave turbulence. The TEXT experiments were Ohmic discharges with toroidal magnetic fields $B=2\,\mathrm{T}$, plasma current $I=200-400\,\mathrm{kA}$, the loop voltage $\mathcal{E}_{/\!/}=2V$ giving $T_e\lesssim 2\,\mathrm{keV}$ and $T_i<1\,\mathrm{keV}$. In contrast, the major confinement experiments have high-power neutral beam injection systems providing injected powers $P_b=5$ to 30 MW, producing $T_e\lesssim 8\,\mathrm{keV}$ and $T_i\lesssim 40\,\mathrm{keV}$. Thus the nature of the instability drive switches from the electron temperature gradient parametrized by

$$\eta_e=\frac{\partial_r \ln T_e}{\partial_r \ln n_e} \tag{14}$$

to the ion temperature gradient parametrized by

$$\eta_i=\frac{\partial_r \ln T_i}{\partial_r \ln n_i} \tag{15}$$

in going from Ohmic discharges in TEXT and ALCATOR, to the high-power neutral beam injection heated discharges in TFTR, JET, DIII-D, and JT60U. The energy-momentum deposition profiles and magnitudes from the auxiliary heating become key control parameters in the later experiments, as will be explained in Sec. IV.C.

Core electron temperature fluctuations δT_e are measured by a multichannel heterodyne receiver of the electron cyclotron emission (Cima *et al.*, 1995) in the TEXT experiment. The electron cyclotron emission instrument loses sensitivity for $k_\theta > 1.5\,\mathrm{cm}^{-1}$ giving rise to the same kind of systematic error problem as the heavy-ion beam probe for the central part of the drift-wave spectrum at $k_\theta \simeq 3\,\mathrm{cm}^{-1}$. The long-wavelength $\delta\tilde{T}_e/T_e$ fluctuation amplitudes, which are free of this problem, are reported to be comparable to the amplitude of the density fluctuations. First, Cima *et al.* (1995) conclude that the directly measured long-wavelength component of the turbulent flux $q_e = \frac{3}{2} n_e \langle \tilde{T}_e \tilde{E}_\theta \rangle / B$ could not account for the thermal flux inferred from power balance. Subsequently, the analysis was improved (Watts and Gandy, 1996; Deng *et al.*, 1998) to show that the shorter-wavelength domain, where the far IR laser scattering shows the dominant drift-wave features, the $\langle \tilde{T}_e \tilde{E}_\theta \rangle$ conductive flux accounts for the electron thermal flux required by the electron power balance equation. The δT_e fluctuation work confirms this important conclusion in detail. It can now be stated that the drift-wave fluctuation studies on TEXT account for both the particle and thermal energy losses for an Ohmically heated tokamak.

C. Conditions for transport and propagation of disturbances

Now we analyze the ion motion in the $\mathbf{E}\times\mathbf{B}$ convection. For the small, localized excess of ion charge shown in Fig. 1, the

$$\mathbf{v}_E = \frac{c\mathbf{E}\times\mathbf{B}}{B^2} \tag{16}$$

convection rotates plasma clockwise around the potential maximum $\phi > 0$ which is also the density and electron pressure maximum in the adiabatic response by Eq. (12). Now, if the ambient plasma is uniform ($\partial_x n_a = \partial_x T_i = 0$) across the convection zone, then the cell rotates without plasma transport. When the plasma has an x gradient of density (pressure), however, there is a net transport of the structure along the symmetry direction $\hat{\mathbf{y}}$ with no net transport across an $x = \text{const}$ surface. Analytically, this follows from the definitions of the net convective flux particle and thermal fluxes across a given surface S as

$$\Gamma_a = \frac{1}{S}\int_S n_a \mathbf{v}_E \cdot d\mathbf{a}, \tag{17}$$

$$q_a = \frac{3}{2S}\int_S n_a T_a \mathbf{v}_E \cdot d\mathbf{a} \tag{18}$$

which, for the situation in Fig. 1, gives $\Gamma_a = (-c/B)\int n_a(\phi)(\partial\phi/\partial y)dy\,dz = 0$ and likewise $q_a = 0$. Clearly, the situation changes in the presence of the phase shift $\delta n - \phi$ in Eq. (13).

Now we show that the localized structure in Fig. 1 translates along the symmetry direction with the electron diamagnetic drift speed $v_{\mathrm{de}} \equiv cT_e/eBL_n$ where $L_n^{-1} = -\partial_r \ln N$.

For the positive potential structure in Fig. 1 the clockwise $\mathbf{E}\times\mathbf{B}$ rotation brings higher density $N_>$ (and higher pressure $N_> T_e$) plasma to the right and lower density $N_<$ (pressure) to the left, resulting in a shift of the maximum density and potential, linked through the electron response by Eq. (12), to the right. The speed of the translation is proportional to the gradient of the density $L_n^{-1} = -\partial_r \ln N$ and inversely proportional to the strength of the magnetic field B. The speed also increases with electron temperature T_e since the potential fluctuation $e\phi$ scales up with T_e. For a negative potential structure the $\mathbf{E}\times\mathbf{B}$ rotation is counterclockwise, but the structure moves to the right with the same speed (in the limit of small $e\phi/T_e$), since now lower density plasma is brought to the right, shifting the minimum in that direction.

To calculate the speed of translation we consider the rate of buildup of the number of ions in a small cell $\Delta x \Delta y$ to the right ($y \equiv \delta y$) of the maximum potential $\phi(x=0, y=0)$ along the $x=0$ (equitorial plane so to speak) of the localized structure. At this location the particle flux $n\mathbf{v}_E$ is purely in the x direction and is $N_> V_x$ into the top of the small cell and $N_< V_x$ out of the cell. Thus, the rate of increase of the ions in the cell is

$$\frac{\partial n_i}{\partial t}\Delta x \Delta y = \Delta y (N_> V_x - N_< V_x) = -\Delta x \Delta y \frac{\partial N}{\partial x}\frac{cE_y}{B}, \tag{19}$$

where $E_y = -[\phi(0,\delta y) - \phi(0,0)]/\delta y = \phi/\delta y$. Now, the ion density at this location builds up to that of the original maximum $\delta n_e = N(e\phi/T_e)$ in the time δt when

$$\delta n_i = -\frac{\delta t c \phi}{B\,\delta y}\frac{\partial N}{\partial x} = N\frac{e\phi}{T_e}, \tag{20}$$

where in the last step we use quasineutrality taking $\delta n_i = \delta n_e = N(e\phi/T_e)$. Thus during the time δt the convection moves the maximum of the structure to the right by $\delta y = v_{\mathrm{de}}\delta t$ where

$$v_{\mathrm{de}} = \frac{\delta y}{\delta t} = -\frac{cT_e}{eBN}\frac{\partial N}{\partial x}. \tag{21}$$

The x displacement of the plasma during this motion is $\xi_x = v_x \delta t = -\delta t\,\delta\phi/B\,\delta y$. When this displacement becomes comparable to δx, the motion is nonlinear leading to the formation of nonlinear vortex structures given in Sec. V.F. Locally, the plasma is mixed over the length δx when $\xi_x = \delta x$ in one rotation period.

D. Drift-wave diffusivities and the ion inertial scale length

It is convenient in the study of drift waves and transport to introduce gradient scale lengths and reference diffusivities. Thus, it is conventional to define L_n as the density gradient scale length through the relation $1/L_n = -\partial_x \ln N$. The temperature gradient scale length L_T is defined similarly. The space-time scales of the waves in

Sec. II.C lead to two different dimensional scalings for the diffusivities. The reference diffusivities are the Bohm diffusivity

$$D_B=\frac{cT_e}{eB} \tag{22}$$

and the drift-wave diffusivity

$$D_{\rm dw}=\left(\frac{\rho_s}{L_n}\right)\left(\frac{cT_e}{eB}\right), \tag{23}$$

also commonly called the gyro-Bohm diffusivity in reference to the factor $\rho_s/L_n \ll 1$. Clearly, the scaling of the Bohm and gyro-Bohm diffusivities are markedly different with $D_B \propto T_e/B$ independent of the system size while $D_{\rm dw}=T_e^{3/2}/B^2L$ decreases with the system size. There is a long history of confinement scaling studies that have correlated the thermal and/or particle confinement with either the Bohm or the drift-wave scaling laws. The issue is still actively debated as to which transport scaling is to occur under given confinement conditions (Christiansen *et al.*, 1993; Petty, Luce, Pinsker, *et al.*, 1995). In Sec. III we will show how the Bohm scaling arises from *mesoscale* toroidal drift-wave structures and thus is expected near marginal stability (Tajima *et al.*, 1994; Kishimoto, Tajima, Horton, *et al.*, 1996; Garbet and Waltz, 1996). When the convective cells scale with ρ_s, the drift-wave diffusivity, more commonly called gyro-Bohm, applies.

A compendium of thermal diffusivity formulas collected from the literature on drift-wave turbulent transport is given by Connor (1993). Currently, large scale particle simulations are used to address this issue from first-principle calculations.

Let us pause to estimate the values of the parameters introduced so far for a tokamak such as the Texas Experimental Tokamak (TEXT) and moderately larger machines such as DIII-D and JT2-FM. For scaling convenience let us take $T_e=T_i=1\,{\rm keV}=10^7$ K, $B=2$ T $=20$ kG, and a pure hydrogen plasma with $L_n=10$ cm. Then we find that $\omega_{ci}=2\times10^8$/s, $c_s=(T_e/m_i)^{1/2}=3\times10^7$ cm/s so that $\rho_s=c_s/\omega_{ci}=1.5$ mm. Then the electron diamagnetic velocity Eq. (21) is $v_{\rm de}=4\times10^5$ cm/s $=4$ km/s and frequencies for the observed fluctuation scales $k_\perp=1$ to 20 cm^{-1} are $\omega/2\pi=7$ kHz to 1 MHz. The drift-wave diffusivity (or gyro-Bohm) is $D_{\rm dw}=(\rho_s/L_n)(\rho_s c_s)=7\times10^4$ cm^2/s$=7$ m^2/s, while the Bohm diffusivity is greater by the factor $L_n/\rho_s=70$. This factor measuring the number of gyroradii or drift-wave scale lengths ρ_s in the system's gradient scale L_n is a key dimensionless measure of the system called ρ_*. In defining ρ_*, it is usual to replace the space-time varying L_n with the relatively constant value a of the plasma minor radius. Thus, a key issue is the scaling of confinement systems with

$$\rho_*\equiv\frac{\rho_s}{a} \tag{24}$$

(Waltz *et al.*, 1990; Perkins *et al.*, 1993). Drift-wave theory seems to be able to account for confinement scaling either as D_B or $\rho_* D_B$. Transport dependent on ρ_* depends on the average mass m_i of the working gas ions since $\rho_s=c(m_iT_e)^{1/2}/eB$.

TABLE I. Plasma drift-wave parameters.

	TFTR	TEXT
Magnetic field	4.8 T	2 T
Major/minor radii	2.45 m/0.8 m	1.0 m/.27 m
Electron temperature	6 keV	500 eV
Density n_e and	4×10^{13} cm^{-3}	3×10^{13} cm^{-3}
Gradient length L_n	20 cm	10 cm
Drift velocity v_d	3×10^5 cm/s	1×10^5 cm/s
k scattering experiment	1–20 cm^{-1}	1.5–15 cm^{-1}
ω scattering experiment	10–500 kHz	10–1000 kHz
$\tilde{n}_e/n_e$	5×10^{-3} to 0.02	0.01 to 0.1

The Perkins *et al.* (1993), Petty, Luce, Burrell, *et al.* (1995), and Erba *et al.* (1995) studies present evidence for the Bohm-like scaling of transport. Power balance in the JET discharge up to 7 MA of plasma current is obtained with $\chi_e=\alpha_e q^2(a/L_p)D_B$ and $\chi_i=\alpha_i\chi_e+\chi_i^{\rm neo}$ with $\alpha_e=2.1\times10^{-4}$ and $\alpha_i=3.0$ (Taroni *et al.*, 1994 and Erba *et al.*, 1995, 1998).

The relevant parameters for TEXT and the large Tokamak Fusion Test Reactor (TFTR) are given in Table I.

The fluctuation measurement at wave numbers $k_\perp \lesssim 1$ cm^{-1} require the techniques of reflectometry (Doyle *et al.*, 1991; Mazzucato and Nazikian, 1993) and the indirect method of beam emission spectroscopy as in the Durst *et al.* (1993) experiment.

In summary, we have shown that the drift wave is a convective disturbance satisfying the wave equation $(\partial_t+v_{de}\partial_y)\phi=0$ in the limit of no dispersion $(k_\perp\rho_s\to0)$ and vanishing amplitude $e\phi/T_e\to0$. In Sec. V, we lift both these conditions showing that the nonlinearity can balance dispersion to form localized coherent structures. The reader may readily find one form of the nonlinear steepening by repeating the arguments given above in Sec. C while retaining the full Boltzmann response $N\exp(e\phi/T_e)$ for the electrons (Tasso, 1967; Petviashvili, 1977).

Let us close this introduction to the drift-wave mechanism by showing the supporting evidence from the far IR scattering experiment in the core of the TEXT experiment and the microwave reflectometry measures in the core of TFTR. From TEXT (Brower *et al.*, 1985, 1987), Fig. 4 shows the peak of the frequency of the electron-density fluctuations inferred from the dynamical scattering factor $S(k_\perp,\omega)$ versus the wave number $k_\perp$ from the scattering geometry. The frequency of the spectrum in the lab frame follows $\omega=\omega_k(\eta_i)+k_\theta v_E$ to a good approximation where $v_E=-cE_r/B$ is the Lagrangian velocity of the plasma (ions and electrons) relative to the laboratory frame of reference, and $\omega_k(\eta_i)$ is the drift-wave frequency in the plasma frame. The plasma rest-frame frequency ω_k is shown by dotted lines for the range of $\eta_i=\partial\ln T_i/\partial\ln n_i$ values in this experiment. The corresponding laboratory frame frequencies

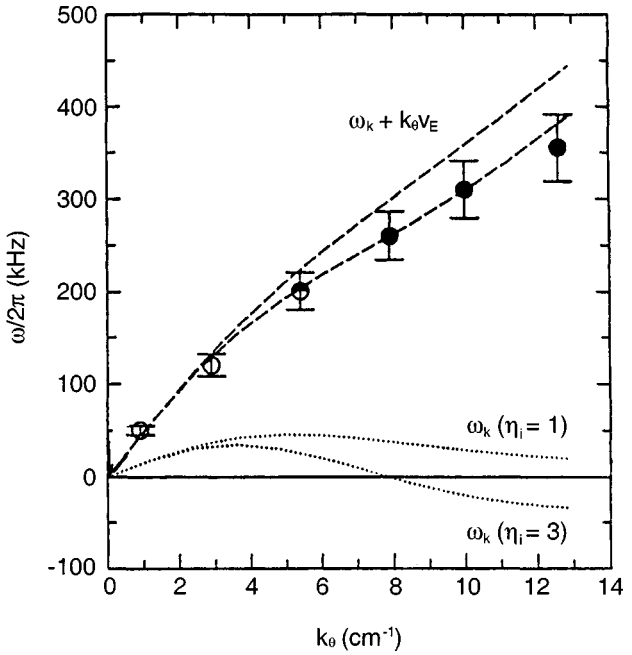

FIG. 4. Frequency spectrum from far infrared laser scattering from the electron density fluctuations associated with drift waves in the TEXT tokamak (courtesy of Brower).

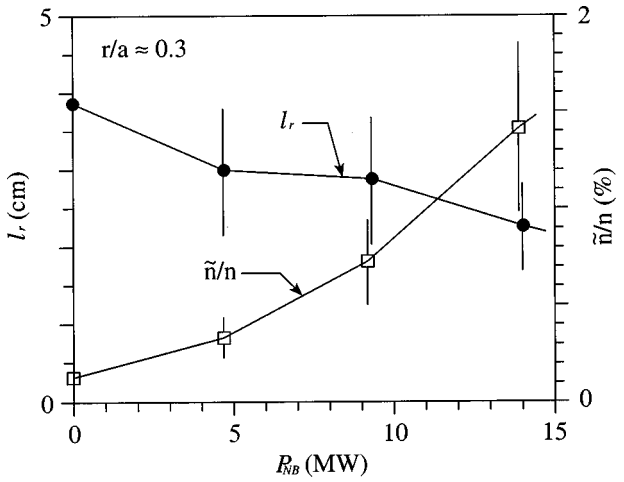

FIG. 5. Microwave reflectometer measurements of the radial correlation length l_r and the fractional fluctuation level in the core of TFTR (courtesy of Mazzucato and Nazikian).

are given by the dashed lines. To find the transformation velocity v_E, and thus the Doppler shift, the HI beam probe diagnostic is used to determine the radial electric field $E_r(r)$. Quasilinear theory predicts the spectrum of density fluctuations

$$S(\mathbf{k},\omega)=\frac{S_0}{VT}\left\langle\left|\frac{\delta n_e(\mathbf{k},\omega)}{n_e}\right|^2\right\rangle\simeq I(\mathbf{k})\,\delta(\omega-\mathbf{k}\cdot\mathbf{u}-\omega_{\mathbf{k}}),$$

where V and T are the sample volume and time interval. Renormalized turbulence theory gives a Lorentzian spectral distribution

$$S^{\rm rn}(\mathbf{k},\omega)=\frac{I(\mathbf{k})\,\nu_{\mathbf{k}}}{(\omega-\omega_{\mathbf{k}})^2+\nu_{\mathbf{k}}^2} \tag{25}$$

with the turbulent decorrelation rate

$$\nu_{\mathbf{k}}\simeq\langle(\mathbf{k}\cdot\mathbf{v}_E)^2\rangle^{1/2}\simeq\frac{ck_\perp^2\tilde{\phi}}{B}. \tag{26}$$

The agreement of the peak of the far IR measurement of $S(k,\omega)$ and the theoretical formula (25) shown by Fig. 4 is a direct signature of the drift-wave turbulence.

The vortex gas description predicts a similarly broadened spectral line but centered along the dispersionless frequency $\omega=k_y u$ with $u\geqslant v_{\rm de}$ rather than along the strongly dispersive wave phase velocity $\omega/k_y\simeq v_{\rm de}(1+k_\perp^2\rho_s^2)^{-1}$. As we shall see in Sec. V, the drift-wave vortices are a natural component of the drift-wave turbulence in the long-time limit where mode coupling effects are dominant.

From TFTR the radial correlation length ℓ_r and the fractional amplitude of the core drift-wave turbulence is shown in Fig. 5 as a function of the total auxiliary heating power $P_{\rm NB}$ (in megawatts) from the neutral beam injectors. The data point at $P_{\rm NB}=0$ is for an Ohmic discharge where the amplitude of the fluctuations is the lowest at $\tilde{n}/n\cong10^{-3}$. The dispersion scale length ρ_s is approximately $\rho_s\simeq0.1$ to 0.2 cm in these deuterium plasmas.

The main features of Figs. 4 and 5 are explained by drift waves and the drift-wave turbulence as will become clear from Secs. III to V. Comparing the fractional fluctuation level $\tilde{n}/n$ from the early smaller machines, such as ATC (Mazzucato, 1976), with intermediate size TEXT and the large TFTR machine shows that the core fractional fluctuation level scaling is consistent with $(\rho_s/a)^\alpha$ scaling with an exponent α that varies from $\frac{1}{2}$ to unity.

Early particle simulations corresponding to the Q-machine drift-wave experiments are found in Lee *et al.* (1987). For both the sheared and shearless slab geometry particle simulations on $(64\Delta)^2$ and $64\Delta\times128\Delta$ grids with $\Delta=\rho_i/2$, $\omega_{ce}/\omega_{pe}=10$, $T_e/T_i=4$–9, and $m_i/m_e=1837$ were performed. The density gradient is strong with $\rho_i/L_n=\frac{1}{5}$, and the saturated state is dominated by single low m modes with convection patterns similar to those shown in Figs. 2 and 3 with $e\tilde{\phi}/T_e\sim\delta\tilde{n}_e/\overline{n}\approx\rho_i/2L_n$. The dominant nonlinear saturation mechanisms are the quasilinear adjustments of the parallel velocity distribution functions and shearing of the convection by the $\mathbf{E}_r(x)\times\mathbf{B}$ flow generated by the $(k_y=k_z=0)$ radial modes.

Finally, in a review article it is important to point out parallels with other areas of physics. The closest and most important parallel to plasma drift waves is the analogy with the Rossby waves and vortices in geophysical atmospheric and oceanographic disturbances with periods long compared to the rotational period of the planet. Hasegawa and Mima (1977, 1978) and Hasegawa *et al.* (1979) developed the limit in which the two models become isomorphic. The correspondence is due to the Coriolis force having the same mathematical form as the Lorentz force. The analogy was also recognized by Petviashvili (1977), which led to the first rotating para-

bolic water tank experiments by Antipov *et al.* (1982, 1985) in Kurchatov and Antonova *et al.* (1983) in Tiblisi. This aspect of the drift-wave–Rossby problem is found in the Horton and Hasegawa (1994) article in the special issue of *Chaos* devoted to such geophysical vortex structures. Further development of the theory from the plasma physics perspective is given in *Chaos and Structures in Nonlinear Plasmas* by Horton and Ichikawa (1996), *Solitary Waves in Plasmas and in the Atmosphere* by Petviashvili and Pokhotelov (1992), and in *Two-Dimensional Turbulence in Plasmas and Fluids* edited by Dewar and Griffiths (1997).

III. DRIFT-WAVE EIGENMODES IN TOROIDAL GEOMETRY

A. Ion acoustic wave coupling and dispersion from the polarization current

The drift wave couples to the ion acoustic wave and through this coupling many important properties of the drift-wave propagation, such as the formation of the eigenmodes, are determined. The ion acoustic waves in a homogeneous, magnetized plasma occur as oscillations parallel to the magnetic field with

$$\omega_{ac}(\mathbf{k})=\pm\left[\frac{k_\parallel^2 c_s^2}{1+k_\perp^2\rho_s^2}\right]^{1/2}, \tag{27}$$

where $c_s=(T_e/m_i)^{1/2}$ and $\rho_s=c(m_iT_e)^{1/2}/eB=c_s/\omega_{ci}$. The waves in Eq. (27) are compressions and refractions of the ion fluid along the magnetic field with the electrons following in the adiabatic Boltzmann distribution Eq. (12) and in the quasineutral limit of Eq. (10) where $\delta n_i=\delta n_e$ for $k_\perp^2\lambda_{\mathrm{De}}^2\ll 1$.

The dispersion of the ion acoustic waves with perpendicular wave number arises from the polarization currents given by

$$\mathbf{j}_p=\frac{c^2\sum_a m_a n_a}{B^2}\frac{d\mathbf{E}_\perp}{dt} \tag{28}$$

in a magnetized plasma. From $\mathbf{j}_p\cdot\mathbf{E}$ we see that the time reversible polarizable currents are associated with the work done in establishing the kinetic energy $\frac{1}{2}m_an_av_E^2$ in the $\mathbf{E}\times\mathbf{B}$ convection. The plasma polarization current $\mathbf{j}_p$ is the same as the polarization current in any polarizable material (Schmidt, 1979) except that the polarization is anisotropic in magnetized plasma. A consequence of the large polarization current across the magnetic field is that transverse electromagnetic waves with frequencies ω below the ion cyclotron frequency, which have the dispersion relation $\epsilon_\perp\omega^2=c^2k_\parallel^2$ where $\epsilon_\perp=1+4\pi c^2\rho_m/B^2\gg 1$, propagate as Alfvén waves $\omega/k_\parallel=c/\sqrt{\epsilon_\perp}\cong B/(4\pi\rho_m)^{1/2}\equiv v_A$ (Jackson, 1975). Here $\rho_m=\Sigma_a m_a n_a$ is the mass density. In toroidal confinement systems we have $\epsilon_\perp\sim 10^3-10^4$ with $v_A=3\times 10^8$ to 10^9 cm/s. While in general the drift waves also couple to the Alfvén waves, and this coupling becomes critical near the onset of the MHD instabilities, we will not attempt to develop this coupling theory in this review article. Results for Alfvén wave coupling are given in the earlier review (Horton, 1990). For a low plasma pressure p to magnetic pressure $B^2/8\pi$ ratio $\beta\equiv 8\pi p/B^2\ll 1$, the ion acoustic coupling is the relevant coupling since $c_s=v_A(\beta/2)^{1/2}\ll v_A$ is the relevant parallel phase velocity for drift-wave eigenmodes.

In the absence of the radial inhomogeneity $\omega_{*e}\equiv k_yv_{de}\to 0$, and the ion acoustic waves are strongly damped by Landau damping from the wave-ion resonance

$$\frac{\gamma_k^{(i)}}{\omega_{\mathbf{k}}}\simeq c_s^2\int \pi\delta(\omega_{\mathbf{k}}-k_\parallel v_\parallel)k_\parallel\frac{\partial f_i(\mathbf{v})}{\partial v_\parallel}d^3v.$$

This is clear from the fact that the parallel phase velocity $\omega_{\mathbf{k}}/k_\parallel\sim c_s$ lies in the thermal ion velocity distribution function $f_i(v_\parallel)$ with $v_\parallel=c_s\sim v_i(T_e/T_i)^{1/2}$ (Goldston and Rutherford, 1995). Turning on the density gradient ($\omega_{*e}\neq 0$) splits the degeneracy of Eq. (27) for the forward and backward waves leading to a fast and slow ion acoustic wave. From the drift-wave–ion acoustic wave coupling we find that the fast waves, which avoid the ion Landau resonance ($\omega/k_\parallel\gg c_s$), are given by

$$\omega_{\mathbf{k}}=\frac{k_yv_{de}}{1+k_\perp^2\rho_s^2}+\frac{k_\parallel^2c_s^2}{k_yv_{de}(1+k_\perp^2\rho_s^2)}, \tag{29}$$

while the slow waves, $\omega_k\simeq -k_\parallel^2c_s^2/k_yv_{\mathrm{de}}$, are strongly damped.

Dispersion relation (29) largely determines the propagation and formation of the drift-wave eigenmodes in the confinement devices when the ion temperature, or its gradient, are not strong effects. The wave (29) propagates fast along the magnetic field with $v_{g\parallel}=\partial\omega/\partial k_\parallel=2c_s(k_\parallel c_s/\omega_{*e})$ and slow across the magnetic field

$$v_{g*}=\frac{\partial\omega}{\partial k_x}=-2c_s\left(\frac{\rho_s}{L_n}\right)(k_xk_y\rho_s^2).$$

Thus the eigenmodes along the magnetic field are rapidly formed. The calculation of these eigenmodes on each magnetic surface ($x=$const) in the torus follows a procedure called ballooning mode theory. Ballooning mode theory gives a method of constructing doubly periodic wave functions for the toroidal system while taking into account the anisotropy of the drift-wave mode structure dictated by the physics in dispersion relation (29). The drift-wave–ion acoustic modes have gradients across the magnetic field determined by $k_\perp\sim\rho_s^{-1}(\omega_{*e}/\omega-1)^{1/2}$ and gradients along the field by $|k_\parallel|\leqslant|\omega_{*e}|/c_s=L_n^{-1}|k_y\rho_s|<L_n^{-1}$. Thus the fluctuations form long, thin filaments aligned with the helical magnetic field line $\mathbf{B}(\mathbf{x})$.

A three-dimensional visualization of the drift-wave convective filaments is shown in Fig. 6 from Parker *et al.* (1996) showing isopotential surfaces. The straightforward WKB representation of the potential filaments, $\phi=\hat{\phi}(s)\exp(i\int^{\mathbf{x}}\mathbf{k}_\perp(\mathbf{x}')\cdot d\mathbf{x}')$ with $\hat{\phi}$ and $\mathbf{k}_\perp$ slowly varying following $\mathbf{B}$, is in direct conflict with the condition of toroidal periodicity. Here $\mathbf{B}\cdot\nabla\phi=B(\partial\hat{\phi}/\partial s)\exp(i\int^{\mathbf{x}}\mathbf{k}_\perp\cdot d\mathbf{x}')=ik_\parallel B\phi$ where s is distance along the field line.

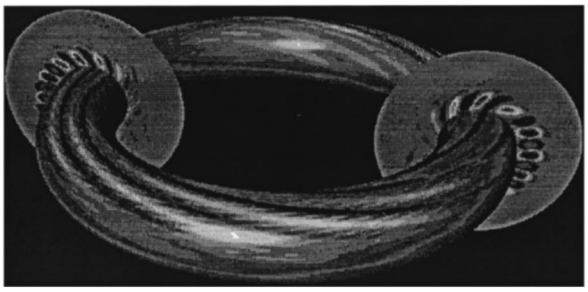

FIG. 6. Contours of the potential filaments aligned along the helical magnetic field lines in a simulation of the tokamak (from Parker *et al.*, 1996, courtesy of Parker).

The resolution of the conflict between periodicity and small $k_\parallel$ is given by the ballooning transformation that uses the local translational symmetry in x between neighboring magnetic surfaces to construct the periodic toroidal functions. The ballooning transform technique is also used for numerical simulations as a way of preventing truncation errors in the large $\nabla_\perp \sim 1/\rho_s$ gradient from projecting on to the small $\nabla_\parallel \sim 1/L_n$ gradient. Thus we will need to present some details of the ballooning transformation. Key early works are Connor, Hastie, and Taylor (1979) and Choi and Horton (1980); more recent developments are found in Romanelli and Zonca (1993), Kim and Wakatani (1994), and Taylor and Wilson (1996). A three-dimensional ballooning theory was developed by Dewar and Glasser (1983).

Briefly stated, the physical results of the ballooning transformation analysis of the drift wave is that in the absence of sheared flows the drift-wave–ion acoustic wave form mesoscale radial eigenmodes with radial widths Δr given by

$$\Delta r = (\rho_s L)^{1/2} \tag{30}$$

in which the ion acoustic term (last term) in Eq. (29) is replaced by a complex frequency shift of order $\Delta\omega \sim \rho_* |\omega_*|$—small compared to the leading drift-wave term, but describing the weak damping due to ion Landau resonance absorption $\gamma_k^{(i)}$. These mesoscale toroidal eigenmodes are readily observed in the global particle simulations (LeBrun *et al.*, 1993; Parker and Lee, 1993; Parker *et al.*, 1993, 1996; Kishimoto, Tajima, LeBrun, *et al.*, 1996; Sydora *et al.*, 1996; Furish *et al.*, 1999). Examples of the toroidal modes from two simulation teams are shown in Figs. 7 and 8.

Figure 7 from Kim *et al.* (1996) shows the change of the global drift-wave functions with the radial electric field $E_r(r)$ where the reduction of the mode's radial width with increasing E_r shear is made clear. In Fig. 7 the direction of the toroidal field is into the page so the electron diamagnetic drift is clockwise and the ion diamagnetic drift and the total diamagnetic current is counterclockwise. The flow arrows at the top show the direction of $\mathbf{E}\times\mathbf{B}$ shear flow, and the angle θ_0 measured from the outside meridional plane where $|\mathbf{B}|$ is minimum shows the location where the elliptical convection cells are most nearly parallel to radial direction ∇r. The determination of θ_0 involves the radial profiles of the diamagnetic flows, the magnetic, and flow shears (Kishimoto, Tajima, LeBrun, *et al.*, 1996; Kim *et al.*, 1996).

Figure 8 from Sydora *et al.* (1996) shows how the turbulence spreads to linearly stable regions in the nonlinear state. Figure 8(a) shows the fluctuating potential during the linear growth of the mesoscale (30) toroidal eigenmode for the toroidal mode number $n=16$. Compare this with the broader spatial range of the fluctuations and the larger number of excited poloidal mode numbers m in Fig. 8(b). Transport simulations containing drift-wave turbulence and the relevant atomic physics for TFTR discharges showed that core plasma is near marginal stability (Bateman, 1992) with the deviation from the critical gradient increasing rapidly toward the edge. The mesoscale eigenmodes are robust, occurring both for the electron drift wave and ion temperature gradient drift wave in the nonlinear saturated states. Scaling studies with ρ_* varying from $\frac{1}{60}$ to $\frac{1}{200}$ were performed. Clusters of these mesoscale toroidal modes, Fig. 8, fill the gradient region of the toroidal cross section, giving rise to a Bohm scaling to the diffusivity and forcing the profile to remain close to marginal stability (Tajima *et al.*, 1994; Kishimoto, Tajima, LeBrun, *et al.*, 1996; Furnish *et al.*, 1999). The idea that the turbulence keeps the profiles close to marginal was proposed by

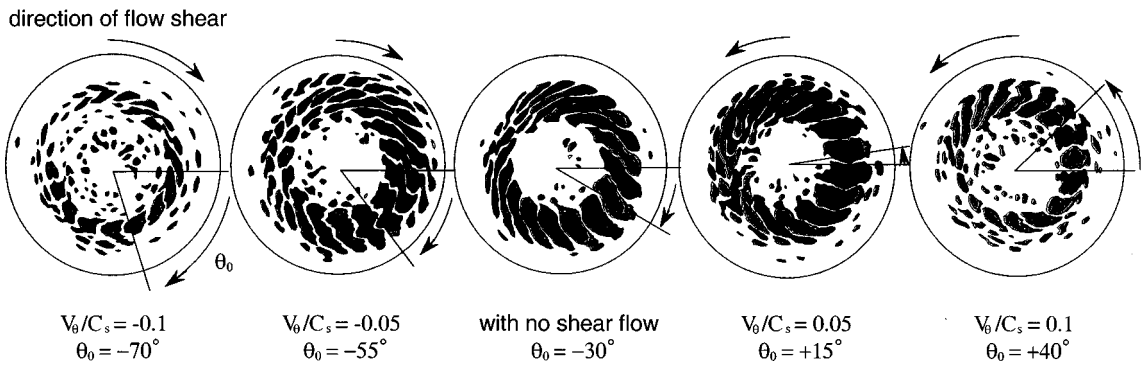

FIG. 7. Contours of the toroidal drift-wave eigenvalues in the cross-sectional plane showing the radial scales given by Eq. (22) for $a/\rho_s = 100$. The angle θ_0 of the Bloch-like wave function where $k_r = 0$ is clearly evident (from Kim *et al.*, 1996, courtesy of Kishimoto).

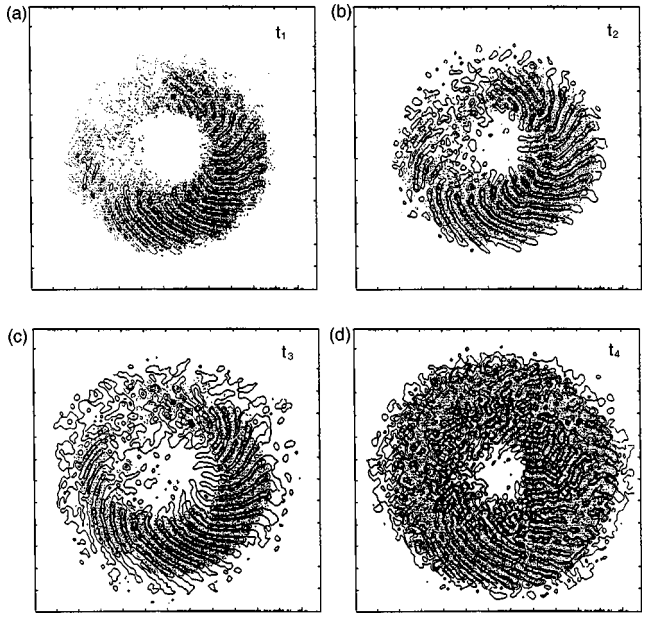

FIG. 8. Evolution of the isopotential contours for the ITG turbulence for $a/\rho_s=128$, $L_T/R=0.2$, $T_i=T_e$ with hyperbolic tangent profiles for the temperature. The density profile is flat (from Sydora *et al.*, 1996, courtesy of Sydora).

Manheimer and Antonsen (1979) and has been extensively developed by Kotschenreuther *et al.* (1995). The mesoscale mode of width $(\rho_s L_T)^{1/2}$ is composed of the phase coherent superposition of a large number of micromodes of width $\Delta r=\rho_s(L_s/L_n)^{1/2}$ localized around each neighboring rational magnetic surface. The number of single-helicity micromodes in each mesoscale mode is $\Delta m\sim(L_T/\rho_s)^{1/2}|S|\sim\rho_*^{-1/2}$, becoming very large for large machines (Connor *et al.*, 1993; Connor and Wilson, 1994). Transport effects associated with density of the rational surfaces are given in Beklemishev and Horton (1992). Another proposed mechanism for Bohm-like scaling is self-organized criticality (Diamond and Hahm, 1995).

Two important physical effects work to break up the mesoscale modes into uncorrelated micromodes restoring the gyro-Bohm diffusivity. In linear theory the introduction of sheared mass flows introduces different Doppler shifts on each rational surface that break up the coherence of the modes. This effect is readily observed in the global toroidal simulations as shown in Fig. 7 from Kim *et al.* (1996). The calculation of the toroidal eigenmodes with sheared flows, while in general a difficult problem, approximately reduces to that of a cylinder due to the loss of the radial coherence. The toroidal theory with sheared flow requires an extension of the standard ballooning transformation (Pegoraro, 1989; Miller and Waltz, 1994; Taylor and Wilson, 1996; Kim *et al.*, 1996). The Taylor, Wilson, and Connor (1996) analysis shows that sheared rotation annuls the toroidal coupling between perturbations associated with neighboring magnetic surfaces, so that the problem closely resembles that of the modes in a cylinder than in a torus. In the cylindrical limit the reduction of the growth rate

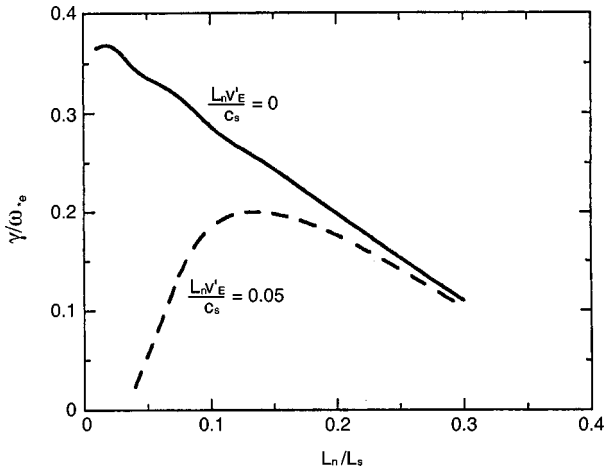

FIG. 9. The gyrokinetic growth rate as a function of magnetic shear $S=L_n/L_s$ with and without $\mathbf{E}\times\mathbf{B}$ shear flow.

is a function of the ratio of $\mathbf{E}\times\mathbf{B}$ flow shear to magnetic shear $S=L_n/L_s$. Thus, the E_r shear stabilization becomes strong at low and reversed magnetic shear. The gyrokinetic calculation for this effect is shown in Fig. 9 from the integral equation eigenvalue problem for single helicity modes (Dong and Horton, 1993). The shear flow also reduces the radial width of the eigenmode. The shear flow and magnetic shear s controlled toroidal drift-wave eigenmode width is

$$\Delta r=\rho_s\left(\frac{v_i}{av_E'}\right)^{1/2}\left(\frac{q}{sk_y\rho_s}\right)^{1/2}, \tag{31}$$

where $k_y v_E'$ is the shear in the Doppler shift frequency due to the $\mathbf{E}\times\mathbf{B}$ flow velocity (Taylor and Wilson, 1996). Large $v_E'(\lesssim 10^5/s)$ are produced in neutral beam heated plasmas through Eq. (1) where the bulk fluid velocity $\mathbf{v}_F$ is driven by the local momentum deposition from the high powered atomic beams. The decrease of χ_r in Fig. 5 correlates with increasing v_E' in Eq. (31).

The second method by which the global drift-wave eigenmodes break into gyroscale vortices is through the nonlinear effect of secondary instabilities (Cowley *et al.*, 1991). Now we consider the descriptions of the cylinder-like single helicity eigenmodes: in the absence of shear flow these modes lock together to form the global (mesoscale) toroidal eigenmodes.

B. Single helicity and ballooning eigenmodes

To calculate drift-wave transport it is important to know the local structure of the eigenmodes. In the absence of toroidal mode coupling the eigenmode analysis is straightforward following the analogous one-dimensional Schrödinger equation generalized to complex eigenvalues and eigenfunctions (Pearlstein and Berk, 1969; Gladd and Horton, 1973; Ross and Mahajan, 1978). Here we give the essential features based on the two-component fluid equations. For the kinetic description based on the Vlasov-Poisson description with arbi-

trary $k_\perp \rho_i$ the system is a one-dimensional integral eigenvalue problem (Dong and Horton, 1993).

In the two-component (ion and electron) hydrodynamic description the ion dynamics is given by

$$\frac{\partial n_i}{\partial t}+\mathbf{v}_E\cdot\nabla n_i+\nabla_\perp\cdot\left(\frac{c^2 n_i m_i}{e_i B^2}\frac{d\mathbf{E}_\perp}{dt}\right)+\nabla_\parallel(n_i u_\parallel)=0, \tag{32}$$

$$n_i m_i\left(\frac{\partial u_\parallel}{\partial t}+\mathbf{v}_E\cdot\nabla u_\parallel\right)=e_i n_i E_\parallel-\nabla_\parallel p_i, \tag{33}$$

$$\frac{3}{2}n_i\left(\frac{\partial T_i}{\partial t}+\mathbf{v}_E\cdot\nabla T_i\right)+n_i T_i(\nabla_\perp\cdot\mathbf{v}_E+\nabla_\parallel u_\parallel)+\nabla\cdot\mathbf{q}_i=0, \tag{34}$$

where $\mathbf{q}_i$ is the heat flux with its moment $\partial\mathbf{q}/\partial t$ linked to the next dropped moment $\mathbf{R}$, the flux of $\mathbf{q}$. In the remainder of this subsection we choose to lower the order of the chain of coupled moment equations by neglecting the ion pressure fluctuation $\nabla_\parallel \delta p_i$ compared with acceleration from $e_i n_i E_\parallel$ in Eq. (33). In Sec. III on the ion temperature gradient-driven modes we include the dynamics of δp_i with an appropriate closure on the heat flux $\mathbf{q}_i$. Inclusion of the thermal fluctuations are important for plasmas with $T_i \gtrsim T_e$ and significant ion temperature gradients $\eta_i \geqslant \frac{2}{3}$.

The electron dynamics is, in general, kinetic with the fluctuating electron distribution function changing form according to the energy range of the electrons. Low-energy electrons have a collisional response while high-energy electrons are collisionless. The collisionless electrons then break up into a passing electron distribution for small pitch angles and a trapped electron population for large pitch angles. Kadomtsev and Pogutse (1971, 1979) develop the kinetic response theory for the passing and trapped particles in toroidal magnetic traps.

The calculations of these electron responses are well covered in earlier reviews (Tang, 1978; Horton, 1990). The original wave-particle dissipation dispersion functions were calculated in the earlier works of Kadomtsev and Pogutse (1971) and Mikhailovskii (1974). For the purpose of this section it is sufficient to take $\delta\tilde{n}_e(\mathbf{k})$ as given in Eq. (13), with the details of the electron-wave interactions $i\delta_{\mathbf{k}}$ left without specification. The form of the operator is $\delta(\mathbf{k})=k_y\hat{\delta}(k_\perp^2,|k_\parallel|)$ where $\hat{\delta}(k_\perp^2,0)=\delta_0+\delta_1 k_\perp^2+\delta_2 k_\perp^4+\cdots$. The two most important cases are the dissipative trapped electron $\hat{\delta}_{\mathrm{TE}}=(\epsilon^{3/2}c_s/L_n\nu_e)\,[\eta_e+k_\perp^2/(1+k_\perp^2)]$ and the plateau regime electrons where $\hat{\delta}_{\mathrm{PT}}=(\pi m_e/2m_i)^{1/2}(qR/L_n)\,[k_\perp^2/(1+k_\perp^2)-\eta_e/2]$. Here $\epsilon=r/R$ and ν_e is the pitch angle collision frequency for the electrons.

For the *toroidal topology* in the cylindrical limit the doubly periodic boundary conditions in the poloidal θ and toroidal $\zeta(=z/R)$ angles force the fields to have the Fourier decomposition in the form

$$n=N(r)+\sum_{m,n}\tilde{n}_{m,n}(r)e^{im\theta-in\zeta-i\omega t}+\text{c.c.},$$

$$u_\parallel=u_\parallel(r)+\sum_{m,n}\tilde{u}_{m,n}(r)e^{im\theta-in\zeta-i\omega t}+\text{c.c.},$$

$$\phi=\Phi(r)+\sum_{m,n}\phi_{m,n}(r)e^{im\theta-in\zeta-i\omega t}+\text{c.c.}, \tag{35}$$

where the integers m, n describe the helicity of the perturbations. For *finite* toroidicity $\epsilon=r/R\neq 0$ the $1/R$ modulation of the magnetic field strength couples the m modes in Eq. (35), leaving only the toroidal mode number n as a good quantum number due to an exact symmetry in the linear system. Clearly, the parallel wave number $k_\parallel$ is determined by the *difference* between the pitch of the phase of the m, n fluctuation and the twist of the helical magnetic field $\mathbf{B}(\mathbf{x})$.

For the helical magnetic field $\mathbf{B}=B_\theta\hat{\mathbf{e}}_\theta+B_\phi\hat{\mathbf{e}}_\phi$ the rotational transform of the magnetic field line is

$$\frac{d\theta}{d\phi}=\frac{1}{q(r)}=\frac{rB_\theta}{RB_\phi}, \tag{36}$$

and the fractional rate of change of the twist of the field line is

$$s=\frac{r}{q}\frac{dq}{dr}. \tag{37}$$

For a monotonically decreasing toroidal current profile the dimensionless shear parameter (37) satisfies $0<s\leqslant 2$ reaching 2 for a radius outside the current channel $(j_\phi=0)$, where $B_\theta=(a/r)B_\theta(a)$ so that $q\propto r^2$. For non-monotonic current profiles with j_ϕ-peaked off axis the shear parameter (37) becomes negative in the core as the twist of the field line $q(r)$ forms a minimum. Such reversed magnetic shear confinement magnetic fields give rise to a breakdown of the ballooning mode symmetry at the $q'(r_{\min})=0$ shear reversal layer. There results a substantial gap in the density of mode rational surfaces at $r_{\min}$ which impedes the convective transport (Beklemishev and Horton, 1992). In this section we exclude the reversed shear case.

For drift waves the m, n-mode numbers in the dominant $\phi_{m,n}$ amplitudes in representation (35) are large and aligned with the magnetic field to keep

$$k_\parallel^{m,n}\equiv -i\hat{\mathbf{b}}\cdot\nabla\ln\phi_{m,n}=\frac{(m-nq)}{qR} \tag{38}$$

small so that $|k_\parallel c_s|\ll|\omega_*|$ for robust drift waves. Consistent with fluctuation experiments, theory gives $k_y\rho_s\gtrsim 0.2$ constant so that $m=k_y r\sim r/\rho_s\gg 1$. The variation of $B=B_0(1+r\cos\theta/R)^{-1}$ with θ couples large numbers of m components in Eq. (35) to form the toroidal eigenmode. To satisfy the conditions of 2π periodicity in θ and small $k_\parallel$ at high mode numbers, the ballooning mode transformation is introduced by

$$\sum_m \phi_m(r)e^{im\theta}=e^{-inq\theta_0}\sum_{\ell=-\infty}^{+\infty}\phi(\theta-2\pi\ell,\theta_0)^{inq(r)(\theta-2\pi\ell)}, \tag{39}$$

where the infinite sum of 2π-displaced localized modes $\phi(\theta)$ creates the required periodic function. The free parameter θ_0 is the Floquet exponent of the wave function

and determines the radial orientation of the convective cells. More globally, $q\theta_0$ should be thought of as an approximation to the eikonal $\int \theta_k dq$ (Dewar and Glasser, 1983).

When the drift modes are strongly localized to the outside of the torus $\phi(\eta,\theta_0)\simeq e^{-\sigma\eta^2/2}$ with $\sigma>1$, then one term, $\ell=0$, in the sum over ℓ in Eq. (39) is sufficient. Such modes ($\sigma>1$) are called "ballooning modes" because they are strongly localized to the outside of the torus. The drift waves tend to localize to the outside of the torus both due to the unfavorable curvature of the magnetic field lines with respect to the interchange instability and due to the resonant interaction with the particles trapped by the minimum of the $B(\theta)$ field. Defining the local radial wave number $k_r=-i\partial_r\phi/\phi$, we obtain from Eq. (39) assuming $\ell=0$ and $n\gg 1$ that

$$k_r=nq'(\theta-\theta_0)=k_\theta s(\theta-\theta_0), \tag{40}$$

where s is the magnetic shear parameter in Eq. (37) and $k_\theta=nq/r$.

Viewed as a function of radius r [or equivalently q for monotonic $q(r)$ profiles] the wave function (39) is of the form of a Bloch function for an electron in a crystal: here the translational symmetry is $q\to q+1/n$ with $\phi\to e^{i(\theta-\theta_0)}\phi$ defines the Floquet exponent. The local translational invariance of the $k_\parallel^2c_s^2/\omega^2$ potential [see Eq. (44)] gives rise to a periodic structure in the radial wave number $k_x=nq'(\theta-\theta_0)+2\pi\ell(nq')$ [cf. Eq. (40) for $\ell=0$]. The ballooning theory can also be approached via a radial Fourier transform in which θ_0 takes on the role of the independent variable just as in quantum mechanics where the position and momentum exchange roles in the momentum representation. In either case of the direct r-space representation (Choi and Horton, 1980) or the "momentum space" representation, the theory leads to a Schrödinger-like equation for the global radial dependence of the toroidal drift waves, with the radial width of the mode given by $\Delta r=(\rho_sL)^{1/2}$ where L is scale length associated with $\omega_*(r)$ variation.

With the representations (35) it is straightforward to solve Eq. (33) to obtain the fluctuating parallel ion fluid velocity

$$\tilde{u}_\parallel=\frac{e_i}{m_i}\frac{\left(k_\parallel+\dfrac{k_\theta}{\omega_{ci}}\dfrac{du_\parallel}{dr}\right)}{\omega-k_\parallel u_\parallel-k_\theta u_\theta}\phi_{m,n}(r), \tag{41}$$

where $k_\theta=m/r$ and $k_\parallel(r)=[m-nq(r)]/qR$. For a spectrum of m, n modes there is a set of mode rational surfaces $r_{m,n}$ where the $nq(r_{m,n})=m$. For those surfaces the pitch of the magnetic field matches the twist of the perturbation so that $k_\parallel=0$. Expanding around this resonant layer gives

$$k_\parallel=\frac{k_\theta x}{L_s} \tag{42}$$

with $x=r-r_{m,n}$ and the magnetic shear length L_s given by

$$\frac{1}{L_s}=\frac{s}{qR}. \tag{43}$$

Expansion (42) must be extended to higher order in the region of shear reversal ($s=0$) where the curvature $L_q^{-1}=r_mq''(r_m)/q_m$ at $r=r_m$ the maximum or minimum of q is required to determine $k_\parallel(r)$.

Now linearizing Eq. (32) and using Eq. (41) (with $u_\parallel'=0$) gives the standard drift-wave equation

$$\frac{\rho_s^2}{r}\frac{\partial}{\partial r}\left(rN(r)\frac{\partial\phi}{\partial r}\right)+N(r)\left[\frac{\omega_*(r)}{\tilde{\omega}}-1+i\delta_k-k_y^2\rho_s^2+\frac{k_\parallel^2(r)c_s^2}{\tilde{\omega}^2}\right]\phi=0, \tag{44}$$

where $\tilde{\omega}=\omega-\mathbf{k}\cdot\mathbf{u}$ is the frequency in the Lagrangian rest frame of the plasma and

$$\omega_*(r)=-\left(\frac{ck_yT_e}{eBN}\right)\left(\frac{dN}{dr}\right)=k_yv_{de}$$

is the long-wavelength drift-wave frequency as derived in Sec. I.C. The key point of Eq. (44) is that for generic profiles the increase of the ion acoustic wave term $k_\parallel^2=k_y^2x^2/L_s^2$ with distance x from the rational surface is so rapid that the modes are localized to the distance $\Delta x=\rho_s(L_s/L_n)^{1/2}$ of the rational surfaces $r=r_{m,n}$ where $x=0$. While the precise formula for the localized modes is derived below this mode width Δx follows from the requirement that $\rho_s^2\partial_x^2\cong\rho_s^2/\Delta x^2$ must balance the term $k_\parallel^2c_s^2/\omega^2\cong k_y^2c_s^2\Delta x^2/\omega^2$ from the ion acoustic waves. For large L_n/ρ_s values there is a high density of the neighboring $k_\parallel(r)=0$ rational surfaces $r=r_{m,n}$ with the spacing $\delta r_n=r_{m+1,n}-r_{m,n}=1/nq'\sim\rho_s[1/(k_y\rho_s)s]$ for fixed $k_y\rho_s$ and s. When $\delta r_n\ll L_n,L_s$ then there is a degeneracy with all neighboring m values satisfying the same local eigenmode equation

$$\left[\rho_s^2\partial_x^2+\left(\lambda(\omega)+\frac{c_s^2k_y^2x^2}{\omega^2L_s^2}\right)\right]\phi=0, \tag{45}$$

where $\lambda=\omega_*/\omega-1-k_y^2\rho_s^2+i\delta_k$. Furthermore, the form of the local drift-wave Eq. (45) is exactly that of the quantum harmonic oscillator except for the unusual feature of a negative spring constant. Pearlstein and Berk (1969) explain the meaning of this feature and show that with the *outgoing radiation* of wave energy boundary conditions

$$\lim_{x^2\to\infty}\rho_s\partial_x\phi=-i\frac{c_s|k_\parallel'|x}{\omega}\phi$$

the solutions of Eq. (45) are localized for $\mathrm{Im}(\omega)>0$. The eigenmodes of the single-helicity system with the outgoing wave boundary condition are

$$\phi_\ell(x)=H_\ell(\sigma x)e^{-\sigma x^2/2} \tag{46}$$

with the ℓth radial eigenvalue given by

$$\lambda_k(\omega)=\frac{\omega_*}{\omega}-1-k_y^2\rho_s^2+i\,\delta_k=i\,\frac{L_n}{L_s}(2\ell+1)\,\frac{|\omega_*|}{\omega}. \tag{47}$$

Thus the outgoing flux of wave energy appears as a magnetic shear $S=L_n/L_s=L_n s/qR$ induced damping of the radial eigenmodes with the complex eigenvalues given by

$$\omega_\ell=\frac{\omega_*[1-i(2\ell+1)S]}{1+k_y^2\rho_s^2-i\,\delta_k}. \tag{48}$$

These basic single helicity localized eigenmodes (46) and eigenvalues (48) have formed the basis for many linear and nonlinear calculations in drift-wave problems. Since the properties of the Hermite eigenfunctions are relatively simple, first- and second-order perturbations theory calculations have been carried out to determine the effects of sheared mass flows, the parallel electron current and nonlinear mode coupling terms with these basis functions. Rewoldt *et al.* (1982, 1987) have built a general toroidal eigenvalue code using functions (46) as the basis functions for the dependence of the modes on the ballooning coordinate along the field line. Cheng and Tsang (1981) report the ballooning mode structure for the ion temperature gradient-driven modes and the toroidicity-induced modes.

IV. ION TEMPERATURE GRADIENT-DRIVEN DRIFT WAVES

A. Kinetic electrostatic ITG modes

The electrostatic kinetic dispersion relation $D_{\mathbf{k},\omega}$ for multiple charge particle species $j=e,i,z,\ldots$ distributed according to local Maxwell-Boltzmann (MB) distribution is given by

$$D_{ES}(\mathbf{k},\omega)=\sum_j\frac{n_j e_j^2}{T_j}\left[1-\left\langle\frac{\omega-\omega_{*j}(\epsilon)}{\omega-\omega_{D_j}-k_\parallel v_\parallel}J_0^2\right\rangle_{M-B}\right], \tag{49}$$

where the density and temperature gradients enter through

$$\omega_{*j}=\frac{k_y c T_j}{e_j n_j B}\frac{dn_j}{dr}\left[1+\eta_j\left(\epsilon-\frac{3}{2}\right)\right] \tag{50}$$

with $\epsilon=m_j v^2/2T_j$ the dimensionless energy variable in the average $\langle A\rangle_{M-B}=\int d^3v\,F_{MB}(\epsilon)A(\mathbf{v})$ where $F_{MB}(\epsilon)=2(\epsilon/\pi)^{1/2}\exp(-\epsilon)$. The wave particle resonance is determined by the resonant denominator $\omega-k_\parallel v_\parallel=\omega_{D_j}$ where the guiding center drift frequency

$$\omega_{D_j}=\frac{k_y c T_j}{eBR}\left(\frac{m_j v_\perp^2}{2T_j}+\frac{m_j v_\parallel^2}{T_j}\right) \tag{51}$$

increases with $v_\perp^2$ and $v_\parallel^2$. The Bessel function $J_0=J_0(k_\perp v_\perp/\Omega_j)$ in Eq. (49) gives the Larmor radius $\rho_j=v_\perp/\Omega_j$ averaging of the electric potential $\phi_k e^{i\mathbf{k}\cdot\mathbf{x}}$ during the fast cyclotron motion $\Omega_j\gg\omega$, ω_{Dj}, $k_\parallel v_j$.

The temperature gradients η_j in Eqs. (49) and (50) give rise to a new unstable drift wave from $D_{es}(\mathbf{k},\omega)=0$ called the eta-i (or the eta-e) mode. The early work by Coppi *et al.* (1967) on the eta-i mode showed the essentially fluid character of the instabilities. In toroidal geometry ($\omega_{Dj}\neq 0$) the mode shares features of the two-dimensional incompressible Rayleigh-Bénard convection (Horton *et al.*, 1981; Hu and Horton, 1997).

For many laboratory experiments it is essential to keep the low-Z impurities in the dispersion relation (Jarmén and Fröjdh, 1993; Dong *et al.*, 1994). In particular, the high power neutral beams used to heat the tokamak produce substantial carbon components from the graphite tiles used as thermal shielding of the metallic walls. Typical high-power experiments have the carbon charge fraction $f_z=Zn_z/n_e=6n_z/n_e\sim\frac{1}{2}$ so that $Z_{\rm eff}=3$. In such hydrogen-carbon plasmas the stability changes with the sign of the carbon density gradient relative to the hydrogen density gradient. For radially decreasing carbon gradient the ITG has a higher critical temperature gradient for instability. For reversed carbon gradient ($\omega_{*i}\omega_{*c}<0$) there is an unstable impurity drift mode producing an inward convection of the carbon and outward flux of hydrogen (Tang *et al.*, 1980). This reversed gradient impurity mode is obviously of considerable concern. The impurity mode brings with it a scaling on the ion mass of the working gas that provides a partial explanation for the mysterious isotope scaling effects seen in tokamak confinement. Lee and Santoro (1997) show how an isotope effect arises from the two-ion component drift-wave transport. The sheared mass flows produced by neutral beam injection can reverse the carbon influx (Fu *et al.*, 1997) to be outward and also introduce a reduction of transport with ion mass due to the scaling of the shear flow velocity effect with $\rho_*\propto m_i^{1/2}$.

B. Wave particle power transfer and the Nyquist diagram

The physical meaning of $\mathrm{Im}\,D_{\mathbf{k}}(\omega,\mu)$ can be understood by calculating the space-time averaged power transfer $\langle\mathbf{j}\cdot\mathbf{E}\rangle$ between the fluctuations $\mathbf{E}=-i\mathbf{k}\phi_{\mathbf{k}\omega}$ and the particles. Using charge conservation $\mathbf{k}\cdot\mathbf{j}=\omega\rho_q(\mathbf{k},\omega)$ and that $\rho_q(\mathbf{k},\omega)=-\Sigma_j(n_j e_j^2/T_j)(1-P_j)\phi_{\mathbf{k}}\equiv -D_{\mathbf{k}}(\omega)\phi_{\mathbf{k}}$ defined through Eq. (49), we reduce the power transfer to

$$\langle\mathbf{j}\cdot\mathbf{E}\rangle=\mathrm{Re}\langle\phi_{*\mathbf{k},\omega}i\mathbf{k}\cdot\mathbf{j}\rangle=\omega\,\mathrm{Im}\,D_{\mathbf{k}}(\omega,\mu)|\phi_{\mathbf{k}}|^2, \tag{52}$$

showing that for $\omega\,\mathrm{Im}\,D_{\mathbf{k}}<0$ there is energy transfer from the particles to the waves. The dispersion relation $D_{\mathbf{k}}(\omega)$ depends on a set of dimensionless system parameters (τ,η_i,ϵ_n), designated by μ in Eq. (52).

Let us examine the transfer rate $\omega\,\mathrm{Im}\,D_{\mathbf{k}}$ in more detail, looking for the critical temperature gradient η_c at which the transfer changes from positive to negative, signifying instability. The dissipation arises from the residue of the pole from the wave-particle propagator $(\omega-\mathbf{k}\cdot\mathbf{v}+i\nu)^{-1}$ that in the collisionless, long-time limit is given by $-i\pi\delta(\omega-\mathbf{k}\cdot\mathbf{v})$. Thus, the wave-particle energy transfer rate from Eq. (52) using Eq. (49) is controlled by

$$\omega \operatorname{Im} D_{\mathbf{k}}(\omega)=\frac{n_i e_i^2}{T_i}\int \frac{d^3v\, e^{-m_i v^2/2T_i}}{(2\pi T_i)^{3/2}} J_0^2\left(\frac{k_\perp v_\perp}{D_i}\right) \times \omega\left\{\omega-\omega_{*i}\left[1+\eta_i\left(\frac{m_i v^2}{2T_i}-\frac{3}{2}\right)\right]\right\} \times \pi\delta\left[\omega-\omega_{Di}\left(\frac{m_i v_i^2}{2T_i}+\frac{m_i v_\parallel^2}{2T_i}\right)-k_\parallel v_\parallel\right] \tag{53}$$

for a single ion species. The positive definite ω^2-term in Eq. (53) is the Landau damping of the uniform plasma existing in the limit $\omega_{*i}\to 0$. The term $\omega\omega_{*i}$ gives the destabilizing transfer for $\omega\omega_{*i}>0$.

A necessary condition for instability is $\omega \operatorname{Im} D_{\mathbf{k}}<0$ which from Eq. (53) occurs from the ion wave resonance for waves in the frequency interval

$$0<\omega<\omega_{*i}(1+\eta_i). \tag{54}$$

Evidently, only the special limit $\eta_i=0$ is simple where $\omega \operatorname{Im} D_{\mathbf{k}}(\omega)=\omega(\omega-\omega_{*i})d_{\mathbf{k}}$ with $d_{\mathbf{k}}>0$. The Nyquist analysis below will show that this limit is stable and that the minimum value of η_i for instability is $\eta_c=\frac{2}{3}$ in the case of adiabatic behavior of all other species.

Stability analysis of dispersion relations is performed by the Nyquist diagram technique (Schmidt, 1979) shown in Fig. 10. Since the semicircle in the upper half ω plane maps to $D(\mathbf{k},\omega)\to D_a>0$ where $D_a(\mathbf{k})$ is the adiabatic response, the critical condition for there to be an unstable mode of $D(\mathbf{k},\omega)=0$ is that $\operatorname{Re} D(\mathbf{k},\omega_m)<0$ where ω_m is the marginal stability frequency at which $\operatorname{Im} D(\mathbf{k},\omega_m)=0$. The condition $\operatorname{Re} D(\mathbf{k},\omega_m,\mu)=0$ determines the marginal stability subspace. The details of the Nyquist analysis for the condition of marginal stability are found in Romanelli (1989), Hong *et al.* (1989), Nordman and Weiland (1989, 1990), and Kim *et al.* (1994). Here we give some of the more interesting details and more important results.

The ion resonance with fluctuations at $\mathbf{k}\omega$ occurs on an ellipse in $v_\parallel - v_\perp$ space with the center at $v_\parallel = -k_\parallel v_T^2/2\omega_D$. The resonant ellipse is given by

$$\left(v_\parallel+\frac{k_\parallel v_T^2}{2\omega_D}\right)^2+\frac{1}{2}v_\perp^2=\frac{\omega}{\omega_{Di}}+\frac{k_\parallel^2 v_T^2}{2\omega_{Di}^2}. \tag{55}$$

The velocity space diagram of the resonant ions is shown in Fig. 11. These features are found in the simulation results (Dimits *et al.*, 1996). Thus only fluctuation frequencies satisfying $\omega>\omega_{br}(k_\parallel,k_\perp)$ where

$$\omega_{br}(k_\parallel,k_\perp)=-\frac{k_\parallel^2 v_T^2}{2\omega_{Di}} \tag{56}$$

are resonant with some ions—namely those ions on the ellipse (55). As the frequency ω approaches $\omega_{br}(\mathbf{k})$ the fractional number $r(\omega)$ of resonant ions vanishes as $r(\omega)\sim(\omega-\omega_{br})^{1/2}$. For frequencies $\omega\gg\omega_{br},\omega_{Di}$ the resonant fraction decays exponentially as $\exp(-\omega/\omega_{Di})$. At the low-frequency end of the toroidal plasma response, the branch point at $\omega=\omega_{\mathrm{br}}$ in the response function $1/D_{\mathbf{k}}(\omega)$ gives rise to long-time correlations in the decay of disturbances. The phase mixing decay of the ballistic response to an initial disturbance δN_0 decays in x space as

$$\delta n_i=\delta N_0\left(\frac{t_*}{t}\right)^{3/2}\cos(\omega_{br}t)$$

for the toroidal system as opposed to the exponential decay $\exp(-k_\parallel^2 v_T^2 t^2)$ for correlations in the slab geometry. This slow phase mixing from the branch point behavior of the collective dynamics makes the toroidal ITG modes for $\eta<\eta_c$ purely oscillatory at $\omega\sim\omega_{Di}$ rather than the continuous transition $\gamma=\gamma'(\eta-\eta_c)$ from growth to damping as η varies through η_c. The details of how the complex $\omega(\eta-\eta_c)$ function behaves is worked out in Kim *et al.* (1994). The behavior of $\omega_k(\eta-\eta_c)$ depends on the parameter $X_k\equiv k_\parallel v_T/|\omega_{Di}|$ and $\epsilon_n=L_n/R$. The $\eta_i-\epsilon_n$ (temperature gradient versus

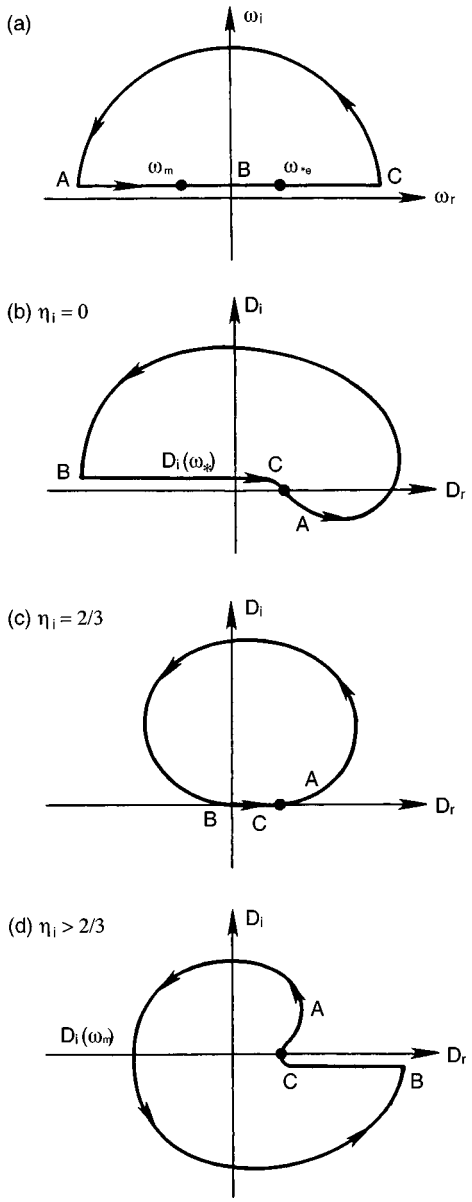

FIG. 10. Nyquist diagram for the ion temperature gradient threshold in the kinetic relation.

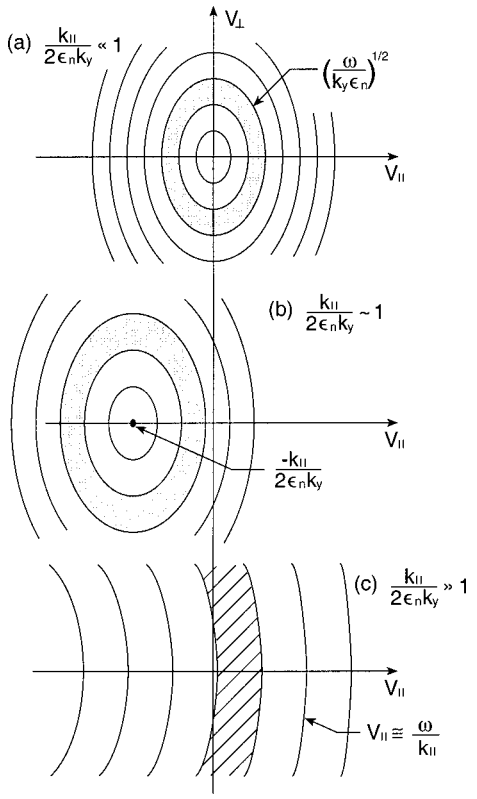

FIG. 11. The band of resonant ion velocities for a given drift-wave fluctuation $(\omega, k_y, k_\parallel)$. (a) the ideal delta function resonance curve from Kim, Horton, *et al.* (1992), (b) the shifted contours of resonant δf, and (c) the slab Landau resonance.

toroidicity) plane divides into three domains; (i) exponentially growing $\eta_i > \eta_c(\epsilon_n, X_k)$, (ii) purely oscillatory $\eta_i < \eta_c(\epsilon_n, X_k)$ and $2\epsilon_n(1+T_i/T_e)(1+b_i)<1$, and (iii) exponentially decaying modes $\eta_i < \eta_c(\epsilon_n, X_k)$ and $2\epsilon_n(1+T_i/T_e)(1+b_i)>1$. For $X_k \to 0$ the minimum critical temperature gradient is $\eta_c = \frac{2}{3}$.

While exact results require numerical evaluation of $D(\mathbf{k}, \omega, \mu)$, there is a useful approximation for obtaining reasonably accurate analytic formulas for the limit $X_k = k_\parallel v_T/\omega_{Di} \to 0$ where the ellipse in Eq. (55) is centered at the origin. If the resonant ellipse is approximated as a circle by taking $1/2 v_\perp^2 + v_\parallel^2 \to 2v^2/3$ then the delta function allows one to obtain an analytic formula for $D(\mathbf{k}, \omega)$ (Romanelli, 1989). The result is that the marginal stability frequency is

$$\omega_m = \frac{\omega_D(\eta_i - 2/3)}{(\eta_i - 4\epsilon_n/3)}. \tag{57}$$

The Nyquist condition for the onset of the unstable root becomes

$$D_k(\omega_m) = 1 + \frac{T_i}{T_e} - \frac{3\eta_i}{4\epsilon_n(1+b_i)} < 0, \tag{58}$$

where we use $\langle J_0^2 \rangle \simeq 1/(1+b_i)$ for $b_i < 2$. Thus, the analytic threshold formula is

$$\eta_c = \frac{4\epsilon_n}{3}\left(1 + \frac{T_i}{T_e}\right)(1+b_i), \tag{59}$$

giving the Romanelli toroidal threshold condition (1989) on $\mu_{i,\mathrm{crit}} = R/L_{Ti}$

$$\frac{R}{L_{Ti}} > \frac{4}{3}\left(1 + \frac{T_i}{T_e}\right) \tag{60}$$

for $b_i = k_y^2 \rho_i^2 \ll 1$ modes. Condition (60) applies when $\omega_m/\omega_{Di} > 0$ ($\eta_i > \frac{2}{3}$) so that there are resonant ions. For small toroidicity, $\epsilon_n \to 0$, there are still marginal ITG modes but they are nonresonant. The marginal condition obtained from the analytic model is then

$$\eta_c = 1 - \frac{2\epsilon_n}{3}\left(1 + \frac{T_i}{T_e}\right)(1+b_i) \tag{61}$$

for $2\epsilon_n(1+T_i/T_e)(1+b_i) \leqslant 1$. At $2\epsilon_n(1+T_i/T_e)(1+b_i) = 1$ the conditions (60) and (61) give $\eta_i > \eta_c = \frac{2}{3}$ for instability. For $X_k = k_\parallel v_{Ti}/\omega_{Di} \neq 0$ there is a low-k_y cutoff to the growth rate given approximately by $(k_\parallel L_n)_{\min} = 0.1 k_y \rho_s$. Thus unstable fluctuations that mode couple to higher $k_\parallel$ modes with $k_\parallel L_n > 0.1 k_y \rho_s$ are limited in amplitude by the associated damping. The result is to produce a peak in the fluctuations spectrum at low k_y within the sector $k_\parallel L_n/k_y\rho_s \leqslant 0.1-0.2$ rate $\gamma(k_\parallel L_n, k_y \rho_s) < 0$. The q dependence of transport enters through $k_n = 1/qR$ in tokamaks.

The transition from the ∇B-curvature drift resonance to the slab drive at $\epsilon_n \sim L_n/R_c = k_\parallel/2|k_y|$ has been observed in a linear mirror geometry representation of the toroidal ITG instability in the same machine used to investigate the slab ITG as discussed in Sec. II. In a mirror system Eq. (51) applies with $1/R = d^2 r(z)/dz^2 = r_p/L_c^2$, where $r(z) = r_0[B_0/B(z)]^{1/2}$ is radial position of a magnetic field line, and $B(z)$ is axial variation of B over the mirror cell length L_c. By varying L_c, Chen and Sen (1995) find the transition from the slab to the equivalent toroidal ITG mode in the three-meter Columbia Linear Machine. The plasma has a variable $\eta_{i\perp}(r)$ and $\eta_{i\parallel}(r)$ with $\rho_* \cong 1/15$. The transition is found to occur at $\epsilon_n \simeq k_\parallel/2|k_y| \simeq 10^{-2}$. Furthermore, the nonlinear amplitude is confirmed to vary as $e\tilde{\phi}/T_e \sim \gamma/|\omega_*| \sim \epsilon_n^{1/2} \propto 1/L_c$ by varying the mirror cell length. The instability occurs as a quasicoherent $m = 2$, 20 kHz oscillation propagating in the ion diamagnetic direction in the plasma rest frame. In the transition from the slab to the ∇B-curvature drift-driven instability the axial wave function becomes flutelike (small $k_\parallel$) in agreement with theory.

C. Scaling laws of the ion temperature gradient turbulent transport

The most important instability with respect to the limits on the ion thermal confinement for nuclear fusion is the ion temperature gradient (ITG) instability. This drift-wave instability goes by both the name ITG and the eta-i ($\eta_i \equiv L_n/L_{T_i}$) mode due to the key dimensionless parameter η_i that measures the strength of the ion temperature gradient. For a specific toroidal machine with major radius R it is advantageous to use the gradient parameter $\mu_i = R/L_{T_i}$ (and its reciprocal ϵ_{T_i}

$=L_{T_i}/R$) since, unlike L_n, the major radius R is fixed. In certain regimes there is a well-defined critical value $\eta_{i,\mathrm{crit}}$, starting at the minimum of $\frac{2}{3}$, above which there is a strong drift-wave instability producing anomalous ion thermal flux q_i. In the classical ITG mode instability the electron dynamics is adiabatic Eq. (12) so that $\Gamma_e=\langle\tilde{n}_e\tilde{v}_x\rangle=0$. From the quasineutrality of the fluctuation it follows that $\Sigma_i Z_i\Gamma_i=0$. Thus, two important cases follow: (1) for the pure hydrodynamic plasma $\Gamma_i=\Gamma_e=0$, and (2) for the carbon-hydrogen plasma $\Gamma_c=-\Gamma_i/6\simeq -D_{\mathrm{dw}}dn_c/dr$ and $\Gamma_e=0$. In general the critical value $\eta_{i,\mathrm{crit}}$ of the temperature gradient is a complicated function of the system stability parameters. Certain simple classical models give well-known simple $\eta_{i,\mathrm{crit}}$ formulas; these formulas (59)–(61), can serve as a guide to the stability threshold.

First studies of the ITG turbulent transport were naturally concerned with regimes where the mode growth per wave period $\gamma_{\mathbf{k}}^{\max}/\omega_{\mathbf{k}}$ is substantial ($\geqslant 0.1$). The $\gamma_k^{\max}$ occurs approximately at the wave numbers $k_y\rho_i\simeq(1+\eta_i)^{-1/2}\ll 1$. In this regime the mixing scale length for an isotropic spectrum ($\lambda_x\simeq\lambda_y$) of fluctuations gives $\chi_i\sim\lambda_\perp^2\gamma_{\max}\simeq(\rho_i/L_{T_i})(cT_e/eB)g(\eta_i,s,q,\epsilon_n)$ at fluctuation levels $\tilde{n}/n=e\tilde{\phi}/T_e\simeq\rho_s/L_{T_i}$. Parameters for such a regime are $\eta_i=3$, $S=L_n/L_s=0.1$, $\tau=T_e/T_i=1$ as in the three-dimensional (3D) FLR fluid simulation (Horton *et al.*, 1980; Hamaguchi and Horton, 1990), and the gyrofluid simulation (Hammett *et al.*, 1992; Waltz *et al.*, 1994; Beer *et al.*, 1995; Beer and Hammett, 1996; Beer *et al.*, 1997).

In this regime away from marginal stability the Vlasov-Poisson kinetic theory (49) has a well-defined asymptotic fluid expansion ($k_\perp\rho_i\ll 1$, $k_\parallel v_i/\omega\ll 1$) in which the linear dispersion relation agrees with that obtained from the two-component FLR-hydrodynamic equations. Thus, many properties of the ITG turbulence have been established based on simulations performed on the two-component (separate ion and electron fluids moments for $n_j,\mathbf{u}_j,p_j,\boldsymbol{\pi}_j,\mathbf{q}_j$) FLR-hydrodynamic equations reduced appropriately for drift waves. The reduced hydrodynamic equations have a clear mathematical structure making the definition of energy, enstrophy, and potential vorticity straightforward. Even exact isolated solitary vortices have been found for the ITG models (Hong, Romanelli, Ottaviani, 1991). Such exact solitary vortices reveal the important nonlinear self-focusing features of the drift-wave turbulence and provide powerful checks on both the numerical simulation procedures and the nonlinear theories.

Within the framework of two-component FLR equations many numerical simulations have reported formulas for the scaling laws of the effective ion thermal diffusivity χ_i defined by the thermal flux $q_i=-n_i\chi_i dT_i/dr$ (some authors insert a factor of $\frac{3}{2}$ in this definition). The simulations include diagnostics for the momentum fluxes $\Pi_{x,\perp}=m_in_i\langle\tilde{v}_x\tilde{v}_E\rangle$ and $\Pi_{x,\parallel}=m_in_i\langle\tilde{v}_x\tilde{v}_\parallel\rangle$ driven by both η_i and the sheared velocity flows $d\overline{v_E}/dx$ and $d\overline{v_\parallel}/dx$. In this section we first review simulations where shear flow effects were excluded. Biglari *et al.* (1990), Artun and Tang (1992), Artun *et al.* (1995), Dong and Horton (1993), Parker *et al.* (1996), and Hahm and Burrell (1995, 1996) analyze models and simulations with shear flow effects.

The 3D-slab model simulations (Horton *et al.*, 1980; Hamaguchi and Horton, 1990; Parker *et al.*, 1994) show ion thermal diffusivity of the form

$$\chi_i^{\mathrm{slab}}=0.3\left(\frac{L_s}{L_n}\right)^{1/2}\frac{\rho_s}{L_n}\frac{cT_e}{eB}(\eta_i-\eta_c)^{1/2} \tag{62}$$

for $S=L_n/L_s>S_1=0.05$ and η_i not close to η_c. For small shear $S<S_1$ the scaling $S^{-1/2}$ is too strong and the parametrization with S is given as $\exp(-S/S_0)$ in Hamaguchi and Horton (1990) and as $q/(S+S_0)$ in Kotschenreuther *et al.* (1995) and Waltz *et al.* (1994). When the turbulence level is high, we expect S_0 independent of ρ_*: for low-turbulence levels S_0 is proportional to ρ_*. Near the critical gradient the exponent on $\eta_i-\eta_c$ in Eq. (62) becomes unity. In an experiment by Sang, Sen, and Tham (1993) in the Columbia Linear Machine on the slab ITG mode this latter linear scaling has been confirmed. The supporting bifurcation analysis is found in Hamaguchi and Horton (1990). Hahm and Tang (1989) give the threshold for the sheared slab as

$$\eta_c=\eta_{\mathrm{KP}}+1.9\left(1+\frac{T_i}{T_e}\right)\frac{L_n}{L_s}$$

where η_{KP} is the local kinetic threshold from Kadomtsev and Pogutse (1970).

For the regime of $\eta_i\gg 1$ the density gradient parameter L_n drops out of the system, and the parametrization of the 3D simulations gives $\chi_i=0.8(\rho_s/L_T)(cT_i/eB)g(q,s,T_i/T_e)$. This is called the flat density regime where $\eta_i\gtrsim 3$–4.

In the slab model $\chi=\chi_i(S,\eta_i,\tau)$. In the toroidal model the two additional parameters are $\epsilon_n=L_n/R$ (or equivalently $\epsilon_T=L_T/R=\epsilon_n/\eta_i$) and q (the slab shear parameter $S=L_n/L_s$ is often expressed in toroidal geometry by $s=rq'/q$ using the relation $S=s\epsilon_n/q$). The instability in the toroidal system changes character from that in the slab system. In the slab the negative compressibility due to $E_\parallel+\nabla_\parallel\delta p_i/en_i=-ik_\parallel(1-\omega_{*p_i}/\omega)\phi_{\mathbf{k},\omega}$ transforms the ion acoustic oscillations in Eq. (27) into unstable compressional waves for $0<\omega<\omega_{*p_i}$. In the toroidal system a cross-field interchange of plasma takes place by electric field arising from the charge separation from the ∇B-curvature drift velocities with $\omega^2\cong-\omega_{*_i}\omega_{Di}/(1+k_\perp^2\rho_s^2)>k_\parallel^2c_s^2(1-\omega_{*p_i}/\omega)$. Different $\mathbf{k}$ vectors describe fluctuations that are driven by the slab and the interchange mechanism. It is the eigenmode problem (Rewoldt and Tang, 1990) that determines how the plasma adjusts through the self-consistent field dynamics to the two driving mechanisms and the sheared toroidal magnetic field to obtain the fastest release of thermal energy stored in the pressure gradient. A major advance in understanding followed from both the FLR-hydrodynamic simulations and the drift-kinetic particle simulations was to make clear the large increase

in the strength of the turbulence and the anomalous ion transport when the toroidal geometry was fully included in the simulations. Thus the charge separation from the unfavorable ∇B and curvature guiding drifts produces electric fields that are a major energy release mechanism for the "free energy" stored in the density and temperature gradients in the confined plasma.

In the toroidal regime the earliest ion thermal diffusivity formula, which still forms the basis for interpreting simulations, is the ITG formula given by Horton, Choi, and Tang (1981):

$$\chi_i^{\mathrm{ITG}} = c_1 \frac{q\rho_s}{sL_n}\frac{cT_e}{eB}[2\epsilon_n(\eta_i-\eta_c)]^{1/2} \tag{63}$$

with c_1 of order unity. Owing to the factor of q, the confinement is inversely proportional to the product of self-field $B_p \approx I_p/a$ and the external toroidal field $B \cong B_\phi$. The peak of the growth rate driving the turbulence is at $k_y = \rho_s^{-1}[1/(1+\eta_i)]^{1/2}$. Near this wave number the phase velocity ω_k/k_y is changing from the electron direction for smaller $k_y\rho_s$ to the ion direction at larger $k_y\rho_s$. Thus there is a critical wave number where the phase of the wave is stationary in the plasma rest frame and the mode grows exponentially at the interchange growth time $\tau = (RL_{T_i})^{1/2}/c_s$ which is of order a few microseconds.

The critical gradient formula η_c has been given in numerous limits (Romanelli, 1989; Hong *et al.*, 1991; Tang *et al.*, 1986; Kim and Horton, 1991; Kim *et al.*, 1994; Kotschenreuther *et al.*, 1995). For systems close to marginal stability the amplitudes and fluxes can be, in principle, calculated by a systematic bifurcation analysis. The structure of the bifurcation theory shows that near marginal stability the thermal flux increases linearly (the exponent on $\eta_i - \eta_c$ is unity). Turbulence theory applies when many modes are linearly unstable. In the turbulent regime the exponent changes to one half as given in Eqs. (62) and (63). Thus some researchers (Kotschenreuther *et al.*, 1995) use the rule $\min[c_1(\eta_i-\eta_c), c_2(\eta_i-\eta_c)^{1/2}]$ to describe the increase of χ_i with the increase of the temperature gradient. A systematic bifurcation analysis for the thermal flux has only been possible for the slab model where the simple harmonic oscillator [Hermite functions, Eq. (46)] eigenfunction make the calculation feasible (Hamaguchi and Horton, 1990).

For comparison we note that in the absence of the ITG fluctuations ($\eta_i < \eta_c$) the calculation of the ion thermal flux in the torus is still a complicated problem due to the geometry and complex ion orbits. The collisional thermal flux for low collisionality $\nu_{*i} \equiv (\nu_i qR/v_{T_i})(R/r)^{3/2} \leqslant 1$ is from the random walk of the banana orbits formed by the guiding center drifts of the trapped ions. Most large tokamaks ($I > 1$ MA) are in this low-collisionality regime. The collisional thermal flux $q_i = -n_i\chi_i^{\mathrm{neo}} dT_i/dr$ (which is only one diagonal element of a large transport matrix) is given by Chang and Hinton (1982, 1986) and Hirshman and Sigmar (1981). In the small $\epsilon = r/R$ limit the ion thermal diffusivity from collisions is

$$\chi_i^{\mathrm{neo}} = \nu_i\rho_{i\theta}^2[0.66 + 1.88(r/R)^{1/2}](r/R)^{1/2}, \tag{64}$$

where the 0.66 arises from the pitch angle scattering and the 1.88 from energy scattering (Bolton and Ware, 1983). Here $\rho_{i\theta} = q\rho_i/\epsilon$ and the postfactor of $(r/R)^{1/2}$ takes into account that only the trapped and barely passing ions, whose fractional density increases as $(r/R)^{1/2}$, contribute to the χ_i^{neo} in the banana regime. At larger collisionality $(R/r)^{3/2} > \nu_{*i} > 1$ the ion detrapping collision occurs before the banana orbit is formed. This is called the plateau regime where most mid-sized tokamaks (TEXT, ALCATOR JT2FM) operate. The ion thermal diffusivity from collisions in this regime is $\chi_i^{\mathrm{neo}} = 2.6(v_i/qR)(q\rho_i)^2$.

In the fluid moment equations, the cross-field transport fluxes Γ_j, q_j arise from the friction forces associated with flow velocities $u_{\|j}$ and thermal fluxes $q_{\|j}$. The calculations of Hirshman and Sigmar (1981) introduce widely-used parallel viscosities that relate the parallel flows $(u_{\|j}, q_{\|j})$ through coefficients μ_1, μ_2, μ_3 to the surface-averaged parallel stresses from $\langle \mathbf{B}\cdot\nabla\cdot\boldsymbol{\pi}_j\rangle$ and $\langle \mathbf{B}\cdot\nabla\cdot\boldsymbol{\Theta}_j\rangle$. In terms of the ion viscosity coefficients, the thermal diffusivity in Eq. (64) is given by the product $1.469(\mu_{i3} - \mu_{i2}^2/\mu_{i1}) = 0.678(r/R)^{1/2}$. The moment method of analysis has an advantage for the systematic development of multispecies transport theory (Balescu, 1988 and Houlberg *et al.*, 1997).

The theoretical structure of the full transport problem treating the collective drift-wave fluctuations and the collisional interactions on equal footing is given in a series of works by Sugama and Horton (1995a, 1997), for electrostatic turbulence, and Sugama *et al.* (1996) for electromagnetic turbulence. Earlier works attempting this complex problem were Shaing (1988a, 1988b) and Balescu (1990). Both transport processes arise from the Coulomb interactions of the charged particles. The collision operator takes into account the thermal fluctuation levels at Debye length space scales $k\lambda_{De} \gtrsim 1$, while the drift wave takes into account the collective Coulomb interactions on space scales covering many Debye lengths $k\lambda_{De} \ll 1$ (see Sec. I.A).

For many years efforts were made to interpret ion thermal losses with the neoclassical formulas. A thorough review of this effort is given by Scott *et al.* (1994). From the first χ_i formulas in Eqs. (62)–(64) applied to tokamaks it becomes clear that these drift-wave turbulent diffusivities are larger than the neoclassical collisional ion diffusivities. The scaling of the drift-wave diffusivity with $T^{3/2}/B^2L_n$ causes the thermal flux to increase rapidly with increasing temperature in sharp contrast to $\chi_i^{\mathrm{neo}} \propto n/T^{1/2}B_\theta^2$ which decreases.

The turbulent diffusion acts on the temperature and density profiles to cause them to relax back toward marginal stability giving a certain stiffness to the profiles. In the absence of external heating to maintain an excess temperature gradient (η_i or $\mu_i = R/L_{T_i}$) there is a pulse of the turbulent energy $W(t)$ after which the profiles are characterized by

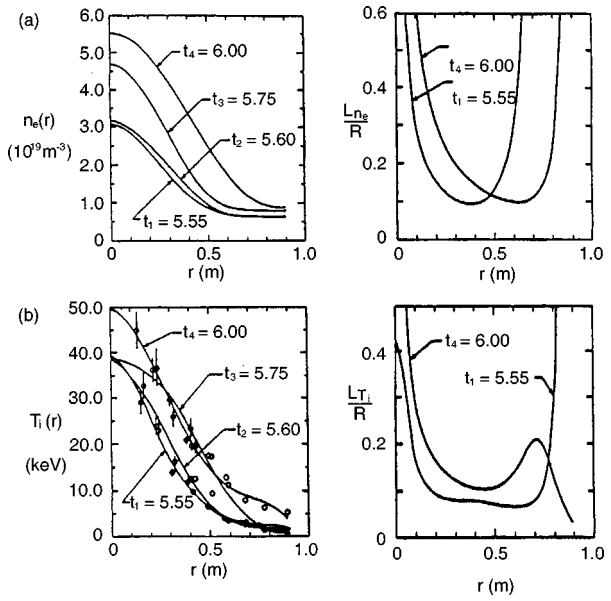

FIG. 12. Evolution of the temperature and density profiles for the JT-60U experiment during the formation of the internal transport barrier at $r/a=0.7$. (a) Smoothed density profiles used to compute the gradient scale lengths at four times during the growth of the core pressure from the internal transport barrier. The insert gives $\epsilon_n = L_n/R$; (b) Ion temperature profiles and the insert shows $\epsilon_{T_i} = L_{T_i}/R$.

$$\mu_i = \frac{-R}{L_{T_i}} \frac{dT_i}{dr} \approx \text{const.} \tag{65}$$

This profile prediction, while it obviously overly simplifies the problem, does correlate with a number of T_i profiles that have a constant $R/L_{T_i} \approx 5$ in the core transport region. Kurki, Suonio, Groebner, and Burrell (1992) successfully analyzed a number of DIII-D discharges on this basis.

The general procedure of predicting the $T_i(r)$ profiles from the energy-momentum deposition profiles for the evolution of the core plasma is carried out with transport codes. An example is shown in Fig. 12 from the IFS/JAERI collaborative analysis of an important discharge (Horton *et al.*, 1997). The normalized gradient scale lengths computed for the JT60-U discharge 17110 is shown in Fig. 12. Here we summarize some features of the analysis. The principal system and plasma parameters for the discharges are given in Table II.

TABLE II. JT-60U high-β_p experiment 17110 with internal transport barrier: Phase I.

R/a	3.1 m/0.7 m
B_ϕ	4.4 T
I_p	2 MA
P_{NBI}	27 MW
$n_D(0)$	$4.1\times10^{19}\,\text{m}^{-3}$
$T_i(0)/T_e(0)$	38 keV/12 keV
$n_D\tau_E T_i$	$1.1\times10^{21}\,\text{m}^{-3}\,\text{s keV}$
$v_\phi(0)$	−100 km/s

An important group of theories called self-organized criticality describe the self-consistent interaction of the turbulence W and the profile gradient $\mu_i(t)$ under the influence of the external heating power $P^{\text{aux}}(r)$. Extending a model proposed by Diamond and Hahm (1995), Newman *et al.* (1996) develop a self-organized critical gradient model for resistive-g turbulence using cellular automata rules for avalanches in sandpiles.

While still under development the self-organized criticality paradigm appears to explain a number of experimental features such as the stiffness, or resiliency, of the temperature profiles (Carreras *et al.*, 1998). A review of progress in self-organized criticality is given by Diamond (1998).

Tajima *et al.* (1994) and Kishimoto, Tajima, Horton, *et al.* (1996) have a simple self-consistent critical gradient model for describing the balance reached by the auxiliary power per ion per unit length $P_i^{\text{aux}}/n_i R$ driving the system away from μ_{crit} balanced by the turbulent diffusivity. The model is given by taking the turbulent thermal diffusivity as

$$\chi = \chi_0 W, \tag{66}$$

where W is the dimensionless turbulence energy density. The turbulence W drives the system toward marginal stability according to the coupled equations for W and μ. The equation for the turbulent energy is

$$\frac{dW}{dt} = 2(\gamma'(\mu) - \gamma^{n\prime} W)W, \tag{67}$$

and the equation for the temperature gradient μ driven by the gradient of external heating is

$$\frac{d\mu}{dt} = -(\chi_i^{\text{neo}} + \chi_0 W)\mu - R\frac{d}{dr}\left(\frac{P^{\text{aux}}}{n_i R}\right)$$

driving the system away from $\mu = \mu_{\text{crit}}$. In Eq. (67) the dependence of the linear growth rate on the temperature gradient is $\gamma' = \gamma_0(\mu - \mu_{\text{crit}})$. The degree to which μ exceeds μ_{crit} is then determined by the strength of $d(P^{\text{aux}}/n)/dr$ compared with $\chi_i dT_i/dr$. At each radius there is a stable fixed point in the (W,μ) plane parameterized by γ_0, $\gamma^{n\prime}$, χ_i^{neo}, χ_0 and $-Rd(P^{\text{aux}}/nR)/dr \simeq P/na$. The theory is straightforward and leads to simple, exact formulas for the increase of the temperature gradient $\mu_i - \mu_c = g(P) \propto P^{1/2}$ and the turbulence level $W = h(P) \propto P^{1/2}$ with auxiliary heating power P. This increase of W and hence χ_i by Eq. (66) gives the L-mode global confinement time scaling:

$$\tau_E = \frac{L_T^2}{\chi_i} = n^\alpha I_p^\beta a^\gamma R^\delta B^\epsilon P^{-1/2} \tag{68}$$

with exponents close to those of the empirical confinement laws. Earlier ITG and trapped electron work lead to related scalings by calculating the increase of the temperature $T = T(P^{\text{aux}})$ from the thermal balance equation $\chi_i n_i T/L_T^2 \cong P_i^{\text{aux}}$, without taking into account the marginal stability consideration, gives $\alpha = 0.6$, $\beta = 0$, $\gamma = 2.7$, $\delta = 0.3$, $\epsilon = 0.8$. These formulas explain the general features of L-mode scaling of ITER89-P (Yushmanov, 1990) scaling but give too weak a dependence on the

plasma current I_p, and too strong a dependence on the toroidal magnetic field B. The ITER89 L-mode law has $\alpha=0.1$, $\beta=0.85$, $\gamma=0.2$, $\delta=1.2$, $\epsilon=0.2$. Close agreement with the ITER89-P empirical formula exponents is obtained by using the Bohmlike formula (Taroni *et al.*, 1994) or the Ottaviani, Horton, and Erba (1997) gyro-Bohm formula. The Bohmlike formula is supported by the mesoscale correlation lengths shown in Figs. 5–8, while the Ottaviani-Horton-Erba model dictates a correlation length $\ell_c = q\rho_s R/L_T$ arising from the low-frequency end of the drift-wave turbulent spectrum.

What formulas (66)–(68) do not take into account is that for $P>P_*$ there is a bifurcation to a new confinement regime in which sheared mass flows occur along with an abrupt reduction in χ_i across a narrow zone with strong sheared flows. Theory shows that for $dv_{E_r}/dr \sim \gamma^{\max}$ or $\max(\Delta x k_y dv_E/dr) > \gamma_k^{\max}$ where Δx is the radial mode width and k_y the wave number, the system is decorrelated by the shear v_E' so as to form a transport barrier.

The nonlinear theory for the suppression of the turbulent diffusivity D gives the reduction factor of $D/[1+\tau_c^2 k_y^2 \Delta x^2 (v_E')^2]$ for broad band $\Delta\omega$ drift-wave turbulence with short correlation time $\tau_c = 1/\Delta\omega$ (Shaing *et al.*, 1990; Biglari *et al.*, 1990; and Zhang and Mahajan, 1992). The typical mode width Δx and the mean k_y have $\Delta x k_y \sim 1$. Hahm (1994) and Hahm and Burrell (1995) generalize the suppression theory to axisymmetric toroidal geometry. A survey of shear flow effects on the drift waves, trapped electron mode, resistive-g, and Rayleigh-Taylor instability is given in Tajima *et al.* (1991). The relation of shear flow stabilization versus the onset of the Kelvin-Helmholtz instability is given in that work. Tokamak-focused simulations showing evidence for the commonly employed $|v_E'| = \gamma_{\max}$ transport suppression rule begin with Waltz, Kerbel, and Milovich (1994) and are followed up in Waltz *et al.* (1997).

There are a number of theoretical models for the occurrence of a bifurcation to the improved confinement regimes through the creation of sheared mass flows. One of the first clear internal transport barriers resulting in the strong growth of the interior ion temperature gradient up to a record value of $\gtrsim$60 keV/m is that shown in Fig. 12 from Koide *et al.* (1994). The edge H-mode barrier forms after the internal transport barrier at $r/a = 0.7$ and is seen by examining the change from $t_3 = 5.75$ s to $t_4 = 6.0$ s in the T_i profile in the lower left frame of Fig. 12 where the region beyond $r/a = 0.7$ lifts up by 3 keV.

D. Properties of the ITG drift-wave instability

Many properties of the drift-wave stability problem are now well established. Here we list some of the more important properties without attempting to give their derivation.

1. For $\eta_i = 0$ there are no unstable roots within the adiabatic electron approximation for the pure hydrogen plasma. With impurities, however, there are unstable modes with $\eta_i = \eta_z = 0$ and $\omega_{*i}\omega_{*z} < 0$ for adiabatic electrons (Tang *et al.*, 1980). The toroidal problem with the transition from hydrogenic to low-z impurity-dominated ion temperature gradient-driven modes is given in Jarmén and Fröjdh (1993) and Dong, Horton, and Dorland (1994).
2. Finite $k_\parallel$ increases the η_i threshold so that unstable growth is localized to small $k_\parallel$ and wave absorption occurs at $k_\parallel c_s > \omega_{*T}$. Numerically, the condition is more restrictive, giving $k_\parallel L_T < 0.1 k_y \rho_i$ for instability. For tokamaks where $\overline{k_\parallel} \gtrsim 1/qR$ this limit introduces a q scaling to the transport (Kim and Horton, 1991; Ottaviani, Horton, and Erba, 1997).
3. The threshold results for toroidal and slab eta-i modes can be understood from the hydrodynamic interchange condition $\eta_i > \Gamma_{\text{eff}} - 1$ when taking into account that the number of degrees of freedom f is effectively given by (1) $f=3$ for the toroidal regime; (2) $f=2$ for the low $k_y\rho_i$ slab; and (3) $f=1$ for the high $k_y\rho_i$ slab and the connection between the adiabatic gas constant $\Gamma_{\text{eff}} = (f+2)/f$ and the number of degrees of freedom. Rigorous results obtained from the Nyquist analysis follow this pattern closely.
4. The T_i/T_e variations of the growth rate and the effect of temperature anisotropy $T_\perp \neq T_\parallel$ in the ion distribution are given in Kim *et al.* (1992). For peaked density profiles increasing T_i/T_e reduces the maximum growth rate and reduces the corresponding wave number $(k_y\rho_s)_{\max}$. For flat density profiles ($\epsilon_n \gtrsim 0.25$) there is a dramatic reduction in the growth rate with increasing T_i/T_e (Chen *et al.*, 1990, 1991; Romanelli and Briguglio, 1990; and Xu and Rosenbluth, 1991a, 1991b). The effect of anisotropic $\eta_i(\eta_{i\parallel}, \eta_{i\perp})$ is given by Mathey and Sen (1991) for the slab mode where the critical destabilizing value of $\eta_{i\parallel}$ is determined. The same for the toroidal mode has been studied by Kim *et al.* (1992), Song and Sen (1993a, 1993b), and Mondt (1996).
5. Electromagnetic coupling to the shear Alfvén wave gives a stabilizing effect of $\gamma \cong \gamma_0(1-\beta/\beta_c)$ where β_c is near the ideal magnetohydrodynamics (MHD) stability limit. The ballooning eigenvalue problem determines the β_c by $\alpha_{\text{MHD}} = -q^2 R(d\beta/dr) = f(s)$. Just below the MHD beta limit there are two unstable modes: (i) the small $E_\parallel$ MHD-like mode destabilized by kinetic resonance with the ions with a wave frequency $\omega_k \cong \omega_{*p_i}/2$, and (ii) the coupled drift wave–shear-Alfvén wave with a substantial $E_\parallel$ polarization with the low frequency $\omega_{Di} \lesssim \omega_k \ll \omega_{*i}$. As the MHD critical beta is crossed, the drift waves become stable.
6. The trapped electron response results in either (1) a new unstable mode (TEM) in addition to η_i mode (ITG) when η_e is significant (or other conditions are met) so that the frequencies $\omega_k^{\text{TEM}}, \omega_k^{\text{ITG}}$ are well separated, or (2) the additional destabili-

zation below $\eta_i < \eta_c^{\rm ITG}$ from a single hybrid mode. The transition between the two regimes is complicated depending on the value of η_i, η_e, and the fraction of trapped electrons. For significant values of all three parameters there are two distinct unstable modes.

7. In the presence of significant low-Z impurity, e.g., carbon with $Z_{\rm eff}\sim 3$, there is an impurity ITG mode in addition to the hydrogenic ITG mode. For density gradients in the same direction and $\eta_z=\eta_i$ the impurity ITG mode becomes stronger as the hydrogenic ITG weakens with increasing impurity charge fraction $f_z=Zn_z/n_e$ (Jarmen and Frödjh, 1993; Dong and Horton, 1995). For a radially increasing impurity profile there is an additional impurity instability, even at $\eta_i=\eta_z=0$, that produces an influx of low-Z impurity balanced by an outflux of hydrogen.
8. Sheared parallel mass flows are in general an additional independent destabilizing drive to the ITG modes. With a low-Z impurity η_i and parallel mass shear flow $\hat{u}_\parallel' = (L_n/c_s)du_\parallel/dx$, regimes are found where a sharp parallel shear flow ($\hat{u}_\parallel' \lesssim 1$) gives an inward hydrogenic flux and outward impurity flux, there is an anomalous parallel momentum flux $\pi_{x,\parallel}$ across the magnetic field (Dong, Horton, Bengston, and Li, 1994; Fu *et al.*, 1997).
9. The $\mathbf{E}_r\times\mathbf{B}$ shear flow is *strongly stabilizing* for $\Upsilon_s = |L_s dv_E/c_s dx| \gtrsim 1$. Small Υ_s values are destabilizing, but the destabilizing effect is second order $(L_s v_E'/c_s)^2$ and not observed in the simulations. In addition, to the direct effect on linear stability the $\mathbf{E}_r\times\mathbf{B}$ shear flow decreases the radial correlation length, reducing the transport for given level of the fluctuations (Biglari *et al.*, 1990; Hamaguchi and Horton, 1992). The generalization to toroidal geometry is given by Hahm and Burrell (1995).
10. Interpolation formulas for ion thermal diffusivity.

Kotschenreuther *et al.* (1995) have combined the information obtained from theory and a simulation database composed of linear gyrokinetic simulations and nonlinear gyrofluid simulations to construct a parametrization of the first critical gradient $R/L_{\rm crit}^{(1)}$ and the ion thermal diffusivity χ_i. The system parameter list is large. There are eight parameters for the hydrogenic working gas

$$\mu_H^8 = \left\{ \frac{R}{L_{T_i}}, \frac{R}{L_n}, q, s\, \frac{T_i}{T_e}, Z_{\rm eff}, \nu_{*i}, \frac{r}{R} \right\}, \tag{69}$$

and with the carbon impurity, the parameter list expands to include six impurity parameters

$$\mu_z^6 = \left\{ Z, \frac{m_z}{m_i}, f_z = \frac{Zn_z}{n_e}, \frac{R}{L_{T_z}}, \frac{R}{L_{nz}}, \frac{T_z}{T_i} \right\} \tag{70}$$

and the fast ion beam component adds at least two parameters. When the injected beam species is the same hydrogenic isotope as the working gas, we add two parameters $\mu_b^2 = \{n_b/n_e = \sigma_b, E_b/T_e\}$. The beam energy E_b is high, $E_b/T_e \gtrsim 15$, so that the beam ion density fluctuations $\delta n_b(\phi)$ is adiabatic, and thus the contribution of the beam to the dispersion relation (49) is to modify the electron and impurity responses by $(T_i/T_e) \to T_i/T_e(1-\sigma_b)$ and $Z_{\rm eff} = \Sigma n_z Z^2/n_e \to Z_{\rm eff}(1-\sigma_b) = Z_{\rm eff}^*$ due to the dilution of the thermal ion density n_i by the beam density fraction $\sigma_b = n_b/n_e$.

Kotschenreuther *et al.* (1995) propose two critical gradients $L_{\rm crit}^{(1)}$ and $L_{\rm crit}^{(2)}$. The parametrization of the first critical gradient is given by

$$\frac{R}{L_{\rm crit}^{(1)}} = f(\{\mu_j\})g(\{\mu_j\})h(\{\mu_j\}), \tag{71}$$

where

$$f = 1 - \frac{0.2(Z_{\rm eff}^*)^{0.5}}{s^{0.7}}\left(\frac{14\epsilon^{1.3}}{\nu^{0.2}} - 1\right), \tag{72}$$

$$g = (0.7 + 0.6s - 0.2R/L_n)^2 + 0.4 + 0.3(R/L_n - 0.8s + 0.2s^2), \tag{73}$$

$$h \equiv 1.5\left(1 + \frac{2.8}{q^2}\right)^{0.26} (Z_{\rm eff}^*)^{0.7}\left(\frac{T_i}{T_e(1-\sigma_b)}\right)^{0.5}. \tag{74}$$

The question arises if other formulas may also parametrize the same computational database within the same tolerance of this parametrization. The uncertainties in the numerous ($\sim$15) exponents and the residuals of the parametrization of $R/L_{T,\rm crit}$ with linear gyrokinetic code are presently unknown.

A formula for the impurity-dominated (carbon) ITG mode threshold $R/L_{L,\rm crit}^{(2)}$ is also given in Kotschenreuther *et al.* (1995). Again the critical gradient is factorized into products of functions in this case containing switches: one for $Z_{\rm eff}^* \gtrless 3$ and the other switch for $R/L_n^* \gtrless \frac{1}{3}$. For a significant carbon component with $n_c(r) \gtrsim n_i(r)/6$ both these switches are on and the second critical gradient $R/L_{T_i}^{(2)} = 0.75(1+\tau_b)(1+s)$ is used. Here $\tau_b = T_i/T_e(1-\sigma_b)$ defines the effective temperature ratio.

For the thermal diffusivity beyond threshold a transition function $G(x) \equiv \min(x, x^{1/2})$ is introduced where x measures the excess of the gradient over the critical gradient: $x \equiv R/L_{T_i} - R/L_{T,\rm crit}^{(1)}$ defined in Eq. (71). Choosing the minimum of x and $x^{1/2}$ assures that for $x<1$ the χ_i increases linearly with the excess $x>0$ as required by bifurcation theory. On the other side ($x>1$) of the $G(x)$ switch, the growth of χ_i with increasing temperature gradient is slowed to match that of formulas (62) and (63) from turbulence theory.

With increasing low Z impurity concentration χ_i changes form. As reported by Dong, Horton, and Dorland (1994) the growth rate and hence diffusivity of the hydrogenic branch of the ITG dispersion relation decreases as the charge fraction $f_z = Zn_z/n_e$ increases. This is taken into account by defining the function $\mathcal{F}(Z_{\rm eff}^*) = \min[1, (3/Z_{\rm eff}^*)^{1.8}]$ so that for $Z_{\rm eff}^* = \Sigma n_z Z^2/n_e(1-\sigma_b) > 3$ the hydrogenic χ_i is decreased as $\chi_i(3/Z_{\rm eff}^*)^{1.8} \propto \chi_i/(Z_{\rm eff}^*)^2$. The low-$Z$ (carbon) branch becomes unstable before $Z_{\rm eff}^*$ reaches 3. So Kotschenreuther *et al.* (1995) added a second hydrogenic thermal diffusivity

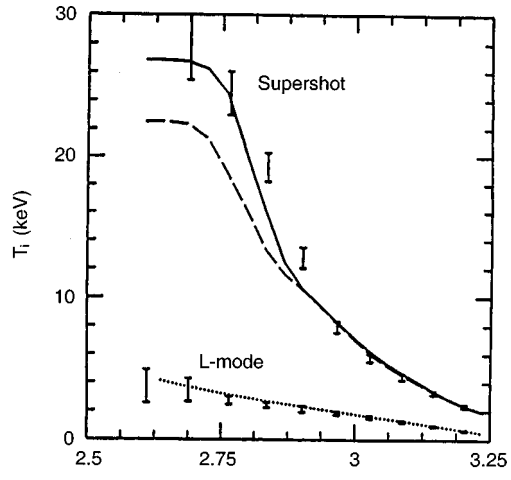

FIG. 13. Comparison of the IFS-PPPL model for an L mode and a supershot discharge in TFTR. The complex χ_i formula is able to account for the large increase in the core ion temperature from the experimental values of T_i at $\rho=0.8$ taken as the boundary condition (from Kotschenreuther *et al.*, 1995).

$\chi_i^{(2)}$ that increases as the $\max(0.25, Z_{\rm eff}^*-3)$. For $Z_{\rm eff}^*>3$ the carbon mode ITG contribution is

$$\chi_i^{(2)}=0.66\left(\frac{T_e}{T_i}\right)^{0.8}\left(\frac{Z_{\rm eff}^*-3}{1+s}\right)\left(\frac{R}{L_{T_i}}-\frac{R}{L_{T,\rm crit}^{(2)}}\right)$$

$$\text{for } x_2=R/L_{T_i}-R/L_{T,\rm crit}^{(2)}>0. \tag{75}$$

Then a final (fourth) switch is introduced in the final ion thermal diffusivity formulas with

$$\hat{\chi}_i=\max(\chi_i^{(1)},\chi_i^{(2)}),$$

where

$$\chi_i^{(1)}=\frac{(q/\tau_b)^{1.1}}{1+s^{0.84}}\left(1+\frac{6.7\epsilon}{q\nu^{0.26}}\right)\left(\frac{R}{R_{T_i}}-\frac{R}{L_{T,\rm crit}^{(1)}}\right) \tag{76}$$

when $Z_{\rm eff}^*<3$. The final formula is

$$\chi_i=C_0\frac{\rho_i^2 v_{T_i}}{R}\hat{\chi}_i. \tag{77}$$

As $R/L_{T_i}\to R/L_{T_i}^{(1)}$ of Eq. (71) a switch is made to the carbon controlled diffusivity of Eq. (75) with critical gradient $R/L_{T,\rm crit}^{(2)}$ given above through the $\max(\chi_i^{(1)},\chi_i^{(2)})$ function.

Thus, with use of switches and interpolating functions obtained by nonlinear regression fits to a simulation database, Kotschenreuther *et al.* (1995) obtain the IFS-PPPL transport model for the ITG mode in the presence of a significant carbon component. An example of the formula's prediction for the ion temperature profiles is shown in Fig. 13. The carbon component switch is the key element allowing the χ_i formula to match both the L mode and supershot data on TFTR. Important features of both $\chi_i^{(1)}$ and $\chi_i^{(2)}$ are the strong inverse dependence on $\tau_b=T_i/T_e(1-\sigma_b)$ and the increase of the critical gradient (71)–(74) with $(\tau_b)^{0.5}$ giving the suppression of χ_i in the hot-ion regime.

A detailed analysis of the enhanced confinement regime shots by Ernst *et al.* (1998) shows that to fully account for the low transport in the steep ion temperature gradients obtained in the enhanced confinement modes in TFTR, the stabilization from E_r shear must be calculated using the formula for E_r from knowledge of the carbon toroidol velocity profile and neoclassical theory to obtain the poloidal velocity profiles of the working gas. The fluctuation measurements (Mazzucato *et al.*, 1996) support the theoretical prediction of suppression of the drift-wave turbulence in the core of the enhanced confinement regimes.

The IFS-PPPL model generated considerable excitement in the fusion community during the period 1995–96 due to its ability to successfully model the TFTR datasets including both the L mode and the supershots. When applied to the large reactor design called ITER, however, the formulas give considerably poorer confinement than projected by the empirical confinement time in Eq. (68). The model gives a radially increasing $\chi_i(r)$ by virtue of the temperature gradient being close to marginal in the core ($r/a<0.5$) and deviating strongly from marginal in the edge. The value of C_0 required is $C_0=12$. It is shown that the global energy confinement time is insensitive to C_0 (varying as $C_0^{-0.15}$). The edge plasma temperature is, however, a sensitive parameter. The analysis starts by specifying the edge temperature taken at $r/a=0.8$ from the database. It is argued that the change from the L mode to the supershot ion temperature profiles is produced by the abrupt change in the edge plasma parameters. As the edge ion temperature increases, there is a positive feedback on the entire ion temperature profile from both the stabilization of the ITG from increasing T_i/T_e ratio [see formulas (74) and (76)] and the decoupling of the ion-electron collisional equilibration allowing T_i to pull away from T_e. The model is capable of strong changes (bifurcations) in the transport behavior due to the four switching functions. The model takes fifteen local parameters to predict the ion thermal diffusivity.

This and other ITG models (Weiland and Nordman, 1991; Ottaviani, Horton, and Erba, 1997; Redd *et al.*, 1998) extrapolated to the ITER parameters predict sensitivity to the edge ion temperature for the fusion power. The sensitivity is such as to lead the Kotschenreuther team to predict that ITER must meet stringent edge conditions in order to meet the design criteria. The abrupt change in the core ion temperature due to critical edge plasma parameters is interpreted as the H-mode condition for this model. More recent studies incorporated the E_r-shear flow stabilization parameter into the model. This critical issue of the difficulty of achieving the edge H mode for the successful operation of ITER was not fully recognized until the Kotschenreuther *et al.* (1996) work.

1. Reversed magnetic shear and the hybrid trapped electron-ITG mode

The reversed magnetic shear (RS mode) has become an important improved confinement mode of operation in tokamaks (Levinton *et al.*, 1995; Strait *et al.*, 1995).

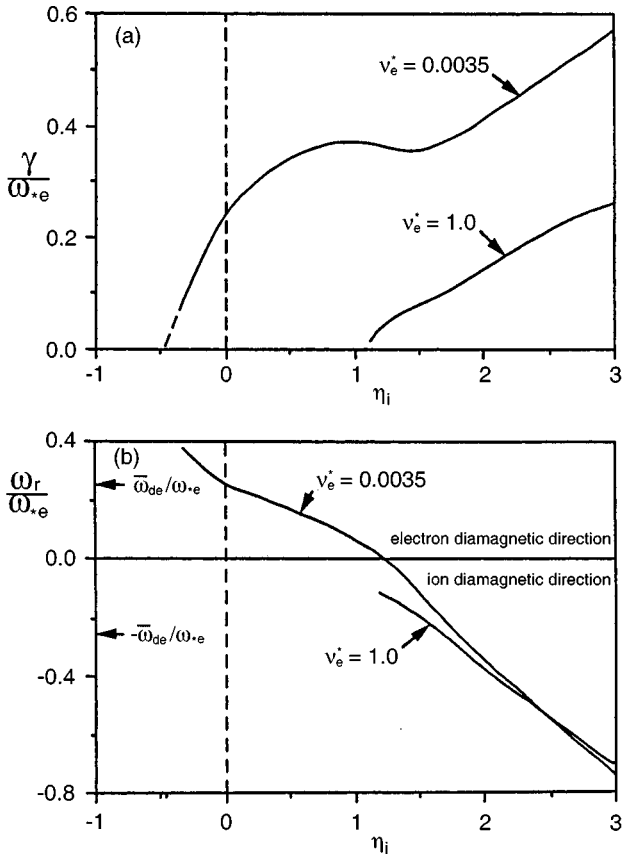

FIG. 14. The normalized (a) growth rate and (b) frequency of the complete kinetic toroidal eigenvalue problem. At high collisionality only the ITG mode appears for $\eta_i > 1.2$ while at low collisionality the trapped electron mode appears for $\eta_i < 1.5$ (from Rewoldt and Tang, 1990).

There are numerous changes that take place in the conventional drift modes, eta-*i* modes, and resistive ballooning modes when $s = rq'/q$ goes through zero and then negative. For a simple explanation and examples of the negative *s* stabilizing effect on the toroidal ion temperature gradient mode, see Kim and Wakatani (1994). The growth rate is a maximum at $s = \frac{1}{2}$ as can be understood from the small θ expansion of $\omega_{D_i}(\theta, s)$.

Dong *et al.* (1996) re-investigate the somewhat subtle issue of the conditions for the existence of *two distinct unstable drift modes*: the eta-*i* (ITG) and the trapped electron (TE) mode. This is the standard case assumed for example in the Weiland transport model implemented in the Bateman-Kinsey transport codes (Kinsey *et al.*, 1996). However, when the η_i and η_e parameters are not large (greater than unity), or especially when the magnetic shear *s* is negative, there is only one unstable root. This situation was first reported by Rewoldt and Tang (1990) who called the single mode the hybrid mode. This hybrid mode does not have a critical η_i value for stabilization. At low η_i values it is driven by the trapped electrons and rotates in the electron diamagnetic direction.

Figure 14 shows an example of the hybrid trapped electron η_i mode compared with pure ITG mode. The results are from the Rewoldt and Tang (1990) investigation of the transition between the trapped electron mode and the η_i mode. At high collisionality $\nu_e^* = 1$ the growth rate in Fig. 14(a) sets in at $\eta_i > \eta_c \simeq 1.2$ and the mode rotates in the ion diamagnetic direction as shown in frame (b). Since the nonadiabatic trapped electron response $\delta_k \propto \epsilon^{1/2} \omega_{*e} \eta_e / \nu_{*e}$, the trapped electron response becomes important at lower collisionality. Thus, in Fig. 14 the $\nu_{*e} = 3.5 \times 10^{-3}$ case shows that the single unstable mode changes direction of rotation from the ion direction to the electron diamagnetic direction for $\eta_i < \eta_c$ with the growth rate now driven by the (trapped) electron-wave interactions. The drift wave remains unstable until η_i reaches -0.5 in this case. Comparing parts (a) and (b) in Fig. 14 shows the large growth per wave period $2\pi\gamma/\omega_r$ from this fully kinetic model for any $\eta_i > 0$ at low collisionality. Thus the trapped electron mode is equally important to the ITG mode in determining the transport properties of confined plasmas.

E. Trapped ion mode low-frequency drift-wave turbulence

An important issue that has recently been settled is the possible existence of a large, Bohm-like transport predicted from the trapped ion mode. The trapped ion mode is a drift instability analogous to the trapped electron mode, but owing to the low frequency of the ion bounce motion $\omega_{bi} (\lesssim 10^5 s^{-1})$, the trapped ion mode occurs only for large space scale ($k_\theta \leqslant k_{bi}$) fluctuations satisfying

$$\omega_* = k_\theta \rho_s \frac{c_s}{L_n} < \omega_{bi} = \frac{\epsilon^{1/2} v_i}{qR}. \tag{78}$$

Here $k_\theta (= k_y) = nq(r)/r$ for toroidal modes $\exp(in\phi - i\omega t)$ and $k_{bi}\rho_s = \epsilon_n \epsilon^{1/2}/q \ll 1$.

In the 1970s there were dire predictions of large ion losses based on the trapped ion mode mixing length $\mathcal{D}^{TI} = \sqrt{\epsilon}\gamma^{TI}/\langle k_x^2 \rangle$ formula for the turbulent diffusivity (Rosenbluth *et al.*, 1972; Adam *et al.*, 1976). Both the magnitude and scaling of this diffusivity formula were disastrous for a fusion reactor. Subsequent nonlinear simulations of the trapped ion mode alone supported this conclusion because the radial correlation length becomes macroscopic, not being tied to the gyroradius.

In sharp contrast to this picture Horton, Choi, *et al.* (1980) argued that the trapped ion mode must coexist in a sea of turbulent drift-wave fluctuations. These shorter scale $k_y \rho_s \sim 0.3$, faster growing modes $(\mathbf{k}, \omega)$ were taken into account and shown to dominate. Thus, the usual drift-wave space-time scale plasma turbulence must be taken into account in considering the dynamics of the trapped ion mode.

Horton, Choi, *et al.* (1980) used standard scale separation procedures $(\mathbf{q}, \Omega) \ll (\mathbf{k}, \omega)$ to show that the trapped ion mode transport $(\mathbf{q}, \Omega)$ is suppressed by the sea of drift-wave fluctuations $(\mathbf{k}, \omega)$. The calculation is complicated and some assumptions must be made in determining the growth rate of the trapped ion mode renormalized by the background drift-wave fluctuations.

Opposed to this conclusion was work by Shapiro *et al.* (1993) who argued that the drift-wave fluctuations would boost the trapped ion mode fluctuation level. Shapiro *et al.* (1993) argued that the energy transfer to the trapped ion mode would create large coherent dipolar vortex convection cells again producing large plasma losses.

The issue has been settled by the simulations of Kingsbury and Waltz (1994), which show fortunately that there are no Bohm scaling losses from large-scale convection in the trapped ion mode dynamics. The diffusion they find is dominated by the drift-wave fluctuations above the ion bounce frequency. The spectral intensity increases as $\tilde{n}/n_e \sim 1/k_\perp L_n$ with decreasing drift wave k_θ until reaching the transition scale given in Eq. (78) when below $k_\theta < k_{bi}$ the fluctuation induced transport drops to a smaller level for the lower wave numbers. They identify the sink of energy as the small $k_y = q_y$ modes whose phase relations between $\delta n_i(q,\Omega)$ and $\phi(q,\Omega)$ have been so strongly shifted by the drift-wave turbulence that they become a *sink* of fluctuation energy rather than a source. These are the same modes that in the linear theory would grow from the trapped ion dynamics. The predicted strong change of the $\delta n(q,\Omega)/\phi(q,\Omega)$ relationship is shown by the computer simulations of the dynamical equations for the two fields and explains the suppression of the linear trapped ion mode.

Clearly, the trapped ion mode alone is an incomplete system: with the same toroidal system parameters the dynamical equations predict the existence of the faster growing and stronger drift-wave turbulence. What is not so clear without the results of the Kingsbury and Waltz simulations is whether the large correlations envisioned by Shapiro *et al.* (1993) can build up or whether the drift-wave turbulence disrupts the trapped ion mode growth mechanism as given by Horton, Choi, *et al.* (1980). The simulations address the issue further by comparing 85^2, 170^2, and 340^2 truncated **k**-space simulations to demonstrate good convergence to the drift-wave diffusion coefficient of $D = 5.2 D_{\rm dw}$ where $D_{\rm dw} = (\rho_s/L_n)(cT_e/eB)$. This value is in comparison to drift waves alone where $D = 6.3 D_{\rm dw}$. The value of 5.2 is broken up into 5.0 from the drift-wave scales and 0.2 from the trapped ion mode scales. Their reference system parameters are $\eta_i = \eta_e = 2$, $T_e/T_i = 1$, $\epsilon_n = 0.15$, $\epsilon = 1/3$, $\nu_{ei} L_n/c_s = 0.08$, $q = 1.5$ so that the banana width is $q\rho_s/\sqrt{\epsilon} = 2.6\rho_s$. For the 170^2 grid the $k_1\rho_s = 0.03$ with $k_{\max}\rho_s = 2.4$. The division between the trapped ion wave and drift-wave dynamics occurs at $k\rho_s = 0.3$. The dynamical system has four ODE's at each wave vector: two for the trapped electron density and pressure that are the same for all **k** and two for the ion density and pressure that change structure form above and below the critical wave number defined by Eq. (78).

These theoretical and simulation studies that appear to eliminate the possibility of the trapped ion mode producing large Bohm-type losses, are in accord with the high ion temperature discharges achieved in the large tokamaks. These conclusions are of paramount importance for the confinement of fusion plasmas. They narrow the scope of the turbulence problem to that of the smaller space scales of the η_i mode and the trapped electron turbulence. The remaining issue of the role of the smaller c/ω_{pe}-scale turbulence, however, is yet to be settled. The status of the short-wavelength turbulence transport problem is given in Sec. V.G.

F. Sheared mass flow generated by turbulence

As the ion temperature of the plasma increases, the viscosity drops, and for a sufficiently strong temperature or pressure gradient, there is a spontaneous symmetry breaking in the turbulence to tilted vortices creating a sheared mass flow. The turbulent fluxes describing this process are the two Reynolds stress tensors $\langle \tilde{v}_x \tilde{v}_y \rangle$ and $\langle \tilde{v}_x \tilde{v}_\parallel \rangle$. The divergence of the Reynolds stress tensors drives the sheared flows $\overline{V_y}(x,t)$ and $\overline{V_\parallel}(x,t)$ against the viscous damping. This shear flow generation phenomena has been observed in computer simulations of the full three-dimensional plasma systems by Carreras *et al.* (1993), Guzdar *et al.* (1993) and Sugama and Horton (1994).

The dominant physical processes at work in the creation of the turbulence-driven sheared flows can be understood from low-order models derived from appropriate truncations of the mode coupling problem as given in Finn *et al.* (1992); Bazdenkov and Pogutse (1993), Hermiz *et al.* (1995), Thiffeault and Horton (1996), and Hu and Horton (1997) for ITG turbulence. The phenomena of turbulence-driven flows has not been identified in plasma experiments due to competing mechanisms such as the torque produced by radial currents (Diamond and Kim, 1991) and ion orbit losses (Shaing *et al.*, 1990; Shaing, 1993). Ida *et al.* (1992) compare their tokamak experiments with five theories without finding substantial agreement.

In hydrodynamics the bifurcation from the usual state of steady, aligned Rayleigh-Bénard vortices to tilted vortices with sheared mass flows was discovered in the experiments reported by Krishnamurti and Howard (1981). The experiments show that for low Prandtl number (Pr = viscosity/thermal diffusivity) there is a critical Rayleigh number above which there is a change in the turbulence to a state with tilted vortices as shown with tracer particles. Subsequently, a simple theoretical explanation was given by Howard and Krishnamurti (1986) using a low-order truncation for the spectral expansion of the two coupled partial differential equations for Rayleigh-Bénard convection. The mathematical structure of the Rayleigh-Bénard equations is the same as the equations for resistive pressure gradient plasma turbulence in the case of no magnetic shear. This similarity simulated a number of low-order models for analysis of the bifurcations in the plasma system (Hermiz *et al.*, 1995, and Horton *et al.*, 1996). The low-order models show a second bifurcation to a limit cycle identified with type III ELM's (edge localized modes) and a final bifurcation to chaos. The issue of convergence to solutions of the partial differential equations is analyzed

in Treve and Manley (1982) and Thiffeault and Horton (1996). Solutions of the three-dimensional partial differential equations are found in Drake *et al.* (1992), Carreras *et al.* (1992, 1993, 1994), and Sugama and Horton (1994).

In more complete descriptions of the global tokamak system with auxiliary heating sources as the control parameters there are further considerations. The spatial nonuniformity of the momentum injected, especially with the high-power neutral beams, leads to driven sheared mass flows. As a result, a further bifurcation to a supersuppressed transport state is possible with a still lower, but finite, level of turbulence. Descriptions of these transport states are given in Newman *et al.* (1993) and Kishimoto, Tajima, LeBrun, *et al.* (1996). The global analysis of a high performance JT-60U discharge is given in Horton *et al.* (1997).

These driven improved plasma confinement states show hysteresis with the back transitions occurring as the power is lowered occurring at lower values than the forward transitions (bifurcations) with rising power. Sugama and Horton (1995a, 1995b) show how the hysteresis can arise from the reduced viscosity in the high-temperature states created through the forward transitions. The hysteresis loop has been explored in the C-MOD experiment in some detail.

The calculation of the shear flow generation from combined neoclassical transport and turbulence is currently an active area of research (Rosenbluth and Hinton, 1998).

V. NONLINEAR DRIFT-WAVE EQUATIONS

For sufficiently small $k_\parallel c_s/\omega$ the parallel compression $\nabla_\parallel(n_i u_\parallel)$ in Eq. (32) is negligible. For the adiabatic electron response in Eq. (12) and using quasineutrality $n_i = n_e$, Eq. (32) reduces to the Hasegawa-Mima equation

$$(1-\rho_s^2\nabla_\perp^2)\frac{\partial\varphi}{\partial t}+v_d\frac{\partial\varphi}{\partial y}-\frac{c}{B}[\varphi,\nabla^2\varphi]=0, \tag{79}$$

where the Poisson bracket arises from the $\mathbf{E}\times\mathbf{B}$ convective derivative in the polarization drift and is defined by

$$\mathbf{v}_E\cdot\nabla f=\frac{c\hat{\mathbf{e}}_z\times\nabla\varphi}{B}\cdot\nabla f=\frac{c}{B}\hat{\mathbf{e}}_z\cdot\nabla\varphi\times\nabla f:=\frac{c}{B}[\varphi,f]. \tag{80}$$

Equation (79) describes the convection of the potential vorticity

$$q=\varphi-\rho_s^2\nabla^2\varphi+v_d x \quad \text{with} \quad \frac{dq}{dt}=0. \tag{81}$$

This nonlinear drift-wave equation has been extensively investigated. The results of these investigations are summarized in Secs. V.A–V.F. Frieman and Chen (1982) give the kinetic derivation of Eq. (79).

The mixture of wave and vortex solutions of Eq. (79) is suggested by the occurrence of the infinite set of Casimir invariants $C_F=\int F(q)\,dx\,dy$ from the conservation of q and the quadratic invariants for the energy W and the potential enstrophy U. The quadratic invariants

$$W=\frac{1}{2}\int[\varphi^2+(\nabla\varphi)^2]dx\,dy$$

$$=\frac{1}{2}\sum_{\mathbf{k}}(1+k_\perp^2\rho_s^2)|\varphi_{\mathbf{k}}|^2, \tag{82}$$

$$U=\frac{1}{2}\int[(\nabla\varphi)^2+(\nabla^2\varphi)^2]dx\,dy$$

$$=\frac{1}{2}\sum_{\mathbf{k}}k_\perp^2(1+k_\perp^2\rho_s^2)|\varphi_{\mathbf{k}}|^2 \tag{83}$$

give rise to the inverse cascade in $\mathbf{k}$-space. The waves $\omega=\omega_k=k_y v_d/(1+k_\perp^2\rho_s^2)$ make the fluctuation spectra anisotropic. The balance between the wavelike turbulence and the vortex turbulence is the subject of the review Horton and Hasegawa (1994). Here we emphasize the wave turbulence.

The solutions of Eq. (79) are best computed and perhaps best understood in the representation

$$\phi(\mathbf{x},t)=\sum_{\mathbf{k}}\phi_{\mathbf{k}}(t)e^{i\mathbf{k}\cdot\mathbf{x}}, \tag{84}$$

where $\phi_{-\mathbf{k}}=\phi_{\mathbf{k}}^*(t)$ are the Fourier amplitudes in an N_F-dimensional $\mathbf{k}$ space. The $\mathbf{k}$-space dynamics is given by

$$\frac{d\phi_{\mathbf{k}}}{dt}+(i\omega_{\mathbf{k}}-\mu_{\mathbf{k}})\phi_{\mathbf{k}}=\sum_{\mathbf{k}_1+\mathbf{k}_2=k}\Lambda^{\mathbf{k}}_{\mathbf{k}_1,\mathbf{k}_2}\phi_{k_1}\phi_{k_2}, \tag{85}$$

where the mode coupling matrix elements are

$$\Lambda^{\mathbf{k}}_{\mathbf{k}_1,\mathbf{k}_2}=\frac{1}{2}\frac{\hat{\mathbf{z}}\cdot(\mathbf{k}_1\times\mathbf{k}_2)}{1+k^2}(k_2^2-k_1^2) \tag{86}$$

and $\mu(k)=\mu k^2/(1+k^2)$ for ion-ion collisional viscosity or $\mu_k=\mu_n k^{2n}/(1+k^2)$ for a hyperviscosity (Benzi *et al.*, 1988). A typical value of $n=8$ and $\mu_n=1.6\times10^{-24}$ (Legras *et al.*, 1988). The hyperviscosity allows the simulations to extend the inertial range of Eq. (79) on a limited grid $N_F=256$ or 512. At the present time 2D simulations are limited to $(1024)^2$-fast Fourier transforms with most published drift-wave simulations on smaller grids.

The dynamics from the mode coupling Eq. (85) is that of the sum over all $\mathbf{k}_1$ of the quadratic interactions of strength $\Lambda^{\mathbf{k}}_{\mathbf{k}_1,\mathbf{k}-\mathbf{k}_1}$ where $\mathbf{k}_1$ is not parallel to $\mathbf{k}$ and $k_1^2 \neq(\mathbf{k}-\mathbf{k}_1)^2$. There are both local interactions where k_1,k_2,k are comparable in magnitude and nonlocal interactions where k_1 is much larger or smaller than k. For a single triplet $\mathbf{k}_1,\mathbf{k}_2,\mathbf{k}=\mathbf{k}_1+\mathbf{k}_2$ there is a conserved quantum number and a useful parametric decay analysis (Horton and Hasegawa, 1994) showing the direction of the energy transfer in each triplet in the dissipationless limit. For the dissipative problem the quanta disappear but the parametric decay analysis is still useful.

The Hasegawa-Mima Eq. (79) has no sources and sinks for the fluctuations. The source of the drift-wave fluctuations is proportional to δ_k in Eq. (13). The nonlinear dynamics from Eq. (32) with Eq. (13) along with

sink from parallel and/or perpendicular ion viscosity is called the Terry-Horton equation (Terry and Horton, 1982, 1983). The spectral properties and transport of the Terry-Horton model have been extensively investigated (Waltz, 1983; Krommes, 1982, 1997) and summarized in Sec. V.E. Both the Hasegawa-Mima and the Terry-Horton models take the plasma as locally homogeneous. The effect of a global density profile $n(x)$ is considered in Sec. V.G for the collisional drift wave.

At sufficiently low-energy levels the Hasegawa-Mima (HM) equation gives rise to regimes of wave turbulence that may be analyzed within the context of the weak turbulence and the renormalized turbulence wave kinetic equations. In regimes where the statistics of the wave field ϕ are sufficiently random to allow the quasi-Gaussian (or quasinormal) truncation of the multifield correlation functions to be valid, the wave kinetic equation provides an analytical method of describing the distribution of the turbulent fluctuation energy spectrum $W(\mathbf{k})=(1+k_\perp^2\rho_s^2)|\phi_\mathbf{k}|^2$ in wave number space.

A. Weak turbulence and Kolmogorov-like spectral laws

The wave kinetic equation provides a method of deriving Kolmogorov-type spectra by methods developed by Zakharov *et al.* (1992). The analysis shows clearly how the Kolmogorov spectral exponents depend on the scale invariance of both the dispersion law $\omega_\mathbf{k}$ and the wave interaction dynamics $\Lambda^{\mathbf{k}_1}_{\mathbf{k}_2\mathbf{k}_3}$. Thus for drift-wave–Rossby wave turbulence the spectral distribution changes slope between the long-wave region $k_\perp\rho_s<1$ and the short-wave region $k_\perp\rho_s>1$ where the scaling properties change. In addition, the dispersion law $\omega_\mathbf{k}=k_y v_d/(1+k_\perp^2\rho_s^2)$ is clearly anisotropic, and thus the spectral distributions are of the form

$$W(\mathbf{k})=P^{1/2}\frac{1}{|k_x|^{\nu_x}|k_y|^{\nu_y}} \tag{87}$$

with separate scaling exponents $\nu=(\nu_x,\nu_y)$ in the two directions. Here P is the flux of energy through the inertial range. In the long wave region ($k\rho_s<1$) the analyses of Novakovskii *et al.* (1988), Balk and Nazarenko (1990), and Balk *et al.* (1991) give $\nu_x=3$ and $\nu_y=\frac{3}{2}$, which was tested in numerical simulations (Horton, Su, and Morrison, 1990). To test the analytic inertial range model an idealized isotropic source-sink model $\gamma^I(k)\phi_\mathbf{k}$ is added to the $\mathbf{k}$-space Hasegawa-Mima equation. The actual plasma fluctuation source-sink physics occurs through the mechanism of dissipation either in the form of finite resistivity from electron-ion collisions or resonant wave-particle interactions.

B. Wave-kinetic equation

Here we review the key elements of this rather technically complex field of study. The principal assumption in the analysis is that the energy-momentum transfer within the turbulent spectrum $W(\mathbf{k})$ occurs along the three-wave resonant manifold defined by

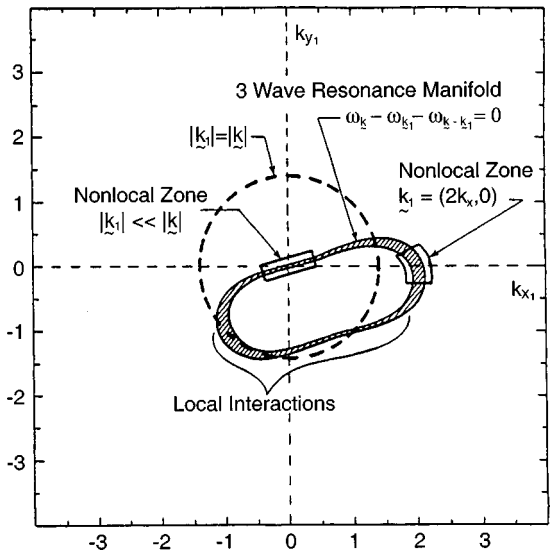

FIG. 15. The resonant three-wave manifold for the drift-wave interaction calculations in weak turbulence theory.

$$\mathbf{k}=\mathbf{k}_1+\mathbf{k}_2,$$
$$\omega_\mathbf{k}=\omega_{\mathbf{k}_1}+\omega_{\mathbf{k}_2} \tag{88}$$

in the $\mathbf{k}\omega$ space. The resonance conditions allow both a local (as in the Kolmogorov hypothesis) and nonlocal interaction. In renormalized turbulence theory the sharp delta-function condition $\delta(\omega_\mathbf{k}-\omega_{\mathbf{k}_1}-\omega_{\mathbf{k}_2})$ on the frequency resonance in condition is replaced by a broadened nonlinear propagator $g_{\mathbf{k}\omega}$ with finite correlation time $\tau_c=1/\nu_k$ that is determined self-consistently with the fluctuation spectrum $W(\mathbf{k})$. Taking $\nu_\mathbf{k}$ into account is important for determining the spectral linewidths $\nu_\mathbf{k}$ observed in the electromagnetic scattering experiments discussed in Sec. II.D. The nonlinear broadening of the propagator $g_{\mathbf{k}\omega}$, however, is not considered to be important in determining the ω-integrated distribution $W(\mathbf{k})=\int d\omega W(\mathbf{k},\omega)$ of the fluctuation energy in $\mathbf{k}$ space.

The transport of fluctuation energy in $\mathbf{k}$ space occurs resonantly along the three-wave manifold (88) which is given in more detail by letting $\mathbf{p}=\mathbf{k}_1$ and $\mathbf{k}_2=\mathbf{k}-\mathbf{p}$

$$\Delta\Omega_{\mathbf{k},p}=\frac{p_y v_d}{1+p_x^2+p_y^2}+\frac{(k_y-p_y)v_d}{1+(k_x-p_x)^2+(k_y-p_y)^2}-\frac{k_y v_d}{1+k_x^2+k_y^2}=0, \tag{89}$$

where for each (k_x,k_y) there is a resonant curve in $\mathbf{p}=\mathbf{k}_1$ shown in Fig. 15.

The interactions are defined as local in $\mathbf{k}$ space when all three-wave vectors are comparable in size $|\mathbf{k}|\sim|\mathbf{k}_1|\sim|\mathbf{k}-\mathbf{k}_1|$. It is the interaction of these comparable space-scale fluctuations that is used in the Kolmogorov picture of the inertial range cascade. In addition, there are *nonlocal* transport processes in which one of the $\mathbf{k}$ vectors is much smaller than the other two. The fluctuation at small $|\mathbf{k}|$ is then part of the large scale turbulent flow. This large scale shear flow can have a dominant influence over the small scale turbulence. One method

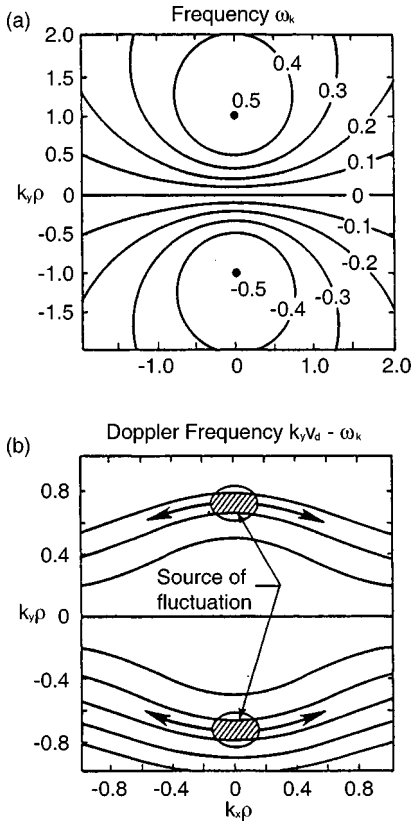

FIG. 16. The flux of wave energy from the source region to the damped modes given by the wave-kinetic equation.

of analyzing the nonlocal fluctuation dynamics is by separating the fluctuation field into $\phi=\phi_L+\phi_s$ where L and s are the large-scale and small-scale parts of the field, respectively. An important example of the turbulence analysis based on this two-scale analysis is given in Sec. V.F.

In the three-wave resonant manifold (a three-dimensional surface in the four-dimensional vector space of $\mathbf{k},\mathbf{k}_1=\mathbf{p}$) shown in Fig. 15 there are two important regions of nonlocal contributions to the $\mathbf{k}$-space transport processes. The region around the origin defined by $|\mathbf{p}|\ll|\mathbf{k}|$ is one in which $\mathbf{k}$ and $\mathbf{k}-\mathbf{p}$ are strongly coupled by the large scale fluctuation at $\mathbf{p}$. These small $|\mathbf{p}|$ interactions reduce to a constrained diffusion of $W(\mathbf{k})$ in $\mathbf{k}$ space along a curve of given $\nu_{\mathbf{k}}=k_y v_d-\omega_{\mathbf{k}}$ as shown in Fig. 16.

Such transport takes energy from the source at $k_x\rho\simeq 0$, $k_y\rho\simeq 0.5$ region of max $\gamma_{\mathbf{k}}$ to the regime of $k_y\rho\to 0$ and finite $k_x\rho$ which is the region of shear flows or zonal flows where $v_y(x,t)\cong -cE_x/B\gg v_x$.

A second region of strong, nonlocal transport occurs from the nonlinear backscattering region around $\mathbf{p}=(2k_x,0)$ also indicated in Fig. 15. These are nonlocal transfer processes. Thus, the combination of the nonlocal and local transport in $\mathbf{k}$ space of fluctuation energy and momentum contained in the turbulent fluctuations is a complex anisotropic process for the Hasegawa-Mima equation.

To formulate the transport analysis in $\mathbf{k}$ space under the resonance condition and to derive the weak-turbulence Kolmogorov scaling exponents it is necessary to transform the mode coupling Eq. (85) to a form showing the symmetry of the exchange of any two of the three waves $\{k_i,\omega_{k_i}\}_{i=1}^3$ where $\mathbf{k}_3=-\mathbf{k}$, $\omega_3=-\omega_{\mathbf{k}}=\omega_{\mathbf{k}_3}$ and $\Sigma^3{}_{i=1}\mathbf{k}_i=\Sigma^3{}_{i=1}\omega_i=0$. The transformation of $\phi_{\mathbf{k}_i}(t)$ to $a_{\mathbf{k}_i}(t)$ required to show the wave exchange symmetry follows from the Hamiltonian formulation of the wave dynamics with $i\dot{a}_j=\delta H/\delta a_j^*$ where the field Hamiltonian is expanded in powers of $a_{k_j}(t)$ with

$$H=\sum_j \omega_{k_j}a_j^*a_j+\frac{1}{3!}\sum_{i,j,k} V_{ijk}a_ia_ja_k\delta_{\mathbf{k}_i+\mathbf{k}_j+\mathbf{k}_{k,0}}+\cdots \tag{90}$$

(Balk *et al.*, 1990; Zakharov *et al.*, 1992). The result of the Hamiltonian analysis is that the usual prescription of introducing the plasmon number spectrum by $n_{\mathbf{k}}=W_{\mathbf{k}}/|\omega_{\mathbf{k}}|=a_{\mathbf{k}}^*a_{\mathbf{k}}$ and thus $a_{\mathbf{k}}(t)=(1+k^2)\phi_{\mathbf{k}}(t)/|k_y|^{1/2}$ gives the desired symmetric interaction elements $V_{\mathbf{k}\mathbf{k}_1\mathbf{k}_2}$.

It is straightforward to show that the mode coupling elements $\Lambda^{\mathbf{k}}_{\mathbf{k}_1\mathbf{k}_2}$ in Eq. (86) are transformed to the fully symmetric $V_{kk_1k_2}$ for the $a_k(t)$ dynamics by

$$\begin{aligned}V_{-k_3,k_1,k_2}&=\left|\frac{k_{1y}k_{2y}}{k_{3y}}\right|^{1/2}\frac{(1+k^2)\Lambda^k_{k_1,k_2}}{(1+k_1^2)(1+k_2^2)}\\&=|k_{1y}k_{2y}k_{3y}|^{1/2}\left[\frac{k_{x1}}{1+k_1^2}+\frac{k_{x2}}{1+k_2^2}+\frac{k_{x3}}{1+k_3^2}\right]\end{aligned} \tag{91}$$

which has complete symmetry in the interchange of any two of the three waves. In making the reduction shown in Eq. (91) the resonance condition (88) must be used. Equation (91) makes clear that the maximum amplitude limit is determined by $1/k_x$.

Now for sufficiently short-wave interaction times the dispersion of the wave frequencies $\omega_{\mathbf{k}}$ over the spectrum of $W(\mathbf{k},t)=|\omega_{\mathbf{k}}|n_{\mathbf{k}}(t)$ allows the fluctuation dynamics to be described by the classical wave kinetic equation (Sagdeev and Galeev, 1968):

$$\begin{aligned}\frac{dn_{\mathbf{k}}}{dt}=4\pi\int d\mathbf{k}_1d\mathbf{k}_2|V_{\mathbf{k}\mathbf{k}_1\mathbf{k}_2}|^2\delta(\mathbf{k}-\mathbf{k}_1-\mathbf{k}_2)\\\times\delta(\omega_{\mathbf{k}}-\omega_{\mathbf{k}_1}-\omega_{\mathbf{k}_2})[n_{\mathbf{k}_1}n_{\mathbf{k}_2}-n_{\mathbf{k}}n_{\mathbf{k}_1}sg(\omega_{\mathbf{k}}\omega_{\mathbf{k}_2})\\-n_{\mathbf{k}}n_{\mathbf{k}_2}sg(\omega_{\mathbf{k}}\omega_{\mathbf{k}_1})].\end{aligned} \tag{92}$$

The kinetic Eq. (92) gives the time rate of change of any functional F with flux $f_{\mathbf{k}}$ defined by

$$F(t)=\frac{1}{2}\int f_{\mathbf{k}}sg(\omega_{\mathbf{k}})n_{\mathbf{k}}(t)d\mathbf{k}$$

as

$$\frac{dF}{dt}=2\pi\sum |V_{\mathbf{k}\mathbf{k}_1\mathbf{k}_2}|^2\delta(\mathbf{k}-\mathbf{k}_1-\mathbf{k}_2)$$
$$\times\delta(\omega_{\mathbf{k}}-\omega_{\mathbf{k}_1}-\omega_{\mathbf{k}_2})n_{\mathbf{k}}n_{\mathbf{k}_1}n_{\mathbf{k}_2}(f_{\mathbf{k}}-f_{\mathbf{k}_1}-f_{\mathbf{k}_2})$$
$$\times\left(\frac{sg(\omega_{\mathbf{k}})}{n_{\mathbf{k}}}-\frac{sg(\omega_{\mathbf{k}_1})}{n_{\mathbf{k}_1}}-\frac{sg(\omega_{\mathbf{k}_2})}{n_{\mathbf{k}_2}}\right)d\mathbf{k}\,d\mathbf{k}_1d\mathbf{k}_2. \tag{93}$$

Thus any flux $f_{\mathbf{k}}$ which is conserved

$$f_{\mathbf{k}}=f_{\mathbf{k}_1}+f_{\mathbf{k}_2} \tag{94}$$

under the resonant interactions defined by Eq. (88) gives an integral of the motion through Eq. (93) with $dF/dt\equiv 0$. Thus from the resonance conditions (88) themselves the total energy-momentum conservation laws for

$$W=\int W(\mathbf{k})d\mathbf{k}\equiv\frac{1}{2}\int|\omega_{\mathbf{k}}|n(\mathbf{k})d\mathbf{k}, \tag{95}$$

$$P_x=\int k_x n(\mathbf{k})sg(\omega_k)d\mathbf{k}, \tag{96}$$

$$P_y=\int k_y n(\mathbf{k})sg(\omega_k)d\mathbf{k} \tag{97}$$

immediately follow. The conserved P_y momentum is equivalent to the enstrophy conservation using $k_y n_{\mathbf{k}}sg(\omega_{\mathbf{k}})=(1+k^2)|\phi_{\mathbf{k}}|^2$ so that $P_y=W+U$ is defined. The momentum $P_x=0$ for a symmetric or antisymmetric wave field $\phi(-x,y,t)=\pm\phi(x,y,t)$ which reduces the invariants to W and U. In general for solutions with a broken symmetry in x the momentum P_x in the direction of the equilibrium gradients $P_x\neq 0$, and the conservation of P_x gives a constraint on the radial transport.

The fastest transport in $\mathbf{k}$ space is the nonlocal transport from the region of $|\mathbf{k}_1|\ll|\mathbf{k}|$ in Fig. 15 where the large scale ($|\mathbf{k}_1|\rho_s\ll 1$) fluctuations produce a flux of energy from ($k_x=0$, $k_y\rho_s\sim 1$) to $|k_x|\gg|k_y|$ along the curves of constant

$$\nu_{\mathbf{k}}=k_y v_d-\omega_{\mathbf{k}}=\frac{k_y v_d(k_x^2+k_y^2)}{1+k_x^2+k_y^2} \tag{98}$$

shown in Fig. 16. The transport of fluctuation energy along the curves of constant $\nu_{\mathbf{k}}$ leads directly to the buildup of strong, small scale zonal flows with $|k_x|\gg|k_y|$. The fluctuation spectrum $W(k_x,|k_y|\ll 1)$ has a steep power lower drop-off $1/|k_x|^{\nu_x}$ with $\nu_x\geqslant 2$ for $k_x>1$. We now derive the various Kolmogorov scaling exponents in the two scaling zones of $\mathbf{k}$ space.

C. Wave number spectral exponents

The dynamics of the turbulent interactions has different strengths in the long-wave $k\ll\rho_s^{-1}$ and short-wave $k\gg\rho_s^{-1}$ regions. The scaling properties for these two regions follow from the scaling laws for the dispersion and interaction elements for the waves

$$\omega_{qk}=q^{\alpha}\omega_k,$$

$$V_{qk,qk_1,qk_2}=q^{\beta}V_{k,k_1,k_2}, \tag{99}$$

where q is the scaling factor for the wave number $k\rightarrow qk$ and $\alpha=(\alpha_x,\alpha_y)$ and $\beta=(\beta_x,\beta_y)$ are the scaling exponents. From Eq. (91) we see that for the short waves $\alpha=(-2,1)$ and $\beta=(-1,\frac{3}{2})$; whereas, for long waves $\alpha=(2,1)$ and $\beta=(3,\frac{3}{2})$. For long waves the relevant dispersion law for scaling is for $\nu_{\mathbf{k}}=\omega_{\mathbf{k}}-k_y v_d$ rather than $\omega_{\mathbf{k}}$. Using the scaling analysis of Zakharov as applied to drift-Rossby waves by Novakovskii *et al.* (1988) and Balk *et al.* (1991) we obtain the following wave number distributions:

$$W(k_x,k_y)=\begin{cases}W_0\left(\frac{k_0}{k_x}\right)^2\left(\frac{k_0}{k_y}\right)^{3/2} & k\rho_s\gg 1\\ W_0\left(\frac{k_0}{k_x}\right)^3\left(\frac{k_0}{k_y}\right)^{3/2} & k\rho_s\ll 1.\end{cases} \tag{100}$$

These scaling laws are required for $dn(\mathbf{k})/dt=0$ in the inertial range of $\mathbf{k}$ where $\gamma(\mathbf{k})=0$. With the omnidirectional k scaling following from Eq. (100) the two scaling law regimes are $W(k)=W_0(k_0/k)^{7/2}$ for $k\rho\gg 1$ and $W_0(k_0/k)^{9/2}$ for $k\rho<1$, where the exponents $\frac{7}{2}$ and $\frac{9}{2}$ bracket the scaling exponent of 4 reported by Hasegawa and Mima (1978). An exponent of 4 leads to the omnidirectional spectral energy density $\int dk\,kW(k)=\int dk\,W_0(k_0/k)^3$ with spectral index 3. The exponent of 3 is commonly used in practical estimates of drift-wave transport and appears consistent with the fluctuation spectrum inferred from electromagnetic scattering measurements. These spectral exponents are only strictly valid in the inertial range, although in regions above the maximum growth rate γ_k they appear to be good approximations to the simulations.

The statistical equilibrium for the undriven Hamiltonian system corresponds to the local thermodynamic equilibrium $n^{eq}(\mathbf{k})=T/[|\omega_{\mathbf{k}}|+|k_y|V]$ corresponding to the Rayleigh-Jeans law for the system. Here T and V are constants determined by the initial data. This thermodynamic equipartition solution has zero energy-momentum flux in $\mathbf{k}$ space. The finite energy-momentum flux through the inertial range is driven by the slope of the Kolmogorov-type spectra (100). Thus the driven damped system must develop spectra of the Kolmogorov-type in the inertial range as we now illustrate with numerical simulations. When the driving damping are turned off in a turbulent state, the spectrum rapidly evolves to the thermodynamic equilibrium $n^{eq}(\mathbf{k})$.

In conclusion we see that the wave-kinetic equation is a useful theoretical tool for understanding the turbulent spectrum. Numerically, however, the method is slow and leaves open many questions as to the role of the missing higher order correlations so that the method is used rarely today. A test of a renormalized form of Eq. (92) with the direct numerical solution to the equation was performed by Waltz (1983) on a relatively small grid. The work shows the difficulties with adopting this procedure. A more precise comparison can be made for the model problem of a single triplet of interactions. For this

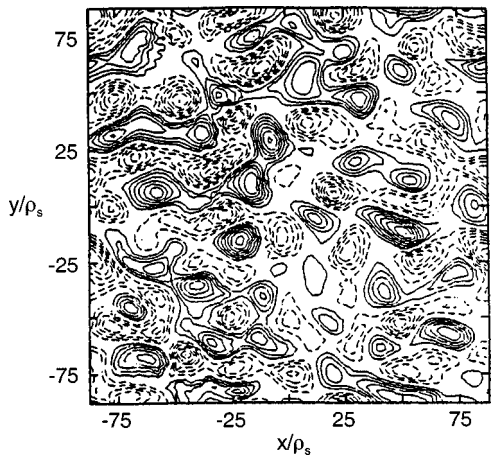

FIG. 17. Isopotential contours computed from direct numerical simulations of the driven damped Hasegawa-Mima equation.

idealized model problem Krommes (1982) shows that by using the direct interaction approximation (DIA) procedure the three-field correlations represented by the delta function on the frequency sum in Eq. (92) is replaced with a nonlinear propagator that allows good agreement to be obtained with the ensemble average for the triplet interaction problem.

D. Inertial range simulations

A test of the scaling exponents and the shape of the long-wavelength spectral density for the driven damped Hasegawa-Mima equation was carried out by Horton, Su, and Morrison (1990). In these tests the Hasegawa-Mima equation is solved in a truncated **k** space using the mode coupling elements $\Lambda^{\mathbf{k}}_{\mathbf{k}_1,\mathbf{k}_2}$. To study the inertial range the source-sink term $\gamma_{\mathbf{k}}\phi_{\mathbf{k}}(t)$ is added to the right-hand side by $\omega_{\mathbf{k}}\rightarrow\omega_{\mathbf{k}}+i\gamma_{\mathbf{k}}$ with the choice

$$\gamma_{\mathbf{k}}=\begin{cases}\gamma_0=+0.005 & \text{for } 0.35\leqslant|\mathbf{k}|\leqslant 0.4\\ 0 & \text{for } 0.4<|\mathbf{k}|<2.0\\ -\gamma_0=-0.005 & \text{for } |\mathbf{k}|>2.0.\end{cases} \tag{101}$$

Computations were carried out on the grid with $\mathbf{k}=(m,n)k_1$ with $k_1\rho_s=0.05$ giving the periodic box size of $(126\rho_s)^2$ for times up to $t_{\max}=1000[L_n/c_s]$. Contour plots of the potential field $\phi(x,y,t=5000)$ are given in Fig. 17. The simulation energy spectra in the steady state are peaked at $k\rho=0.35$ (the source region) and decay in the inertial range as shown in Fig. 18. Parametrizing the numerically computed one-dimensional projections with regression fits to

$$W^{\rm num}(k_x)=\sum_{k_y} W(k_x,k_y)\leftrightarrow\frac{1}{|k_x|^{m_x}},$$
$$W^{\rm num}(k_y)=\sum_{k_x} W(k_x,k_y)\leftrightarrow\frac{1}{|k_y|^{m_y}}, \tag{102}$$

the simulation determines the values of $m_x\pm\delta m_x$ and $m_y\pm\delta m_y$ for mean and uncertainty in the exponents.

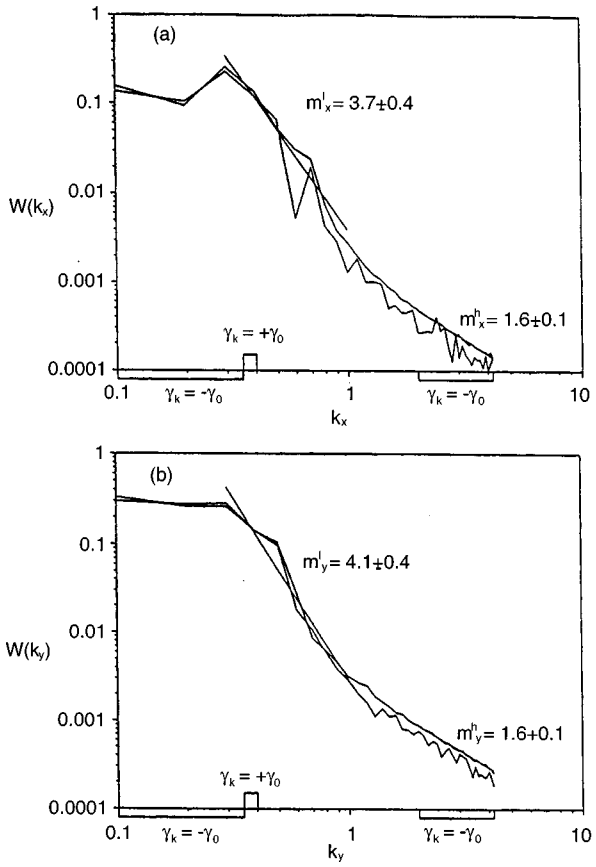

FIG. 18. The anisotropic spectral distribution of wave energy for the driven damped Hasegawa-Mima equation. Spectral indices are computed for comparison with weak turbulence theory.

The simulations show the change in the indices m_x, m_y in the high (m^h) and low (m^l) wave number regimes as expected from the scaling theory Eq. (100). The exponents found in the example given in Eq. (101) shown in Fig. 18 are

$$m^h_x=1.6\pm0.1,\quad m^h_y=1.6\pm0.1\quad\text{for } k>1,$$
$$m^l_x=3.7\pm0.4,\quad m^l_y=4.1\pm0.4\quad\text{for } k<1, \tag{103}$$

which confirms the trend but not the values of the scaling laws based on the asymptotic forms in Eq. (100). The steeper decrease of the numerical k_xk_y spectrum is presumably due to the compressed inertial range used in the test.

In the steady state shown in Figs. 17 and 18 the total turbulent energy density and enstrophy are $W=0.8$ and $U=0.3$ in units of $(\rho_s/L_n)^2n_0T_e$. The space-time averaged kurtosis and skewness of ϕ are 2.9 and -0.1, respectively. The equipotential contours at time $tv_d/\rho_s=5000$ are shown in Fig. 17 along with the maximum and minimum values of ϕ. The system appears to be within the state of weak turbulence ($\Omega_E=2\phi_m/r_0^2\lesssim|\omega_*|\simeq v_d/r_0$) for these small values of γ_0.

Even in the isotropic, 2D Euler limit the question of the value of spectral index remains an active area of research. High-resolution simulations of the forced

damped 2D Euler equation persistently show energy spectral decays faster than the rate $k^{-3}[\ln(k/k_1)]^{-1/3}$ predicted by space filling, isotropic, homogeneous turbulence theory. The reason for the larger decay indices has been traced to the emergence of long-lived, coherent vortex structures (McWilliams, 1984; Legras *et al.*, 1988). The high-resolution simulations of Legras *et al.* (1988) show clearly the correlation of larger decay indices ($m \simeq 4$) with the appearance of monopole, dipole, and tripolar vortices. Legras *et al.* (1988) compare the spectral indices and the associated vortex structures for $(512)^2$ simulations obtained with the three types of drivers: (i) constant, single mode $\mathbf{k}=(k_I,0)$ external forcing, (ii) stochastic, narrow-band external forcing $\tilde{F}(k_1<|\mathbf{k}|<k_2)$ taken with new random phases at each time step, and (iii) narrow-band linear growth rate similar to that given in Eq. (101). A large-scale damping rate $-\nu_L\phi(\mathbf{k})$ and a hyperviscosity $-\nu_s(k_\perp^2)^p\phi(\mathbf{k})$ are used to produce the steady state. The resulting turbulence is characterized by the spectral index m and its vortex content as follows: (i) $m=3.6$ and a low-packing fraction of relatively large vortices, (ii) $m=3.5$ and a denser packing of smaller vortices, and (iii) $m=4.2$ and the prominence of several dipolar vortices and one tripolar vortex. Thus, it appears that for 2D turbulence the space-filling, inverse cascade spectrum of $k^{-3}[\ln(k/k_1)]^{-1/3}$ is an idealization that is not achieved in practice due to the strong, self-organization properties of these turbulent flows. Further, clear demonstrations of the suppression of turbulent cascades by coherent vortices in 2D turbulence are given by McWilliams (1990a, 1990b) and Larichev and McWilliams (1991).

In contrast, in the next subsection we consider the case where self-consistent wave growth and damping due to electron-ion collisions are used to drive the system. For typical values of these parameters the system enters a state of strong turbulence which is a more isotropic state of turbulence with a short correlation time. The system has no inertial range since the linear growth/damping $\gamma(\mathbf{k})$ extends throughout the $\mathbf{k}$ space.

E. Self-consistent driven damped nonlinear drift-wave equation

Fluctuations in tokamaks with characteristics of the drift waves are widely observed in many confinement experiments since the 1976–78 electromagnetic scattering experiments described in Sec. II.B. The exact nature of the driving and damping mechanisms has proven difficult to determine experimentally (Bravenec *et al.*, 1992) and presumably varies widely with the confinement system parameters, the plasma parameters, and plasma profiles as linear stability theory predicts. The simplest and earliest studied form of driving and damping of the drift-wave fluctuations occurs through the electron-ion collisions that determine the plasma resistivity $\eta=m_e\nu_{ei}/n_e e^2$ and the ion-ion collisions that determine the plasma viscosities $\mu_\perp=0.3\nu_{ii}\rho_i^2$ and $\mu_\parallel=(T_i/m_i\nu_{ii})$. For fluctuations with wave numbers $k_\perp, k_\parallel$ perpendicular to and parallel to the magnetic field the associated decay rates ν are

$$\nu_\parallel^\eta=\frac{k_\parallel^2 T_e}{\eta e^2 n_e}=\frac{k_\parallel^2 v_e^2}{\nu_{ei}}\leqslant|k_\parallel|v_e,$$
$$\nu_\parallel^\mu=\frac{k_\parallel^2 v_i^2}{\nu_i}\leqslant|k_\parallel|v_i, \tag{104}$$
$$\nu_\perp^\mu=\frac{k_\perp^2\mu_\perp}{1+A_p/(k_\perp\rho_s)^2}=\begin{cases}0.3k_\perp^2\rho_i^2\nu_{ii} & A_p=0\\ 0.3k_\perp^4\rho_s^2\rho_i^2\nu_{ii} & k_\perp^2\rho_s^2\ll A_p=1,\end{cases}$$

where $A_p=0$ for resistive-g modes and the Hasegawa and Wakatani (1983) model and $A_p=1$ for adiabatic electrons in the ITG and Hasegawa-Mima models (1978). For drift waves the resistive diffusion $\nu_\parallel^\eta$ is destabilizing and the viscous dampings $(\nu_\perp^\mu,\nu_\parallel^\mu)$ are stabilizing. In the limit of low collision frequency the dissipation is replaced with the collisionless Landau damping which is adequately described by the limiting formulas $\nu_\parallel^\eta\to|k_\parallel|v_e$ and $\nu_\parallel^\mu\to|k_\parallel|v_i$ and $\nu_\perp^\mu\to 0$.

There are two well-known descriptions of the resistive-dissipative drift-wave turbulence: (1) the $i\delta_k$ model (Horton, 1976; Terry and Horton, 1982) that retains the single field description but introduces an anti-Hermitian operator $\hat{\mathcal{L}}^{ah}\phi$ to include the effects of the dissipation, and (2) the Hasegawa-Wakatani model (1983) that introduces two fields, the density and the electrostatic potential to describe the dissipative dynamics and the partial decoupling of the density and potential that occurs when the dissipation is strong. For weak dissipation the Hasegawa-Wakatani equation reduces to the $i\delta_k$ model (Horton, 1986). A more complete collisional description that includes the coupling to the ion acoustic waves and the electron temperature fluctuations $(\tilde{\phi},\tilde{n},\tilde{u}_\parallel,\tilde{T}_e)$ is given by Hinton and Horton (1971) in a work that interprets the first collisional drift-wave experiments. The drift-wave measurements analyzed were those of Hendel *et al.* (1968) in a long, straight cylindrical geometry containing a thermionically ionized cesium plasma, a device called a Q machine for the quiescent plasma produced. The four-field system $(\tilde{\phi},\tilde{n},\tilde{u}_\parallel,\tilde{T}_e)$ and other reduced equations drift-wave models are analyzed in detail in Scott (1992) and Brizzard (1992, 1996). Here we restrict the discussion to the Terry-Horton $i\delta_k$ model and the Hasegawa-Wakatani equations.

In the limit of weak dissipation the electron density response to the electrostatic potential is nonlocal and dissipative as given by

$$\tilde{n}(x,y,t)=\frac{en_0}{T_e}\left[\phi+\delta_0(c_1+\nabla^2)\frac{\partial\phi}{\partial y}\right]$$
$$=\left(\frac{en_0}{T_e}\right)(1+\hat{\mathcal{L}}^{ah})\phi, \tag{105}$$

where the anti-Hermitian operator $\mathcal{L}^{ah}$ is of strength δ_0 has the power series expansion $\delta_0(c_1+c_2\nabla^2+c_3\nabla^4+\cdots)\partial_y$. With the generalization of the electron density

response in Eq. (105) it is straightforward to repeat the analysis to obtain the dissipative drift-wave equation used by Horton and his collaborators:

$$\hat{\mathcal{L}}\frac{\partial\phi}{\partial t}+v_d\frac{\partial\phi}{\partial y}+\left[\frac{\partial\phi}{\partial x}\frac{\partial}{\partial y}(\hat{\mathcal{L}}\phi)-\frac{\partial\phi}{\partial y}\frac{\partial}{\partial x}(\hat{\mathcal{L}}\phi)\right]+\mu\nabla^4\phi=0, \tag{106}$$

where

$$\hat{\mathcal{L}}=1-\nabla^2+\hat{\mathcal{L}}^{ah} \tag{107}$$

and μ is the perpendicular ion viscosity that arises from the divergence of the ion cross-field current

$$\mathbf{j}_\perp=\left(\frac{c\mathbf{B}}{B^2}\right)\times\left[m_i n_i\left(\frac{d\mathbf{v}_\perp}{dt}\right)-\mu_\perp\nabla^2\mathbf{v}_\perp\right] \tag{108}$$

with $\mathbf{v}_\perp=c\mathbf{E}\times\mathbf{B}/B^2=c\hat{\mathbf{z}}\times\nabla\phi/B$. The model equation is also called the $\mathbf{E}\times\mathbf{B}$ nonlinear drift-wave model since the nonlinearity of the Poisson bracket now contains both the polarization drift $[\phi,\nabla^2\phi]$ nonlinearity and the nonlinearity due to the $\mathbf{E}\times\mathbf{B}$ convection of the density

$$\mathbf{v}_E\cdot\nabla n=[\phi,n]=[\phi,\hat{\mathcal{L}}^{ah}\phi]. \tag{109}$$

Waltz (1983, 1990) has compared the contributions of the two nonlinearities and shown from simulations that the $\mathbf{E}\times\mathbf{B}$ nonlinearity is essential for saturation at the mixing length level. Without the $\mathbf{E}\times\mathbf{B}$ nonlinearity the rms amplitude of the fluctuations continues to increase with δ_0 beyond the mixing length (ml) level given by

$$\frac{\tilde{n}^{ml}}{n}\sim\frac{e\tilde{\phi}^{ml}}{T_e}\sim\frac{\lambda_x}{n_0}\frac{dn_0}{dx}. \tag{110}$$

The linear modes for the dissipative equation are given by

$$\omega_{\mathbf{k}}+i\gamma_{\mathbf{k}}=\frac{k_y v_d-i\mu_\perp k_\perp^4}{1+k_\perp^2+i\delta_0 k_y(c_1-k_\perp^2)} \tag{111}$$

with γ_k being positive in the region of $k\rho<1$ with $\gamma_{\mathbf{k}}^l\simeq k_y^2\delta_0(k_\perp^2-c_1)/(1+k_\perp^2)^2$ and negative in the short wave region $k\rho>1$ with $\gamma_{\mathbf{k}}\simeq-\mu_\perp k_\perp^4/(1+k_\perp^2)$. A typical distribution of $\gamma(k_x,k_y)$ is shown in Fig. 14.

The importance of the $\mathbf{E}\times\mathbf{B}$ nonlinearity in Eq. (109) and how this term is responsible for the mixing length level of saturation in Eq. (110) rather than the $\mathbf{v}_E\cdot\nabla\nabla^2\varphi$ nonlinearity of the Hasegawa-Mima Eq. (79) was made clear by Waltz and Dominguez (1983) and Waltz (1983). Figure 19 from that work shows the dependence on the amplitude in frame (a) and the diffusivity in frame (b) with the driving damping scaling factor $S=\delta_0$ as defined here. With only the vorticity advection nonlinearity the amplitude of the fluctuations increases linearly with δ_0 as opposed to Eq. (110). With the $\mathbf{E}\times\mathbf{B}$ nonlinearity the amplitude remains close to the mixing length level of Eq. (110) until $\delta_0>0.5$ whereupon there is an increase shown in Fig. 19. The diffusivity follows the mixing length rule $D=\gamma/\langle k_x^2\rangle\propto\delta_0$ with the $\mathbf{E}\times\mathbf{B}$ nonlinear present, but D increases with δ_0^3 with only the advection of vorticity as shown in Fig. 19.

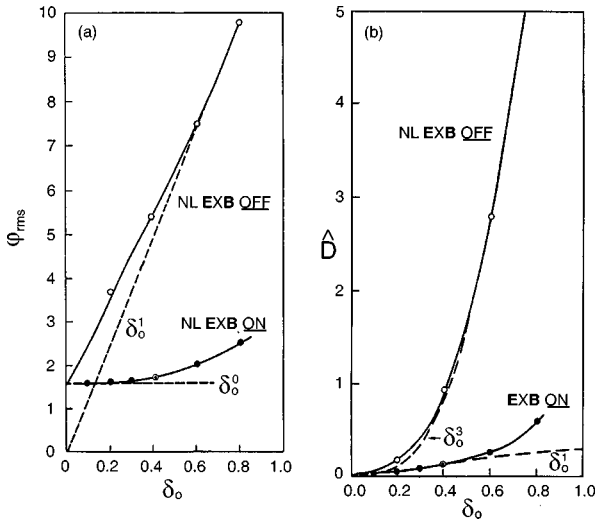

FIG. 19. Scaling of the drift-wave turbulence with δ_0. In frame (a) the scaling of the rms potential fluctuation level and (b) the normalized diffusivity $D/D_{\rm dw}$ for the Hasegawa-Mima nonlinearity (open circles) and the self-consistent nonlinear drift-wave Eq. (99) (solid circles) containing the $\mathbf{E}\times\mathbf{B}$ nonlinearity in the convection of the density (from Waltz and Dominguez, 1983).

Both the direct numerical simulation (Waltz, 1983) and the "direct interaction approximation" (Waltz and Dominguez, 1983) show the results given in Fig. 19.

The relationship between the "mixing length" description of turbulence and the "direct interaction approximation" and renormalized toroidal turbulence theories are analyzed by Sudan and Pfirsch (1985). Sudan and Keskinen (1979) show the importance of the $\mathbf{E}\times\mathbf{B}$ convection of the plasma density for the ionospheric equivalent of the drift wave. The details of the wave number spectrum and the appearance of coherent structures in the ionospheric convective-drift problem were established by Sudan *et al.* (1997).

The dissipative nonlinear drift-wave equation shows both regimes of weak turbulence with $W=\Sigma_{\mathbf{k}}W(\mathbf{k})\ll1$ and strong turbulence $W\gg1$ where the vortex gas dynamics dominates. An example of the vortex gas regime is shown in Fig. 17 where the parameter set is $\{\delta_0,c_1,\mu\}=\{1/4,-1/4,0.005\}$, taken to be representative of the trapped electron turbulence in tokamaks, is used. The total energy and enstrophy in the saturated state is $W=25.6$ and $U=2.1$, which gives a mean wave number of $\bar{k}\rho_s=(U/W)^{1/2}=0.28$. The dimensionless dissipative Reynolds number for the system is

$$R_{en}=\frac{\tilde{v}_E L}{\mu}=2\times10^3, \tag{112}$$

where $L=62.8\rho_s$. The dimensionless $\mathbf{E}\times\mathbf{B}$ rotation number, sometimes called the Kubo number, formed by the ratio of the convective derivative nonlinearity and the wave frequency $\omega_{\bar{k}}$ is

$$R_E=\frac{\bar{k}\tilde{v}_E}{\omega_{\bar{k}}}\simeq2, \tag{113}$$

a value of R_E characteristic of drift-wave vortices with speeds close to the drift-wave speed. Having $R_E>1$ puts the drift-wave dynamics in the regime of self-trapping of the wave energy into vortices. With $\omega_{\mathbf{k}}\rightarrow\omega_{\mathbf{k}}-\mathbf{k}\cdot\mathbf{u}$ the rotation number R_E is a Galilean invariant giving the amount of rotation around vortex as in Fig. 1, during the oscillation period of the intrinsic collective modes $(\mathbf{k},\omega_{\mathbf{k}})$. This regime of self-trapping significantly reduces the effect of inhomogeneities on the waves, as shown in Sec. V.F, and greatly increases the lifetime of the fluctuations.

Newman *et al.* (1993) give further insight into the different roles of the $n\mathbf{E}\times\mathbf{B}$ nonlinearity and the $\mathbf{v}_E\cdot\nabla\mathbf{v}_E$ polarization current nonlinearity. The steady-state spectrum is subjected to an impulse of energy localized at a fixed annulus $|\mathbf{k}|=k_0$ and the relaxation to the original steady state is observed. It is found that the $\mathbf{E}\times\mathbf{B}$ nonlinearity gives a prompt nonlocal transfer throughout $\mathbf{k}$ space by means of lattice structure of nonlocal couplings. In contrast, the polarization drift gives a diffusivelike local transfer. Newman *et al.* (1993) show that there is a cross-coupling effect from the two nonlinearities giving rise to nonlinear frequency shifts that lead to intermittency in the time dependence of the turbulence.

The Terry-Horton model given by Eq. (106) has been extended by Crotinger and Dupree (1992) and Naulin and Spatschek (1997) to take into account the nonlinear phase shift in Eq. (105). The resulting equation describes accurately the electron Landau damping of vortex structures with $\omega>k_y v_{\mathrm{de}}$. The turbulence generated by the extended model shows an intermittent creation and damping of coherent vortex structures. The vortices are shown to have a radial drift down (up) the density gradient when $\delta n=n_0(e\phi/T_e)>0(\delta n<0)$.

Signal processing techniques for directly testing for the quadratic mode coupling as in Eq. (85) have been developed (Kim and Powers, 1978). An example from the torsatron stellarator edge fluctuation data confirming the importance of the quadratic mode coupling components is given by Hidalgo *et al.* (1993).

F. Onset of self-trapping from $\mathbf{E}\times\mathbf{B}$ nonlinearity: Drift-wave vortices

The condition for self-trapping is that the amplitude of a disturbance be just above the mixing length level corresponding to Eq. (110). Noting that a circular vortex of radius r_0 has an effective wave number $\overline{k}r_0\simeq\pi$ and using $\omega_{\overline{k}}/k_y\cong v_d$ and $\tilde{v}_E=\overline{k}c\tilde{\phi}/B$ we obtain from Eq. (113)

$$\frac{c\phi_{\max}}{B}>r_0 v_d=\frac{r_0}{L_n}\frac{cT_e}{eB}\frac{2}{\pi} \tag{114}$$

which corresponds to an amplitude just above the mixing length level (110).

In the vortex regime (114) there is trapped fluid or plasma (Horton and Petviashvili, 1993) that rotates around the potential maximum at the rate Ω_E. We calculate the rotation rate from the local model of a vortex with $\phi=\phi_{\max}(1-r^2/r_0^2)$ to obtain the angular rotation frequency

$$\Omega_E=\frac{v_\theta}{r}=\frac{c}{rB}\frac{d\phi}{dr}=-\frac{2c\phi_{\max}}{Br_0^2} \tag{115}$$

which is clockwise for $\phi_{\max}>0$ where the pressure and density are high (anticyclone) and counterclockwise for $\phi_{\max}<0$ where the pressure and density are low (cyclone).

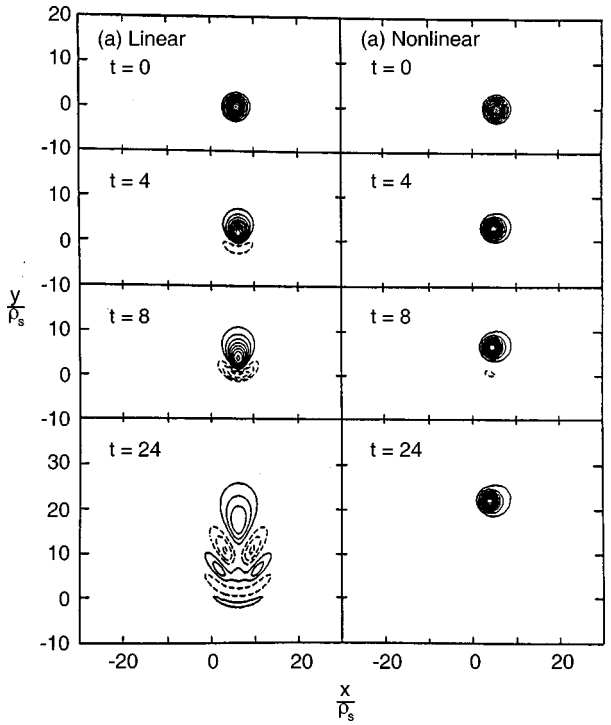

FIG. 20. An initial value experiment with the Hasegawa-Mima equation illustrating the self-trapping for amplitudes satisfying the trapping condition (114). The time values are in units of L_n/c_s.

In Fig. 20 we show an example of the self-trapping of the drift wake field by the $\mathbf{E}\times\mathbf{B}$ nonlinearity. We compare the propagation from the initial Gaussian disturbance of radius $6\rho_s$ given by the Hasegawa-Mima Eq. (79). The small amplitude linear wave propagation is shown in the left column (a) and the nonlinear evolution for an initial amplitude well above the trapping condition (107) is shown in the right column. In the linear wave the energy propagates with all speeds between zero and v_d (=1 in the simulation space-time units $\rho_s, L_n/c_s$) and spreads in x. In the high-amplitude disturbance the rapid angular rotation (115) traps the fluctuation energy except for small wake seen at $t=80[L_n/c_s]$ on the linear scale. Note that a small dipolar distortion under the large anticyclone is created in Fig. 20. A theory for the interaction of coherent vortices with the wave turbulence is developed in Muhm *et al.* (1992). A search for vortex structures in the shear flow layer of the TEXT tokamak (see Table I) is given in Filippas *et al.* (1995) using conditional averaging techniques.

These vortices, as shown in Fig. 18, are observed in rotating water tank experiments by Nezlin (1986), Antonova *et al.* (1983), Antipov *et al.* (1982), and Behringer *et al.* (1991). In accord with the Hasegawa-Mima equation vortices of positive (anticyclones) and negative $\phi_{\max}$ (cyclones) are equivalent having the same lifetime. Both are observed to have long lifetimes when $2\pi/\Omega_E$ is small compared to the linear wave period and the dissipation time scale from the friction of the rotating fluid with the walls of the vessel. Some experiments (Nezlin, 1986; Nezlin and Snezhkin, 1993), however, show that the anticyclone has a longer lifetime than the cyclone which is not a property predicted by the dissipative Eq. (113) which has the symmetry $\phi(-x,y,t)=-\phi(x,y,t)$. The resolution of this problem is that for larger scale vortices ($r_0 \gg \rho_s$) there is a structural change in the nonlinear equation that brings in the new nonlinearity

$$\alpha\phi\frac{\partial\phi}{\partial y} \equiv \text{scalar or KdV nonlinearity} \tag{116}$$

that has the property of removing the degeneracy of the cyclones and anticyclones. Nezlin (1986) argues, as supported by theory and simulations, that this nonlinearity (116) is important in the rotating water tank experiments and has the sign of the strength parameter α such that the anticyclonic vortices form the long-lived self-organized structures. Historically, the KdV nonlinearity of the drift-wave problem was the first nonlinearity to be found (Tasso, 1967). Petviashvili (1977, 1980) used this nonlinearity extensively in the earlier work on drift waves.

G. Resistive drift-wave turbulence

The collisional drift wave is a paradigm for anomalous transport that has been extensively investigated with many different modelings. A particularly simple 2D model, called the Hasegawa-Wakatani model, with an adiabaticity parameter α has been investigated by Wakatani and Hasegawa (1984), Krommes and Hu (1994), Sugama *et al.* (1988), Gang, Diamond, and Rosenbluth (1991), Koniges *et al.* (1992), Biskamp *et al.* (1994), and Hu *et al.* (1995). To understand the origin of the simple α model and to appreciate its limits we briefly present the 3D resistive drift model.

For finite resistivity $\eta=m_e\nu_e/n_e e^2$ the parallel current carried by the electrons in Eq. (10) yields $j_\parallel=-(n_e e^2/m_e\nu_e)\nabla_\parallel(\phi-(T_e/e)\ln n)$ using the isothermal approximation $\delta p_e=T_e\delta n_e$. The collisional drift-wave equation follows from the divergence of the current $\nabla\cdot\mathbf{j}=0$ with the polarization current balancing $j_\parallel$ through $\nabla\cdot\mathbf{j}_p=-\nabla_\parallel j_\parallel=\eta^{-1}\nabla_\parallel^2(\phi-(T_e/e)\ln n)$ and the electron continuity equation. The rotational part of the plasma momentum for the vorticity $\nabla^2\varphi$ is equivalent to the current closure equation. The vorticity equation and the electron continuity equation give, in dimensional form

$$\frac{m_i n c}{B_0}\frac{d}{dt}\nabla^2\varphi=\frac{B_0}{c}\nabla_\parallel j_\parallel+\hat{\mathbf{z}}\cdot\nabla p_e\times\nabla\Omega, \tag{117}$$

$$\frac{d}{dt}(n_0+n_1)=\frac{1}{e}\nabla_\parallel j_\parallel+\frac{cT_e n_0}{eB_0}\hat{\mathbf{z}}\cdot\nabla\left(\frac{n_1}{n_0}-\frac{e\varphi}{T_e}\right)\times\nabla\Omega, \tag{118}$$

where $\nabla\Omega$ is the effective $\mathbf{g}$ force used to relate the curvature and gradient-B effects to the classical Rayleigh-Taylor instability. The computation of $\Omega(r)$ for the average curvature of the magnetic field line is extensively used in stellarator/heliotron research (Carreras *et al.*, 1987). The derivatives on the left side of Eqs. (117) and (118) are the $\mathbf{E}\times\mathbf{B}$ convective derivatives defined by $df/dt=\partial_t f+\mathbf{v}_E\cdot\nabla f$ using Eq. (80). The model Eqs. (117) and (118) have a conserved potential vorticity ζ given by

$$\zeta=\frac{m_i c^2}{eB^2}\nabla_\perp^2\varphi-\ln n_0-\frac{n_1}{n_0}-\Omega \tag{119}$$

which generalizes the potential vorticity already defined in Eq. (81). It is useful to first consider the dimensionless form of the model Eqs. (117) and (118) in global coordinates before using the local drift-wave units ρ_s and L_n/c_s. Using the minor radius a for the cross-field $B_0\hat{\mathbf{z}}$ dimensions, the major radius R for the dimensionless $z/R\to z$ and time in units $\omega_{ci}t(\rho_s/a)^2\to t$ [equivalent to $(cT_e/eBa^2)t\to t$], one finds that the natural amplitude variables are $e\varphi/T_e=\varphi$ and $n_1/n_0=n$, and the dimensionless parameters of the model are $\epsilon=a/R$, $\rho=\rho_s/a$, $\nu=\nu_e/\omega_{ce}$. The dimensionless model is then

$$\rho^2\frac{d}{dt}\nabla_\perp^2\varphi=\frac{\epsilon^2}{\nu}\nabla_\parallel^2(n-\varphi)-g\frac{\partial n}{\partial y}+\mu\nabla^2\varphi, \tag{120}$$

$$\frac{dn}{dt}=\frac{\epsilon^2}{\nu}\nabla_\parallel^2(n-\varphi)+\partial_x\ln n_0\frac{\partial\varphi}{\partial y}-g\frac{\partial}{\partial y}(n-\phi)+D\nabla^2 n, \tag{121}$$

where $g=d\Omega/dr$. This 3D model has resistive drift waves driven by the density gradient $(\partial_x n_0)^2$ through the charge separation from finite $k_\perp^2\rho_s^2$ and the resistive interchange driven modes from $\omega_*\omega_D>0$ where $\omega_D=(ck_\theta T/eB)(d\Omega/dr)$ is the averaged gradient-B/curvature drift frequency (Chen *et al.*, 1980). The linear eigenmodes are of two types: localized to the rational surfaces where $k_\parallel=0$ and global modes (Sugama *et al.*, 1988; Hong, Horton, *et al.*, 1991). The global modes are observed in the Heliotron and in the $H1$-Heliac (Schatz *et al.*, 1995).

Sugama, Wakatani, and Hasegawa (1988) carried out 3D simulations of this system and the results for one case are shown in Fig. 21. The density fluctuations are large and give a qualitative explanation of the similar tokamak and stellarator/helical device edge density fluctuations. The electric potential has the important property of developing an $m=0/n=0$ component with a well-defined circular null surface. This $\varphi_{0,0}(r,t)=0$ surface partially blocks the turbulent losses from the core of the cylindrical model. For stellarators the $m=1$, $n=1$ rational surface is near the edge of the plasma and the dominant modes in this simulation are the $m=3/n=2$ and $m=2/n=1$ fluctuations and the $m=0/n=0$ background profile for $v_\theta=-cE_r/B$. These simulations with

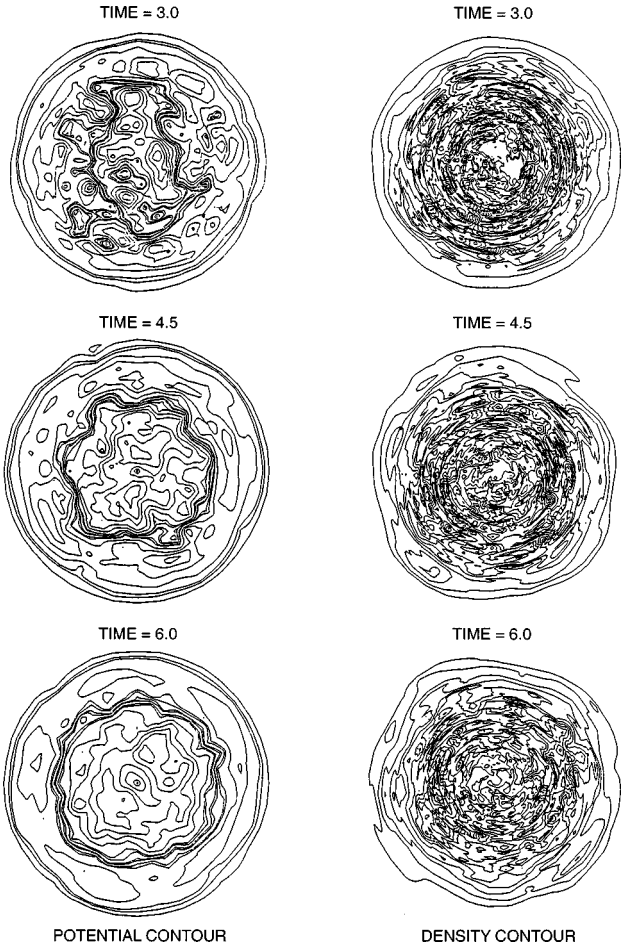

FIG. 21. The evolution of (a) the electrostatic potential and (b) the density contours for the 3D turbulence given by the resistive drift-wave model with average unfavorable toroidal curvature (courtesy of Wakatani). The time values are in units of $eBa^2/cT_e=(a/\rho_s)^2\omega_{ci}^{-1}$.

$\nu_e/\omega_{ce}=1.4\times10^{-4}$ are too collisional to apply to edge of major toroidal confinement devices (where $\nu_e/\omega_{ce}\lesssim10^{-6}$).

Wakatani *et al.* (1992) extend the investigation of the models (120) and (121) to include an externally imposed electric field $E_r(r)$ exceeding the strength of self-consistently field generated from the $m=0/n=0$ modes. The $E_r<0$ field suppresses the turbulence during the growth phases, but produces only a weak reduction of the flux in the saturated state. The collisionality dependence of the particle flux is shown to increase with ν_e for $\nu/\omega_{ce}<10^{-3}$ and then to increase as $\nu_e^{1/3}$ for $\nu/\omega_{ce}>10^{-3}$.

In the widely investigated 2D model of the Hasegawa-Wakatani Eqs. (120) and (121) the operator $\nabla_\parallel^2\to-\overline{k_\parallel^2}$ or $-1/\mathcal{L}_c^2$, where $\overline{k_\parallel}$ is the relevant mean parallel wave number and $\mathcal{L}_c$, is the connection length to the divertor end plates in the scrape-off layer (open field lines) modeling.

The space-time units are changed to the local scales of ρ_s and L_n/c_s in these 2D studies. The standard form of the Hasegawa-Wakatani 2D model is then

$$\frac{d}{dt}(\nabla^2\phi)=\alpha(\phi-n)+\mu\nabla^4\phi, \tag{122}$$

$$\frac{dn}{dt}=-\kappa\frac{\partial\phi}{\partial y}+\alpha(\phi-n)+D\nabla^2 n, \tag{123}$$

where the viscosity μ and D are taken small, but finite to absorb all fluctuation energy reaching the smallest resolved space scales in the simulation system. The system's strong turbulence features at small α where $\alpha/\overline{\omega}\sim1$ where $\overline{k},\overline{\omega},\overline{\gamma}$ are taken at the peak of the energy spectrum. Here the overbar on k, ω, γ denotes a mean value near the peak of the energy spectrum E_k. One can show that $\overline{k}\approx\alpha^{1/3},\overline{\gamma}\approx\alpha^{1/3}$ and that $E_{\overline{k}}\simeq\overline{\gamma}^2/\overline{k}^3\simeq1/\alpha^{1/3}$ (Krommes and Hu, 1994). In the large α limit the density $n\to\phi[1+\mathcal{O}(1/\alpha)]$ approaches the adiabatic limit, and a weaker turbulence appears with $E_k\simeq\overline{\gamma\omega}/\overline{k}^3\approx1/\alpha$ since $\overline{\gamma}\sim1/\alpha$, and $\overline{k}=\alpha^0$ and $\overline{\omega}=\alpha^0$ independent of α.

The new parameter $\alpha=k_\parallel^2T_e/m_e\nu_e\omega_0$ measuring the parallel electron diffusion in a characteristic wave period $(1/\omega_0)$ determines the properties of the waves. For $\alpha\gtrsim1$ the electrons tend to the Boltzmann distribution $\tilde{n}=e\phi/T_e$ and the Hasegawa-Mima equation is recovered. In Xu *et al.* (1995) the dimensionless measure of this dissipation coefficient α was varied from 1 to 10^{-5}. Both fixed and time evolving background densities were considered in bounded and periodic systems. Their reference value of the gradient scale length is $L_n=100\rho_s$. Xu *et al.* (1995) show that for an exponential density profile for which the gradient parameter $K=-\rho_s\boldsymbol{\nabla}\ln n$ is constant the local turbulence theory works well and the diffusivity and fluctuation levels are given by

$$D=1.4\frac{cT_e}{eB}\frac{\rho_s}{L_n}\left(\frac{1}{\alpha^{1/3}}\right), \tag{124}$$

$$\frac{\tilde{n}}{n}=3.0\frac{\rho_s}{L_n}\left(\frac{1}{\alpha^{1/3}}\right). \tag{125}$$

For the exponential density profile without constant K the coefficients increase to 1.56 and 3.72 in Eqs. (124) and (125). For the hyperbolic tangent step-down density profile mode the authors define a nonlocal transport associated with the correlation length being an appreciable fraction of the gradient length scale. They report that formulas of the form (124) and (125) remain valid with $L_n\to L_n(x)$ and the coefficients increase to 1.6 and 3.6, respectively. The effect of the Kelvin-Helmholtz terms in the vorticity equation are investigated with two models for the radial electric field.

The Xu *et al.* (1995) simulations were subsequently extended to include both a core plasma with magnetic shear at separatrix $(x=0)$, and a scrape-off layer with magnetic field lines ending on conducting end plates. In these simulations of the Berk *et al.* (1991) scrape-off layer instability the effective value of $\alpha_{\rm eff}=(4\rho_s/L_\parallel)(e\Phi_0/T_e)^2$ where Φ_0 is the sheath potential drop along the open field lines and $L_\parallel$ is the length of the magnetic field line terminated by the two conducting plates. This

configuration of a separatrix outside of which fields are terminated on conducting plates is the important divertor configuration in fusion reactors. The turbulent diffusivity on the open field lines with $\alpha_{\rm eff}$ used in Eq. (124) scales as

$$D_{\rm SOL} \simeq \frac{cT_e}{eB}\left(\frac{\rho_s}{L_n}\right)^{2/3}\left|\frac{T_e}{e\Phi_0}\right|^{2/3}$$

which is a hybrid between Bohm and gyro-Bohm. Connor (1993) has compiled a list of the special forms of the turbulent diffusivities applicable to the scrape-off layer plasma.

The divertor allows a sharp edge to the confined plasma to form and provides for the efficient removal of low-temperature plasma containing impurities that ordinarily can recycle into the core plasma. It is with the use of the divertor in the ASDEX experiment that the *H*-mode transition was discovered by Wagner *et al.* (1982). The Princeton divertor experiment also found the *H* mode at essentially the same time with the same technique. The achievement of the edge *H* mode has been repeated with many different techniques and is now assumed to be essential for the successful operation of a nuclear fusion reactor based on low beta toroidal confinement. The *H*-mode transition from biased limiters was found by Taylor *et al.* (1989) and Weynants *et al.* (1991).

H. Radial propagation of the drift wave and edge turbulence

An alternative theory for the high level of the edge turbulence is developed by Mattor (1995) and Mattor and Diamond (1994). The theoretical model argues that the drift waves are driven in the core plasma and propagate to the edge. The WKB theory for wave propagation is used to calculate the amplitude of the waves at the edge. Brizzard (1996) extended the adiabatic theory introducing a Lagrangian density for the drift waves. Mattor (1995) argues that the theory predicts sufficiently high edge amplitudes in the *L*-mode plasma. Then Mattor extends the theory to include parallel velocity shear and the radial electrostatic potential $\Phi(r)$ with a component of $v_\theta = c\Phi'/B$ driven by the Reynolds stress $\langle \tilde{v}_r \tilde{v}_\theta \rangle$. By steeping the edge radial electric field, Mattor (1995) reflects the drift waves reducing the edge transport, thus making an *L*- to *H*-mode transition. Mattor calls the basic increase of the edge fluctuation amplitude from radial propagation the "beach scenario," for the *H*-mode transition and argues that this mechanism is quite different from the shear flow suppression of turbulence from E_r shear. Mattor supports his arguments with detailed discussions of well-known data from TEXT and DIII-D which, aside from his model, gives a useful perspective on the fluctuation data.

Edge turbulence may also arise from a resistive-drift wave mode that balloons in the region of unfavorable magnetic curvature on the outside of the torus. The theory and simulations of the resistive-drift-ballooning modes (Guzdar *et al.*, 1993; Carreras *et al.*, 1987, 1992) yield the diffusivity

$$D^{RB} = C_{RB}(2\pi q_a^2)\rho_e^2 \nu_{ei}\left(\frac{R}{L_p}\right) \tag{126}$$

that has been used with $C_{RB}=15$ in the transport modeling with some success (Kinsey *et al.*, 1996; Redd *et al.*, 1997). The theory and simulation for the resistive-drift-ballooning modes as straightforward extensions of the turbulence modeling described in the previous Sec. V.E requiring the ion acoustic wave coupling. A recent work by Novakovski *et al.* (1995) shows there are *two branches* of the ballooning mode equation. The first conventional branch with weak ballooning is stabilized when the magnetic shear $s = rq'/q$ exceeds unity. The second branch is more localized to the outside of the torus and remains unstable for $s \sim 1$. The time scale for growth of the resistive drift ballooning is the usual interchange time $(RL_n)^{1/2}/c_s$ and the space scale is $q(2R/L_n)^{1/2}(2\nu_{ei}R\rho_s/\Omega_{ce})^{1/2}$. The asymptotic techniques needed to obtain analytic results are explained well in Novakovski *et al.* (1995) and the references therein. The wave functions become quite complicated extending along the ballooning mode coordinate up to $\theta \sim 100$ [rad]. The correction to the η_i-mode is given in Zeiler *et al.* (1998).

I. Short-wavelength drift-wave turbulence

Short-wavelength fluctuations $k_\perp \rho_i \gg 1$ with finite electron inertia are driven unstable by the electron temperature gradient. The modes are electron analogs of the better studied η_i modes reviewed in Sec. IV. Their properties are developed in Lee *et al.* (1987) and Horton, Hong, and Tang (1988).

There are two experimental studies of short scale high-frequency turbulence. One with magnetic probes in a steady state device and one in electromagnetic scattering in a large confinement tokamak.

Using a toroidal multipole machine operated so as to simulate a tokamak (the Tokapole), Haines *et al.* (1995) use assorted sizes (diameters) of magnetic and Langmuir probes to form a coarse filtering (or binning) of the fluctuation spectrum. In this manner electromagnetic fluctuations with frequencies from 10 kHz to 5 MHz and the wavelength scales from 2 to 13 mm are binned. Haines *et al.* (1995) correlate the measured fluctuations with the c/ω_{pe}-turbulence theories that are favored as an origin of χ_e (electron thermal diffusivity) by a number of researchers. This experimental study reports that the fluctuation properties do not correlate well with the theoretical models. The studies do, however, report a peak in the wave number spectrum at short wavelengths $\lambda_\theta \gtrsim 2$ mm that exceeds the power in the $\lambda_\theta \gtrsim 13$ mm bin by a factor of 20. At $\lambda_\theta = 4$ mm the power is greater than the $\lambda_\theta \sim 13$ mm waves by a factor of four. The 2 mm wavelength corresponds to $k_\theta c/\omega_{pe} \gtrsim 1$. These result are for the high-frequency ($\gtrsim$1 MHz) magnetic fluctuations

inside the separatrix where the electron plasma beta is into the electromagnetic drift-wave regime, since the local $\beta_e \sim 10 m_e/m_i$.

This enhancement in the small λ_θ power drops as the measurement position is moved toward the separatrix and is not measurable outside the separatrix where $\beta_e \ll m_e/m_i$. The radial profile of the measure $\tilde{B}_r/B$ for λ_θ are binned according to [2, 4, 13 mm] and show a sharp increase of $\tilde{B}_r/B$ at the 2 mm scale to $\gtrsim 2\times 10^{-5}$. The enhancement of the high-frequency spectrum at $r = 11$ cm is in qualitative agreement with the results of the 3D electromagnetic simulations (Horton, Hong, Tajima, and Bekki, 1990). While the measurements versus simulations show differences, in for example the anisotropy of the spectrum, the general feature of the enhancement at the 2 mm probe in the core that disappears toward the edge is consistent with the c/ω_{pe} theory. Haines *et al.* (1995) argue that since the total $dk d\omega$-integrated fluctuation power is much larger in the 10 to 300 kHz region the particle transport must come from the large scales ($\geqslant$4 mm). There can still be a substantial χ_e contribution from the c/ω_{pe}-correlation scale lengths taken at the $\gtrsim$1 MHz decorrelation rate ($\epsilon^{1/2} v_e/qR$) associated with the broad high-frequency component of the fluctuation spectrum. The final argument by Haines *et al.* (1995) against the c/ω_{pe} model is that the saturation level predicted by theory is too large by one order of magnitude. For the theoretical estimate they take $\tilde{B}_r/B = ck_\parallel/\omega_{pe} \sim 10^{-3}$ using $k_\parallel = 1/qR$. They report that the fluctuation level at the c/ω_{pe} scale is measured to be $\tilde{B}_r/B \sim 5\times 10^{-5}$. They acknowledge, however, that the approach to the theoretical level may occur with higher β_e plasmas. The highest β_e in the experiment is at about 1/2 the value used in the simulations of Horton, Su, and Morrison (1990). Haines *et al.* (1995) conclude that there is important dynamics in between the c/ω_{pe} and ρ_i scales suggesting that more work needs to be performed on the nonlinear dynamics at these small scales. Extensive test-particle electron transport studies from the small-scale fluctuations in Kim *et al.* (1990) show how the stochastic electron orbits lead to the c/ω_{pe}-diffusivities.

Tokamak Fusion Test Reactor (TFTR) discharges with high core temperatures ($T_{e0} \lesssim 8$ kev, $T_{i0} \lesssim 25$ keV) from the improved confinement regime (enhanced reversed shear) and high neutral beam heating power (28 MW) have small-scale fluctuations at $k_\perp \cong 0.85\omega_{pe}/c \sim 5\rho_i^{-1} \simeq 9\ \mathrm{cm}^{-1}$ (Wong *et al.*, 1997). These electron density fluctuations $\langle \delta n_e^2 \rangle_k$ are measured by scattering a microwave beam with $|\Delta \mathbf{k}| = k_\perp = 8.9\ \mathrm{cm}^{-1}$ from the core plasma continuously in time. Power balance studies are then performed to determine the electron thermal diffusivity $\chi_e(r,t)$ required to give the measured $n_e, T_e(r,t)$ profiles from the fraction of the beam power deposited into the electrons. The resulting $\chi_e(r,t)$ is shown to track the fluctuation level over a period of one second while χ_e varies from 0.5 to 4 m^2/s.

A related instability based on the electron inertial in the nonlinear Ohm's law and a single pressure field driving interchange instability in the unfavorable magnetic curvature is called the current diffusive ballooning mode. Yagi *et al.* (1994) develop the properties of this turbulence estimating the thermal diffusivity as

$$\chi = f(s)\frac{q^2}{\omega_{pe}^2}\frac{v_A}{R}\left(-R\frac{d\beta}{dr}\right)^{3/2},$$

where $f(s)$ is a complicated function of magnetic shear s obtained from the ballooning mode calculation of $\langle k_x^2 \rangle$. Comparison of the current diffusive χ, in the form given by Fukuyama *et al.* (1994), with the ITG for a high beta poloidal discharge is given in Horton *et al.* (1997).

The importance of the electron transport at the c/ω_{pe} scale has been pointed out and developed by many authors: Ohkawa (1978), Kadomtsev and Pogutse (1979), Lee *et al.* (1987), Horton *et al.* (1988), Horton, Hong, *et al.* (1990), Connor (1993), Itoh *et al.* (1994), and Fukuyama *et al.* (1994). The resulting formula for χ_e is able to explain the electron flux in numerous power balance studies (Taroni *et al.*, 1994). It is the author's view that these fluctuations are an important mechanism, albeit poorly understood, for thermal transport. These electron scale fluctuations may be responsible for holding the electron temperature down in discharges where the ion confinement has improved dramatically.

J. Long-wavelength electron drift waves

In the long-wavelength regime defined by

$$\frac{L_T}{qR} \lesssim k_\theta \rho_s \lesssim \left(\frac{L_{T_i}}{R}\right)^{1/4}, \tag{127}$$

the eigenfunction $\phi(\theta)$ is more extended along the field lines and the transit (passing) ion response is important (Chen *et al.*, 1990). In this regime the trapped electron mode exists even in the limit of flat density. The fluctuation spectrum integrated over k_x varies as $I(k_\theta) = I_0(k_0/k_\theta)^3$. The quasilinear fluxes from the trapped electron response are dominant over the η_i drive since the long-wavelength fluctuations rotate in the electron diamagnetic direction. The scaling of the quasilinear thermal fluxes are as $Q_i = 4T_i\Gamma$ and $Q_e = 2T_e\Gamma$ for the collisionless electron response. Here $\Gamma = \langle \tilde{n}_e \tilde{v}_x \rangle$ is the ambipolar electron response which has the following approximate forms (Hahm, 1991):
collisional regime

$$\Gamma_e = 1.6\frac{ncT_e}{eB}\left(\frac{T_i}{T_e}\right)^{2/3}\frac{\rho_s}{s^{4/3}L_{T_i}^{3/4}R^{5/4}}\left(\frac{r}{R}\right)^3\left(\frac{c_s}{\nu_{ei}L_{T_e}}\right)^2, \tag{128}$$

collisionless regime

$$\Gamma_e = 1.85\frac{ncT_e}{eB}\left(\frac{T_i}{T_e}\right)^{7/6}\frac{q^2\rho_s}{s^{4/3}L_{T_i}^{1/2}R^{3/2}}\left(\frac{R}{L_{T_e}}\right)^2\left(\frac{r}{R}\right). \tag{129}$$

These formulas are given in the limit that $L_n \gtrsim R$ so that L_n drops out of the transport problem. The corresponding formulas for the peaked density regime can be found

in Hahm and Tang (1996). The transition occurs for $\Gamma = \min(\Gamma_e^1, \Gamma_e^2)$. The particle flux Γ_e is driven by the temperature gradient.

The wavelength regime in Eq. (127) also sees changes in the ITG turbulence. At the lower end of this wavelength range where $\lambda_\theta = 2\pi\rho_s(qR/L_{T_i})$ the correlation lengths are of order a few centimeters in TFTR which is in agreement with the correlation length reported in the microwave reflectometry measurements by Mazzucato and Nazikian (1993). Simulations indicate that the turbulence remains approximately isotropic at this scale so that the radial correlation length is also $\lambda_c = \rho_s(qR/L_{T_i})$. Since the decorrelation rate $\tau_c = (L_{T_i}R)^{1/2}/c_s$ remains connected to the maximum growth rate, the turbulent diffusivity becomes

$$\chi_i = C_{\rm OHE}\frac{q^2\rho_s}{L_{T_i}}\frac{cT_e}{eB}\left(\frac{R}{L_{T_i}}\right)^{3/2}. \tag{130}$$

This formula for the ion thermal diffusivity is given by Ottaviani, Beer *et al.* (1997) and has been applied to the ITER profile database with some success (Erba *et al.*, 1995; Redd *et al.*, 1998). The similarity of the scaling of Eq. (129) with Eq. (130) is to be noted. In the derivation of Eq. (130) no attempt was made to account for the magnetic shear s dependence. The Ottaviani-Horton-Erba model takes into account that the transport is dominated by the largest, most energetic scale eddies in the turbulence while the source of the turbulence remains at the short scales where the linear growth rate is a maximum.

The measurement of large space fluctuations ($\lambda_\perp = 2\pi/k_\perp \gtrsim 6$ cm) are made using special techniques with diagnostic neutral beams, the heating neutral beams, and microwave reflectometry. The beam emission spectroscopy measurements of Durst *et al.* (1993) show fluctuations at the level of $\tilde{n}/n \sim 0.01$ in the range $r/a = 0.7$ to 0.8 with a peak in the k_θ spectrum at about 1 cm^{-1}. The reflectometry measurements of Mazzucato and Nazikian (1993), shown in Fig. 5, show core fluctuations with the radial correlation length of 3 to 4 cm. The reflectometry measurements of Doyle *et al.* (1991) show evidence for the bifurcation in the fluctuation levels associated with a change in the confinement properties.

In conclusion, a deep understanding of the low-frequency plasma turbulence responsible for the cross-field transport of particles, thermal energy, and momentum has been obtained through experimental and theoretical research programs devoted to plasma confinement with magnetic fields. The properties of the fluctuations agree with the predictions of drift-wave theory which encompasses a broad range of gradient-driven instabilities whose details vary with both the plasma parameters and the parameters of the confinement geometry. The TEXT Ohmic tokamak equipped with a full complement of fluctuation and transport diagnostic probes and sensors provided, for example, the details of the correlation between drift wave fluctuations and transport. The conclusion of the transport research program was that both the particle and the electron thermal energy balance could be accurately accounted for in terms of the turbulent transport fluxes. The program also showed the difficulty of identifying the particular driving terms of the turbulence which is also consistent with theory where growth rates and turbulence levels are complicated functions of many different radial gradients and other plasma system parameters as shown in Secs. III to V. Simpler devices, particularly the Q machines, have identified the dissipative electron drift wave, and the Columbia Linear Machine have been able to isolate the trapped electron drift waves and the ion temperature gradient instability in quasicoherent low m modes to make definitive identification with drift wave theory.

As in geophysical turbulence, the problem of making predictions in turbulence systems is in itself an issue. There does seem to be some degree of predictability with drift-wave turbulence based transport coefficients. Modeling with the multimode model, and other parametrizations with sufficient complexity are able to reproduce a particular database. New machine designs in the past have relied principally on empirical scaling laws, but as the cost of future fusion machines escalates to the multibillion dollar level, modeling with drift-wave turbulence models is gaining acceptance as an alternative route for predicting performance.

The next major step in transport research is to gain a fuller understanding of the bifurcations that occur to different confinement regimes. The improved confinement regimes found experimentally are now being interpreted by a variety of theoretical models. Many of these bifurcation models are based on the changes in the drift-wave turbulence as it is self-consistently determined with the background transport, especially of plasma momentum. Thus a thorough understanding of the topic of this review, drift-wave turbulence, is presupposed in the research on bifurcations leading to improved confinement regimes.

ACKNOWLEDGMENTS

The author would like to thank H. L. Berk, J. Q. Dong, G. Hu, J.-Y. Kim, and H. Sugama for many helpful comments during the writing of this work. The work was supported by the Department of Energy under Grant No. DE-FG03-96ER-54346.

REFERENCES

Adam, J. C., W. M. Tang, and P. H. Rutherford, 1976, Phys. Fluids **19**, 561.

Antipov, S. V., M. V. Nezlin, E. N. Snezhkin, and A. S. Trubnikov, 1982, Zh. Eskp. Teor. Fiz. **82**, 145 [Sov. Phys. JETP **55**, 85].

Antipov, S. V., M. V. Nezlin, E. N. Snezhkin, and A. S. Trubnikov, 1985, Sov. Phys. JETP **62**, 1097.

Antonova, R. A., B. P. Zhvaniya, D. K. Lominadze, Dzh. Nanobashvili, and V. I. Petviashvili, 1983, Pisma Zh. Eksp. Teor. Fiz. **37**, 545 [JETP Lett. **37**, 651].

Artun, M., and W. M. Tang, 1992, Phys. Fluids B **4**, 1102.

Artun, M., W. M. Tang, and G. Rewoldt, 1995, Phys. Plasmas **2**, 3384.
Balescu, R., 1988, *Transport Processes in Plasmas, Vol. I: Classical Transport, Vol. 2: Neoclassical Transport* (North Holland, Amsterdam).
Balescu, R., 1990, Phys. Fluids B **2**, 2100.
Balk, A. M., and S. V. Nazarenko, 1990, Sov. Phys. JETP **70**, 1031.
Balk, A. M., S. V. Nazarenko, and V. E. Zakharov, 1990, Phys. Lett. A **146**, 217.
Balk, A. M., S. V. Nazarenko, and V. E. Zakharov, 1991, Phys. Lett. A **152**, 276.
Balk, A. M., V. E. Zakharov, and S. V. Nazarenko, 1990, Sov. Phys. JETP **71**, 249.
Bateman, G., 1992, Phys. Fluids B **4**, 634.
Bazdenkov, S. V., and O. P. Pogutse, 1993, JETP Lett. **57**, 410.
Beer, M. A., S. Cowley, and G. W. Hammett, 1995, Phys. Plasmas **2**, 2687.
Beer, M. A., and G. W. Hammett, 1996, Phys. Plasmas **3**, 4046.
Beer, M. A., G. W. Hammett, G. Rewoldt, E. J. Synakowski, M. C. Zarnstorff, and W. Dorland, 1997, Phys. Plasmas **5**, 1792.
Behringer, R. P., S. D. Meyers, and H. L. Swinney, 1991, Phys. Fluids A **3**, 1243.
Beklemishev, A. D., and W. Horton, 1992, Phys. Fluids B **4**, 200.
Benzi, R., G. Paladin, and A. Vulpiani, 1988, Phys. Rev. A **42**, 3654.
Berk, H. L., D. D. Ryutov, and Yu. A. Tsidulko, 1991, Phys. Fluids B **3**, 1346.
Berk, H. L., R. H. Cohen, D. D. Ryutov, Yu. A. Tsidulko, and X. Q. Xu, 1993, Nucl. Fusion **33**, 263.
Biglari, H., P. H. Diamond, and P. W. Terry, 1990, Phys. Fluids B **2**, 1.
Biskamp, D., S. J. Camaargo, and B. D. Scott, 1994, Phys. Lett. A **186**, 239.
Bolton, C., and A. A. Ware, 1983, Phys. Fluids **26**, 459.
Bowman, J. C., and J. A. Krommes, 1996.
Bowman, J. C., J. A. Krommes, and M. Ottaviani, 1993, Phys. Fluids B **5**, 3558.
Braginskii, S. I., 1965, *Reviews of Plasma Physics*, edited by M. A. Leontovich (Consultants Bureau, New York), Vol. I, p. 205.
Bravenec, R. V., K. W. Gentle, B. Richards, D. W. Ross, D. C. Sing, A. J. Wootton, D. L. Brower, N. C. Luhman, W. A. Peeples, C. X. Yu, T. P. Crowley, J. W. Heard, R. L. Hickok, P. M. Schock, and X. Z. Zhang, 1992, Phys. Fluids B **4**, 2127.
Brizard, A. J., 1992, Phys. Fluids B **4**, 1213.
Brizard, A. J., 1996, Phys. Plasmas **3**, 744.
Brower, D. L., W. A. Peebles, S. K. Kim, N. C. Luhmann, W. M. Tang, and P. E. Phillips, 1987, Phys. Rev. Lett. **59**, 48.
Brower, D. L., W. A. Peebles, and N. C. Luhmann, Jr., 1985, Phys. Rev. Lett. **54**, 689.
Burrell, K. H., 1997, Phys. Plasmas **4**, 1499.
Carreras, B. A., L. Garcia, and P. H. Diamond, 1987, Phys. Fluids **30**, 1338.
Carreras, B. A., V. E. Lynch, L. Garcia, and P. H. Diamond, 1993, Phys. Fluids B **5**, 1491.
Carreras, B. A., D. Newman, P. H. Diamond, and Y-M. Liang, 1994, Phys. Plasmas **1**, 4014.
Carreras, B. A., D. Newman, V. E. Lynch, and P. H. Diamond, 1996, Phys. Plasmas **3**, 2903.
Carreras, B. A., K. Sidikman, P. H. Diamond, P. W. Terry, and L. Garcia, 1992, Phys. Fluids B **4**, 3115.
Carreras, B. A., V. E. Lynch, P. H. Diamond, and M. Medvedev, 1998, Phys. Plasmas **5**, 1206.
Chandrasekhar, S., 1961, *Hydrodynamic and Hydromagnetic Stability* (Dover Publications, Inc., New York).
Chang, C. S., and F. L. Hinton, 1982, Phys. Fluids **25**, 1493.
Chang, C. S., and F. L. Hinton, 1986, Phys. Fluids **29**, 3314.
Chang, Z., and J. D. Callen, 1992, Phys. Fluids B **4**, 1167.
Charney, J. G., 1948, Geophys. Public. Kosjones Nors. Videnshap.-Akad. Oslo **17**, 3.
Chen, J., and A. K. Sen, 1995, Phys. Plasmas **2**, 3063.
Chen, L., S. Briguglio, and F. Romanelli, 1990, Phys. Fluids B **29**, 3715.
Chen, L., S. Briguglio, and F. Romanelli, 1991, Phys. Fluids B **3**, 611.
Chen, L., M. S. Chance, and C. Z. Cheng, 1980, Nucl. Fusion **20**, 901.
Chen, L., and C. Z. Chen, 1980, Phys. Fluids **23**, 2242.
Cheng, C. Z., and K. T. Tsang, 1981, Nucl. Fusion **21**, 643.
Choi, D.-I., and W. Horton, 1980, Phys. Fluids **23**, 356.
Christiansen, J. P., P. M. Stufferfield, J. G. Cordey, C. Gormezano, C. W. Gowers, J. O'Rourke, D. Stork, A. Taroni, and C. D. Challis, 1993, Nucl. Fusion **33**, 863.
Cima, G., R. V. Bravenec, A. J. Wootton, T. D. Rempel, R. F. Gandy, C. Watts, and M. Kwon, 1995, Phys. Plasmas **2**, 720.
Connor, J. W., 1993, Plasma Phys. Controlled Fusion **35**, 757.
Connor, J. W., G. F. Counsell, S. K. Erents, S. J. Fielding, B. LaBombard, and K. Morel, 1998, ''Scrape-off Layer Models,'' UKAEA Fus. 396.
Connor, J. W., R. J. Hastie, and J. B. Taylor, 1979, Proc. R. Soc. London, Ser. A **365**, 1.
Connor, J. W., J. B. Taylor, and H. R. Wilson, 1993, Phys. Rev. Lett. **70**, 1803.
Connor, J. W., and H. R. Wilson, 1994, Plasma Phys. Controlled Fusion **36**, 719.
Coppi, B., M. N. Rosenbluth, and R. Z. Sagdeev, 1967, Phys. Fluids **10**, 582.
Coppi, B., 1977, Phys. Rev. Lett. **39**, 939.
Cowley, S. C., R. M. Kulsrud, and R. N. Sudan, 1991, Phys. Fluids B **3**, 1803.
Crotinger, J. A., and T. H. Dupree, 1992, Phys. Fluids B **4**, 2854.
Deng, B. H., D. L. Brower, G. Cima, C. W. Domier, N. C. Luhmann, Jr., and C. Watts, 1998, Phys. Plasmas **5**, 4117.
Denton, R. E., and M. Kotschenreuther, 1987, J. Comput. Phys. **72**, 612.
Dewar, R. L., 1997, Plasma Phys. Controlled Fusion **39**, 453.
Dewar, R. L., and A. H. Glasser, 1983, Phys. Fluids **26**, 3038.
Dewar, R. L., and R. W. Griffiths, Eds. 1997, *Two-Dimensional Turbulaence in Plasmas and Fluids*, Research Workshop, Canberra, Australia, June–July, 1997, AIP Conf. Proc. No. **414**, (AIP, Woodbury, NY).
Dewar, R. L., Y. Z. Zhang, and S. M. Mahajan, 1995, Phys. Rev. Lett. **74**, 4563.
Diamond, P. H., 1998, ''Review of Self-Organized Criticality in Plasmas,'' APS-DPP Review talk.
Diamond, P. H., and T. S. Hahm, 1995, Phys. Plasmas **2**, 3640.
Diamond, P. H., and Y-B. Kim, 1991, Phys. Fluids B **3**, 1626.
Diamond, P. H., V. B. Lebedev, D. E. Newman, B. A. Carreras, T. S. Hahm, W. M. Tang, G. Rewoldt, and K. Avinash, 1997, Phys. Rev. Lett. **78**, 1472.

Dimits, A. M., J. F. Drake, P. N. Guzdar, and A. B. Hassam, 1991, Phys. Fluids B **3**, 620.
Dimits, A. M., T. J. Williams, J. A. Byers, and B. I. Cohen, 1996, Phys. Rev. Lett. **77**, 71.
Dong, J. Q., and W. Horton, 1995, Phys. Plasmas **2**, 3412.
Dong, J. Q., and W. Horton, 1993, Phys. Fluids B **5**, 1581.
Dong, J. Q., W. Horton, R. D. Bengtson, and G. S. Li, 1994, Phys. Plasmas **1**, 3635.
Dong, J. Q., W. Horton, and W. Dorland, 1994, Phys. Plasmas **1**, 3635.
Dong, J. Q., W. Horton, and J.-Y. Kim, 1992, Phys. Fluids B **4**, 1867.
Dong, J. Q., W. B. Xu, Y. Z. Zhang, and W. Horton, 1998, Phys. Plasmas **5**, 4328.
Dong, J. Q., Y. Z. Zhang, S. M. Mahajan, and P. N. Guzdar, 1996, Phys. Plasmas **3**, 3065.
Dorland, W., and G. W. Hammett, 1993, Phys. Fluids B **5**, 812.
Doyle, E. J., R. J. Groebner, K. H. Burrell, P. Gohil, T. Lehecka, N. C. Luhmann, Jr., H. Matsumoto, T. H. Osborne, W. A. Peebles, and R. Philipona, 1991, Phys. Fluids B **3**, 2300.
Drake, J. F., J. M. Finn, P. N. Guzdar, V. Shapiro, V. Shevchenko, F. Waelbroeck, A. B. Hassam, C. S. Liu, and R. Sagdeev, 1992, Phys. Fluids B **4**, 488.
Drake, J. F., A. Zeiler, and D. Biskamp, 1995, Phys. Rev. Lett. **75**, 4222.
Dupree, T. H., 1982, Phys. Fluids **25**, 277.
Durst, R. D., R. J. Fonck, J. S. Kim, S. F. Paul, N. Bretz, C. Bush, Z. Chang, and R. Hulse, 1993, Phys. Rev. Lett. **71**, 3135.
Efthimion, P. C., D. K. Mansfield, B. C. Stratton, E. Synakowski, A. Bhattacharjee, H. Biglari, P. H. Diamond, R. J. Goldston, C. C. Hegna, D. McCune, G. Rewoldt, S. Scott, W. M. Tang, G. Taylor, R. E. Waltz, R. M. Wieland, and M. C. Zarnstorff, 1991, Phys. Rev. Lett. **66**, 421.
Erba, M., T. Ariel, V. Basiuk, A. Becoulet, and X. Litaudon, 1998, Nucl. Fusion **38**, 1013.
Erba, M., V. Parail, E. Springmann, and A. Taroni, 1995, Plasma Phys. Controlled Fusion **37**, 1249.
Ernst, D. R., M. G. Bell, R. E. Bell, *et al.* 1998, Phys. Plasmas **5**, 665.
Filippas, A. V., R. D. Bengston, G.-X. Li, M. Mejer, Ch. P. Ritz, E. J. Powers, 1995, Phys. Plasmas **2**, 839.
Finn, J. M., J. F. Drake, and P. N. Guzdar, 1992, Phys. Fluids B **4**, 2758.
Frieman, E. A., and L. Chen, 1982, Phys. Fluids **25**, 502.
Fu, X. Y., J. Q. Dong, W. Horton, C. T. Ying, and G. J. Liu, 1997, Phys. Plasmas **4**, 588.
Fukuyama, K., S.-I. Itoh, M. Itoh, M. Yagi, and M. Azumi, 1994, Plasma Phys. Controlled Fusion **36**, 1385.
Furnish, G., W. Horton, Y. Kiskimoto, M. LeBrun, and T. Tajima, 1999, Phys. Plasmas **6**, 1227.
Fyfe, D., and D. Montgomery, 1979, Phys. Fluids **22**, 246.
Gang, F. Y., P. H. Diamond, J. A. Crotinger, and A. E. Kroniges, 1991, Phys. Fluids B **4**, 955.
Gang, F. Y., P. H. Diamond, and M. N. Rosenbluth, 1991, Phys. Fluids B **3**, 68.
Garbet, X., L. Laurent, A. Samain, and J. Chinardt, 1994, in *Transport, Chaos and Plasma Physics*, edited by S. Benkadda, F. Doveil, and Y. Elskens (World Scientific, Singapore), p. 284.
Garbet, X., and R. E. Waltz, 1996, Phys. Plasmas **3**, 1898.
Gentle, K. W., 1995, Rev. Mod. Phys. **67**, 809.
Gentle, K. W., R. V. Bravenec, G. Cima, H. Gasquet, G. A. Hallock, *et al.* 1995, Plasma Phys. Controlled Fusion **2**, 2292.
Gladd, N. T., and W. Horton, 1973, Phys. Fluids **16**, 879.
Goldston, R. J., and P. H. Rutherford, 1995, *Introduction to Plasma Physics* (Institute of Physics, Bristol), p. 420.
Guzdar, P. N., J. F. Drake, D. McCarthy, A. B. Hassam, and C. S. Liu, 1993, Phys. Fluids B **5**, 3712.
Hahm, T. S., 1991, Phys. Fluids B **3**(6), 1445.
Hahm, T. S., 1994, Phys. Plasmas **1**, 2940.
Hahm, T. S., and K. H. Burrell, 1995, Phys. Plasmas **2**, 1648.
Hahm, T. S., and K. H. Burrell, 1996, Phys. Plasmas **3**, 427.
Hahm, T. S., and W. M. Tang, 1989, Phys. Fluids B **1**, 1185.
Hahm, T. S., and W. M. Tang, 1996, Phys. Plasmas **3**, 242.
Haines, E. J., I. H. Tan, and S. C. Prager, 1995, Phys. Plasmas **2**, 1521.
Hamaguchi, S., and W. Horton, 1990, Phys. Fluids B **2**, 1833.
Hamaguchi, S., and W. Horton, 1992, Phys. Fluids B **4**, 319.
Hammett, G. W., W. Dorland, and F. W. Perkins, 1992, Phys. Fluids B **4**, 2052.
Hammett, G. W., and F. W. Perkins, 1990, Phys. Rev. Lett. **64**, 3019.
Hasegawa, A., C. G. Maclennan, and Y. Kodama, 1979, Phys. Fluids **22**, 2122.
Hasegawa, A., and K. Mima, 1977, Phys. Rev. Lett. **39**, 205.
Hasegawa, A., and K. Mima, 1978, Phys. Fluids **21**, 87.
Hasegawa, A., and M. Wakatani, 1983, Phys. Rev. Lett. **50**, 682.
Hasegawa, A., and M. Wakatani, 1987, Phys. Rev. Lett. **59**, 1581.
Hazeltine, R. D., and J. D. Meiss, 1992, *Plasma Confinement* (Addison-Wesley, Redwood City, CA).
Hendel, H. W., T. K. Chu, and P. A. Politzer, 1968, Phys. Fluids **11**, 2426.
Hermiz, K. B., P. N. Guzdar, and J. M. Finn, 1995, Phys. Rev. E **51**, 325.
Hernandez, J. V., T. Tajima, W. Horton, *et al.* 1996, Nucl. Fusion **36**, 1009.
Hidalgo, C., E. Sánchez, T. Estrada, B. Branas, and Ch. P. Ritz, 1993, Phys. Rev. Lett. **71**, 3127.
Hinton, F. L., and W. Horton, 1971, Phys. Fluids **14**, 116.
Hirshman, S. P., and D. J. Sigmar, 1981, Nucl. Fusion **21**, 1079.
Hong, B. G., and W. Horton, 1990, Phys. Fluids B **2**, 978.
Hong, B. G., G. Horton, and D. I. Choi, 1989, Phys. Fluids B **1**, 1589.
Hong, B. G., W. Horton, S. Hamaguchi, M. Wakatani, M. Yagi, and H. Sugama, 1991, Phys. Fluids B **3**, 1638.
Hong, B. G., R. Romanelli, and M. Ottaviani, 1991, Phys. Fluids B **3**, 615.
Horton, W., 1976, Phys. Rev. Lett. **19**, 1269.
Horton, W., 1986, Phys. Fluids **29**, 1491.
Horton, W., 1990, Phys. Rep. **192**, 1.
Horton, W., D.-I. Choi, and W. M. Tang, 1981, Phys. Fluids **24**, 1077.
Horton, W., D.-I. Choi, P. W. Terry, and D. Biskamp, 1980, Phys. Fluids **23**, 590.
Horton, W., R. Estes, and D. Biskamp, 1980, Phys. Plasmas **22**, 663.
Horton, W., and A. Hasegawa, 1994, Chaos **4**, 227.
Horton, W., B.-G. Hong, T. Tajima, and N. Bekki, 1990, Comments Plasma Phys. Control. Fusion **13**, 207.
Horton, W., B. G. Hong, and W. Tang, 1988, Phys. Fluids **31**, 2971.

Horton, W., and Y.-H. Ichikawa, 1996, *Chaos and Structures in Nonlinear Plasmas* (World Scientific, Singapore), p. 234.
Horton, W., D. Lindberg, J.-Y. Kim, J. Q. Dong, G. W. Hammett, S. D. Scott, M. C. Zarnstorff, and S. Hamaguchi, 1992, Phys. Fluids B **4**, 953.
Horton, W., J. Liu, J. Sedlak, and J. Meiss, 1986, Phys. Fluids **29**, 1004.
Horton, W., and V. Petviashvili, 1993, in *Research Trends in Physics: Chaotic Dynamics and Transport in Fluids and Plasmas*, edited by W. Horton, Y. Ichikawa, I. Prigogine, and G. Zaslavsky (AIP, New York).
Horton, W., and W. Rowan, 1994, Phys. Plasmas **1**, 901.
Horton, W., X. N. Su, and P. J. Morrison, 1990, Sov. J. Plasma Phys. **16**, 562.
Horton, W., T. Tajima, J-Q. Dong, J.-Y. Kim, and Y. Kishimoto, 1997, Plasma Phys. Controlled Fusion **39**, 83.
Horton, W., and R. K. Varma, 1972, Phys. Fluids **15**(4), 620.
Horton, W., M. Wakatani, and A. J. Wootton, 1994, *Ion Temperature Gradient Driven Turbulent Transport* (AIP, New York).
Houlberg, W., K. C. Shaing, S. P. Hirshman, and M. C. Zarnstorff, 1997, Phys. Plasmas **4**, 3230.
Howard, L. N., and R. Krishnamurti, J., 1986, J. Fluid Mech. **170**, 385.
Hu, G., and W. Horton, 1997, Phys. Plasmas **4**, 3262.
Hu, G., J. A. Krommes, and J. C. Bowman, 1995, Phys. Lett. A **202**, 117.
Hu, G., J. A. Krommes, and J. C. Bowman, 1996, Phys. Plasmas **1**, 3211.
Huld, T., A. H. Nielsen, H. L. Pécseli, and J. Juul Rasmussen, 1991, Phys. Fluids B **3**, 1609.
Ida, K., S. Hidekuma, M. Kojima, Y. Miura, S. Tsuj, K. Hoshino, M. Mori, N. Suzuki, T. Yamuchi, and the JFT-2M Group 1992, Phys. Fluids B **4**, 2552.
Itoh, S.-I., and K. Itoh, 1988, Phys. Rev. Lett. **60**, 2376.
Jackson, J. D., 1975, *Classical Electrodynamics* (John Wiley & Sons, New York), p. 469.
Jarmén, A., and M. Fröjdh, 1993, Phys. Fluids B **5**, 4015.
Kadomtsev, B. B., and O. P. Pogutse, 1970, *Reviews of Plasma Physics* Vol. 5, edited by M. A. Leontovich (Consultants Bureau, New York) p. 249.
Kadomtsev, B. B., and O. P. Pogutse, 1971, Nucl. Fusion **11**, 67.
Kadomtsev, B. B., and O. P. Pogutse, 1979, Nucl. Fusion Supp. **1**, 649.
Kim, C. B., W. Horton, and S. Hamaguchi, 1993, Phys. Fluids B **5**, 1516.
Kim, D. E., E. G. Heo, and D.-I. Choi, 1990, Phys. Fluids.
Kim, J.-Y., D-I. Choi, W. Horton, P. N. Yushmanov, and V. V. Parail, 1990, Phys. Fluids B **2**, 547.
Kim, J.-Y., and W. Horton, 1991, Phys. Fluids B **3**, 1167.
Kim, J.-Y., W. Horton, D-I. Choi, S. Migliuolo, and B. Coppi, 1992, Phys. Fluids B 152.
Kim, J.-Y., W. Horton, and J. Q. Dong, 1993, Phys. Fluids B **5**, 4030.
Kim, J.-Y., Y. Kishimoto, W. Horton, and T. Tajima, 1994, Phys. Plasmas **1**, 927.
Kim, J.-Y., Y. Kishimoto, M. Wakatani, and T. Tajima, 1996, Phys. Plasmas **3**, 3689.
Kim, J.-Y., and M. Wakatani, 1994, Phys. Rev. Lett. **73**, 2200.
Kim, Y. C., and E. J. Powers, 1978, Phys. Fluids **21**, 1452.
Kingsbury, O. T., and R. E. Waltz, 1994, Phys. Plasmas **1**, 2319.
Kinsey, J. E., G. Bateman, A. Kritz, and A. Redd, 1996, Phys. Plasmas **3**, 561.
Kishimoto, Y., J.-Y. Kim, T. Fukuda, S. Ishida, T. Fujita, T. Tajima, W. Horton, G. Furnish, and M. J. LeBrun, 1997, *Plasma Physics and Controlled Nuclear Fusion Research, 1996* (International Atomic Energy Agency, Vienna), paper IAEA-CN-64/DP-10.
Kishimoto, Y., T. Tajima, W. Horton, M. J. LeBrun, and J.-Y. Kim, 1996, Phys. Plasmas **3**, 1289.
Kishimoto, Y., T. Tajima, M. J. LeBrun, W. Horton, J.-Y. Kim, J. Q. Dong, F. L. Waelbroeck, S. Tokuda, M. Kawanobe, and T. Fukuda, 1996, "Self-organized critical gradient transport and shear flow effects for the ion temperature gradient mode in toroidal plasmas," *Plasma Physics and Controlled Nuclear Fusion Research, 1994* (International Atomic Energy Agency, Vienna), Vol. 3, p. 299.
Koide, Y., M. Kikuchi, M. Mori, S. Tsuji, S. Ishida, N. Asakura, Y. Kamada, T. Nishitani, Y. Kawano, T. Hatae, T. Fujita, T. Fukuda, A. Sakasai, T. Kondoh, R. Yoshino, and Y. Neyatani, 1994, Phys. Rev. Lett. **72**, 3662.
Koniges, A. E., J. A. Crotinger, and P. H. Diamond, 1992, Phys. Fluids B, 2785.
Kotschenreuther, M., W. Dorland, M. Beer, and G. W. Hammett, 1995, Phys. Plasmas **2**, 2381.
Krall, N. A., and A. W. Trivelpiece, 1973, *Principles of Plasma Physics* (McGraw Hill, New York), p. 21, Bohm Diffusion; p. 206, drift waves; p. 464, Nyquist method.
Krishnamurti, R., and L. N. Howard, 1981, Proc. Natl. Acad. Sci. USA **78**, 1985.
Krommes, J. A., 1980, Phys. Fluids **23**, 736.
Krommes, J. A., 1982, Phys. Fluids **25**, 1393.
Krommes, J. A., 1986, Phys. Fluids **29**, 2756.
Krommes, J. A., 1997, Phys. Rep. **283**, 5.
Krommes, J. A., and G. Hu, 1994, Phys. Plasmas **1**, 3211.
Kurki-Suonio, T., R. J. Groebner, and K. H. Burrell, 1992, Nucl. Fusion **32**, 138.
Larichev, V. D., and J. C. McWilliams, 1991, Phys. Fluids A **3**, 938.
LeBrun, M. J., T. Tajima, M. Gray, G. Furnish, and W. Horton, 1993, Phys. Fluids B **5**, 752.
Lee, Y. C., J. Q. Dong, P. N. Gudzar, and C. S. Liu, 1987, Phys. Fluids **30**, 1331.
Lee, W. W., and R. A. Santoro, 1997, Phys. Plasmas **4**, 169.
Legras, B., P. Santangelo, and R. Benzi, 1988, Europhys. Lett. **5**, 37.
Levinton, F. M., M. C. Zarnstorff, S. H. Batha, M. Bell, R. E. Bell, R. V. Budny, C. Bush, Z. Chang, E. Fredrickson, A. Janos, J. Manickam, A. Ramsey, S. A. Sabbagh, G. L. Schmidt, E. J. Synakowski, and G. Taylor, 1995, Phys. Rev. Lett. **75**, 4417.
Manheimer, W. M., and T. M. Antonsen, 1979, Phys. Fluids **22**, 957.
Mathey, O., and A. K. Sen, 1991.
Mattor, N., 1991, Phys. Fluids **3**, 1913.
Mattor, N., 1995, Phys. Plasmas **2**, 766.
Mattor, N., and P. H. Diamond, 1994, Phys. Rev. Lett. **72**, 486.
Mazzucato, E., 1976, Phys. Rev. Lett. **36**, 792.
Mazzucato, E., 1978, Phys. Fluids **21**, 1063.
Mazzucato, E., 1982, Phys. Rev. Lett. **48**, 1828.
Mazzucato, E., S. H. Batha, M. Beer, M. Bell, R. E. Bell, R. V. Budny, C. Bush, T. S. Hahm, G. W. Hammett, F. M. Levinton, R. Nazikian, H. Park, G. Rewoldt, G. L. Schmidt,

E. J. Synakowski, W. M. Tang, G. Taylor, and M. C. Zarnstorff, 1996, Phys. Rev. Lett. **77**, 3145.
Mazzucato, E. and R. Nazikian, 1993, Phys. Rev. Lett. **71**, 1840.
McWilliams, J. C., 1984, J. Fluid Mech. **146**, 21.
McWilliams, J. C., 1990a, Phys. Fluids A **2**, 547.
McWilliams, J. C., 1990b, J. Fluid Mech. **219**, 361.
Meiss, J. D., and W. Horton, Jr., 1983, Phys. Fluids **26**, 990.
Mikhailovskii, A. B., 1974, *Theory of Plasma Instabilities* (Consultants Bureau, New York), Vol. II.
Mikhailovskii, A. B., S. V. Nazarenko, S. V. Novakovskii, A. P. Churikov, and O. G. Onishchenko, 1988, Phys. Lett. A **133**, 407.
Mikhailovskii, A. B., A. M. Pukhov, and O. G. Onishchenko, 1989, Phys. Lett. A **141**, 154.
Miller, R. L., F. L. Waelbroeck, A. B. Hassam, and R. E. Waltz, 1995, Phys. Plasmas **2**, 3676.
Miller, R. L., and R. E. Waltz, 1994, Phys. Plasmas **1**, 2835.
Mondt, J. P., 1996, Phys. Plasmas **3**, 939.
Morrison, P. J., J. D. Meiss, and J. R. Cary, 1984, Physica D **11**, 324.
Muhm, A., A. M. Pukhov, K. H. Spatschek, and V. Tsytovich, 1992, Phys. Fluids B **4**, 336.
Mynick, H. E., and S. E. Parker, 1995, Phys. Plasmas **2**, 2231.
Naulin, V., and K. H. Spatschek, 1997, Phys. Rev. E **55**, 5883.
Newman, D., B. A. Carreras, P. H. Diamond, and T.-S. Hahm, 1996, Phys. Plasmas **3**, 1858.
Newman, D., P. W. Terry, P. H. Diamond, and Y.-M. Liang, 1993, Phys. Fluids B **5**, 1592.
Newman, D., P. W. Terry, P. H. Diamond, Y.-M. Liang, G. G. Craddock, A. E. Koniges, and J. A. Crottinger, 1992, Phys. Plasmas **1**, 1592.
Nezlin, M. V., 1986, Sov. Phys. Usp. **29**, 807 [Usp. Fiz. Nauk. **150**, 3 (1986)].
Nezlin, M. V., and E. N. Snezhkin, 1993, in *Rossby Vortices, Spiral Structures, Solitons* (Springer, Berlin), p. 196.
Nilsson, J., and J. Weiland, 1994, Nucl. Fusion **34**, 803.
Nordman, H., and J. Weiland, 1989, Nucl. Fusion **29**, 251.
Nordman, H., J. Weiland, and A. Jarmen, 1990, Nucl. Fusion **30**, 983.
Novakovskii, S. V., A. B. Mikhailovskii, and O. G. Onischenko, 1988, Phys. Lett. A **132**, 33.
Novakovskii, S. V., P. N. Guzdar, J. F. Drake, C. S. Liu, and F. L. Waelbroeck, 1992, Phys. Plasmas **2**, 781.
Ohkawa, T., 1978, Phys. Lett. A **67**, 35.
Ohkawa, T., and M. Yoshikawa, 1967, Phys. Rev. Lett. **19**, 1374.
Okabayashi, M., and V. Arunasalam, 1977, Nucl. Fusion **17**, 497.
Ottanviani, M., M. A. Beer, S. C. Cowley, W. Horton, and J. A. Krommes, 1997, Phys. Rep. **283**, 121.
Ottaviani, M., W. Horton, and M. Erba, 1997, Plasma Phys. Controlled Fusion **39**, 1461.
Ottaviani, M., F. Romanelli, R. Benzi, M. Briscolini, P. Santangelo, and S. Succi, 1990, Phys. Fluids B **2**, 67.
Park, H.-B., E.-G. Heo, W. Horton, and D.-I. Choi, 1997, Phys. Plasmas **4**, 3273.
Parker, S. E., W. Dorland, R. A. Santoro, M. A. Beer, Q. P. Liu, W. W. Lee, and G. W. Hammett, 1994, Phys. Plasmas, 1461.
Parker, S. E., and W. W. Lee, 1993, Phys. Fluids B **5**, 77.
Parker, S. E., W. W. Lee, and R. A. Santoro, 1993, Phys. Rev. Lett. **71**, 2042.
Parker, S. E., H. E. Mynick, M. Artun, J. C. Cummings, V. Decyk, J. V. Kepner, W. W. Loe, and W. M. Tang, 1996, Phys. Plasmas **3**, 1959.
Pearlstein, L. D., and H. L. Berk, 1969, Phys. Rev. Lett. **23**, 220.
Pécseli, H. L., J. Juul Rasmussen, and K. Thomsen, 1984, Phys. Rev. Lett. **52**, 2148.
Pécseli, H. L., J. Juul Rasmussen, and K. Thomsen, 1985, Plasma Phys. Controlled Fusion **27**, 837.
Pegoraro, F., 1989, Phys. Lett. A **142**, 384.
Perkins, F., C. W. Barnes, D. W. Johnson, S. D. Scott, M. C. Zarnstorff, M. G. Bell, R. E. Bell, C. E. Bush, B. Grek, K. W. Hill, D. K. Mansfield, H. Park, A. T. Ramsey, J. Schivell, B. C. Stratton, and E. Synakowski, 1993, Phys. Fluids B **5**, 477.
Persson, M., J. L. V. Lewandowski, and H. Nordman, 1995, Phys. Plasmas **2**, 3440.
Persson, M., J. L. V. Lewandowski, and H. Nordman, 1996, Phys. Plasmas **3**, 3720.
Petty, C. C., T. C. Luce, K. H. Burrell, S. C. Chiu, J. S. deGrassie, C. B. Forest, P. Gohil, C. M. Greenfield, R. J. Groebner, R. W. Harvey, R. I. Pinsker, A. Prater, R. E. Waltz, R. A. James, and D. Wroblewski, 1995, Phys. Plasmas **2**, 2342.
Petty, C. C., T. C. Luce, R. I. Pinsker, K. H. Burrell, S. C. Chiu, P. Gohil, R. A. James, and D. Wroblewski, 1995, Phys. Rev. Lett. **74**, 1763.
Petviashvili, V. I., 1977, Fiz. Plazmy **3**, 270 [Sov. J. Plasma Phys. **3**, 150].
Petviashvili, V. I., 1980, JETP Lett. **32**, 619.
Petviashvili, V. I., and O. A. Pokhotelov, 1992, *Solitary Waves in Plasmas and in the Atmosphere* (Gordon and Breach, Philadelphia).
Phillips, M. W. Z., 1996, Phys. Plasmas **3**, 1673.
Prager, S. C., A. K. Sen, and T. C. Marshall, 1974, Phys. Rev. Lett. **33**, 692.
Rajendran, K., J. Q. Dong, and S. M. Mahajan, 1997, Phys. Plasmas **4**, 908.
Redd, A. J., A. H. Kritz, G. Bateman, and W. Horton, 1998, Phys. Plasmas **5**, 1369.
Redd, A. J., A. H. Kritz, G. Bateman, and J. E. Kinsey, 1997, Phys. Plasmas **4**, 2207.
Rewoldt, G., L. L. Lao, and W. M. Tang, 1996, Phys. Plasmas **3**, 4074.
Rewoldt, G., L. L. Lao, and W. M. Tang, 1997, Phys. Plasmas **4**, 3293.
Rewoldt, G., and W. M. Tang, 1990, Phys. Fluids B **2**, 318.
Rewoldt, G., W. M. Tang, and M. S. Chance, 1982, Phys. Fluids **25**, 480.
Rewoldt, G., W. M. Tang, and E. A. Frieman, 1978, Phys. Fluids **21**, 1513.
Rewoldt, G., W. M. Tang, and R. J. Hastie, 1987, Phys. Fluids **30**, 807.
Rogister, A., 1995, Phys. Plasmas **2**, 2729.
Romanelli, F., 1989, Phys. Fluids B **1**, 1018.
Romanelli, F., and S. Briguglio, 1990, Phys. Fluids B **2**, 754.
Romanelli, F., and F. Zonca, 1993, Phys. Fluids B **5**, 4081.
Rosenbluth, M. N., H. L. Berk, I. Doxas, and W. Horton, 1987, Phys. Fluids **30**, 2636.
Rosenbluth, M. N., and F. L. Hinton, 1998, Phys. Rev. Lett. **80**, 724.
Rosenbluth, M. N., D. W. Ross, and D. P. Kostomarov, 1972, Nucl. Fusion **12**, 3.
Ross, D. W., and S. M. Mahajan, 1978, Phys. Rev. Lett. **40**, 324.

Sagdeev, R. Z., and A. A. Galeev, 1969, in *Nonlinear Plasma Theory*, edited by T. M. O'Neil and D. L. Book (Benjamin, New York) p. 89.
Sang, B., A. K. Sen, and P. Tham, 1993, Phys. Fluids B **5**, 4341.
Scarmozzino, R., A. K. Sen, and G. A. Navratil, 1986, Phys. Rev. Lett. **57**, 1729.
Schatz, M. G., J. H. Harris, K. M. Likin, J. B. Wilgen, L. R. Baylor, J. D. Bell, C. H. Ma, M. Murakami, K. A. Sarksyan, S. C. Aceto, T. S. Bigelow, G. L. Bell, R. J. Colchin, R. A. Dory, J. L. Dunlap, G. R. Dyer, A. C. England, R. C. Goldfinger, G. R. Hanson, D. P. Hutchinson, R. C. Isler, T. C. Jerrigan, R. A. Langley, D. K. Lee, J. F. Lyon, A. L. Qualis, D. A. Rasmussen, R. K. Richards, M. J. Saltmarsh, J. E. Simpkins, K. L. Vander Sluis, and J. J. Zielinski, 1995, Phys. Plasmas **2**, 398.
Schmidt, G., 1979, *Physics of High Temperature Plasmas*, 2nd Ed. (Academic, New York), p. 161, polarization; p. 354, drift waves.
Scott, S. B., 1992, Phys. Fluids B **4**, 2468.
Scott, S. D., C. W. Barnes, D. Ernst, J. Schivell, E. J. Synakowski, M. G. Bell, R. E. Bell, C. E. Bush, E. D. Fredrickson, B. Grek, K. W. Hill, A. Janos, D. L. Jassby, D. Johnson, D. K. Mansfield, D. K. Owens, H. Park, A. T. Ramsey, B. C. Stratton, M. Thompson, and M. C. Zarnstorff, 1994, in U.S.-Japan Workshop on "Ion Temperature Gradient-Driven Turbulent Transport," AIP Conf. Proc. No. 284 (AIP, New York), p. 255.
Sen, A. K., J. Chen, and M. Mauel, 1991, Phys. Rev. Lett. **66**, 429.
Shaing, K. C., 1993, Phys. Fluids B **5**, 2122.
Shaing, K. C., 1988a, Phys. Fluids **31**, 8.
Shaing, K. C., 1988b, Phys. Fluids **31**, 2249.
Shaing, K. C., and E. C. Crume, Jr., 1989, Phys. Rev. Lett. **63**, 2369.
Shaing, K. C., E. C. Crume, Jr., and W. A. Houlberg, 1990, Phys. Fluids B **2**, 1496.
Shapiro, V. D., P. H. Diamond, V. B. Lebedev, G. Isoloview, and V. I. Shevchenko, 1993, Plasma Phys. Controlled Fusion **35**, 1032.
Slough, J., G. A. Navratil, and A. K. Sen, 1982, Phys. Rev. Lett. **47**, 1057.
Slusher, R. E., and C. M. Surko, 1978, Phys. Rev. Lett. **40**, 400.
Song H., and A. K. Sen, 1993a, Nucl. Fusion **36**, 895.
Song H., and A. K. Sen, 1993b, Phys. Fluids B **5**, 2806.
Strait, E. J., L. L. Lao, M. E. Mauel, B. W. Rice, T. S. Taylor, K. H. Burrell, M. S. Chu, E. A. Lazarus, T. H. Osborne, S. J. Thompson, and A. D. Turnbull, 1995, Phys. Rev. Lett. **75**, 4421.
Su, X. N., W. Horton, and P. J. Morrison, 1991, Phys. Fluids B **3**, 921.
Su, X. N., W. Horton, and P. J. Morrison, 1992, Phys. Fluids B **4**, 1238.
Sudan, R. N., A. V. Gruzinov, W. Horton, and N. Kukharkin, 1997, Phys. Rep. **283**, 95.
Sudan, R. N., and M. J. Keskinen, 1979, Phys. Fluids **22**, 2305.
Sudan, R. N., and D. Pfirsch, 1985, Phys. Fluids **28**, 1702.
Sugama, H., and W. Horton, 1994, Phys. Plasmas **1**, 345.
Sugama, H., and W. Horton, 1995a, Phys. Plasmas **2**, 2989.
Sugama, H., and W. Horton, 1995b, Plasma Phys. Controlled Fusion **37**, 345.
Sugama, H., and W. Horton, 1997, Phys. Plasmas **4**, 405.
Sugama, H., M. Okamoto, W. Horton, and M. Wakatani, 1996, Phys. Plasmas **3**, 2379.
Sugama, H., M. Wakatani, and A. Hasegawa, 1988, Phys. Fluids **31**, 1601.
Surko, C. M., and R. E. Slusher, 1976, Phys. Rev. Lett. **36**, 1747.
Surko, C. M., and R. E. Slusher, 1978, Phys. Rev. Lett. **40**, 400.
Sydora, R. D., V. K. Decyk, and J. M. Dawson, 1996, Plasma Phys. Controlled Fusion **38**, 281.
Synakowski, E. J., *et al.*, 1997, Phys. Plasmas **4**, 1725.
Tajima, T., W. Horton, P. J. Morrison, J. Schutkeker, T. Kamimura, K. Mima, and Y. Abe, 1991, Phys. Fluids B **3**, 938.
Tajima, T., Y. Kishimoto, M. J. LeBrun, M. G. Gray, J.-Y. Kim, W. Horton, H. V. Wong, and M. Kotschenreuther, 1994, in U.S.-Japan Workshop on "Ion Temperature Gradient-Driven Turbulent Transport," in AIP Conf. Proc. No. **284** (AIP, New York), p. 255.
Tang, W. M., 1978, Nucl. Fusion **18**, 1089.
Tang, W. M., G. Rewoldt, and L. Chen, 1986, Phys. Fluids **29**, 3715.
Tang, W. M., R. B. White, and P. N. Guzdar, 1980, Phys. Fluids **23**, 167.
Taroni, A., M. Erba, F. Tibone, and E. Springmann, 1994, Plasma Phys. Controlled Fusion **36**, 1629.
Tasso, H., 1967, Phys. Lett. **24A**, 618.
Tasso, H., 1983, Phys. Lett. **96A**, 33.
Tasso, H., 1987, Phys. Lett. A **120**, 464.
Taylor, R. J., M. L. Brown, B. D. Fried, H. Grote, J. R. Liberati, G. J. Morales, and P. Pribyl, 1989, Phys. Rev. Lett. **63**, 2365.
Taylor, J. B., and H. R. Wilson, 1996, Plasma Phys. Controlled Fusion **38**, 1999.
Taylor, J. B., H. R. Wilson, and J. W. Connor, 1996, Plasma Phys. Controlled Fusion **38**, 243.
Terry, P. W., and W. Horton, 1982, Phys. Fluids **38**, 1999.
Terry, P. W., and W. Horton, 1983, Phys. Fluids **26**, 106.
Terry, P. W., and P. H. Diamond, 1985, Phys. Fluids **28**, 1414.
TFTR Group, 1997, in *Plasma Physics and Controlled Nuclear Fusion Research*, Proceedings of the 6th International Conference, Berchtesgaden (IAEA, Vienna), Vol. I, p. 35.
Thiffeault, J. L., and W. Horton, 1996, Phys. Fluids **8**, 1715.
Treve, J. M., and O. P. Manley, 1984, J. Fluid Mech. **147**, 1.
Varma, R. K., and W. Horton, 1972, Phys. Fluids **15**, 1469.
Waelbroeck, F. L., and L. Chen, 1991, Phys. Fluids B **3**, 601.
Waelbroeck, F. L., J. Q. Dong, W. Horton, and P. N. Yushmanov, 1994, Phys. Plasmas **1**, 3742.
Wagner, F., G. Becker, K. Behringer, D. Campbell, A. Eberhagen, W. Engel-hardt, G. Fussmann, O. Gehre, J. Gernhardt, G. v. Gierke, G. Haas, M. Huang, F. Karger, M. Keilhacker, O. Klueber, M. Kornherr, K. Lackner, G. Lisitano, G. G. Lister, H. M. Mayer, D. Meisel, E. R. Mueller, H. Murmann, H. Niedermeyer, W. Poschenrieder, H. Rapp, H. Rohr, F. Schneider, G. Siller, E. Speth, A. Staebler, K. H. Steuer, G. Venus, O. Vollmer, and Z. Yu, 1982, Phys. Rev. Lett. **49**, 1408.
Wakatani, M., and A. Hasegawa, 1984, Phys. Fluids **27**, 611.
Wakatani, M., K. Watanabe, H. Sugama, and A. Hasegawa, 1992, Phys. Fluids B **4**, 1754.
Waltz, R. E., 1983, Phys. Fluids **26**, 169.
Waltz, R. E., 1985, Phys. Fluids **28**, 577.
Waltz, R. E., 1986, Phys. Fluids **29**, 3684.
Waltz, R. E., 1988, Phys. Fluids **31**, 1962.
Waltz, R. E., 1990, Phys. Fluids B **2**, 2118.
Waltz, R. E., 1995, Phys. Plasmas **2**, 2408.

Waltz, R. E., J. C. DeBoo, and M. N. Rosenbluth, 1990, Phys. Rev. Lett. **65**, 2390.
Waltz, R. E., and R. R. Dominguez, 1983, Phys. Fluids **26**, 3338.
Waltz, R. E., R. R. Dominguez, and G. W. Hammett, 1992, Phys. Fluids B **4**, 3138.
Waltz, R. E., G. D. Kerbel, and J. Milovich, 1994, Phys. Plasmas **1**, 2229.
Waltz, R. E., G. D. Kerbel, J. Milovich, and G. W. Hammett, 1995, Phys. Plasmas **2**, 2408.
Waltz, R. E., G. M. Staebler, W. Dorland, G. W. Hammett, M. Kotschenreuther, and J. A. Konings, 1997, Phys. Plasmas **4**, 2482.
Watts, C. and R. F. Gandy, 1996, Phys. Plasmas **3**, 2013.
Weiland, J., A. B. Jarmén, and H. Nordman, 1989, Nucl. Fusion **29**, 1810.
Weiland, J., and H. Nordman, 1991, Nucl. Fusion **31**, 390.
Weynants, R. R., *et al.*, 1991, in *Plasma Physics and Controlled Nuclear Fusion, 1990*, Vol. 1 (International Atomic Energy Agency, Vienna), p. 473.
White, R. B., 1989, *Theory of Tokamak Plasmas* (North-Holland, Amsterdam).
Wong, K. L., N. L. Bretz, T. S. Hahm, and E. Synakowski, 1997, Phys. Lett. A **236**, 339.
Xu, X. Q., R. H. Cohen, J. A. Crotinger, and A. I. Shestakov, 1995, Phys. Plasmas **2**, 686.
Xu, X. Q., and M. N. Rosenbluth, 1991a, Phys. Fluids B **3**, 627.
Xu, X. Q., and M. N. Rosenbluth, 1991b, Phys. Fluids B **3**, 1807.
Yagi, M., and W. Horton, 1994, Phys. Plasmas **1**, 2135.
Yagi, M., K. Itoh, S.-I. Itoh, A. Fukuyama, and M. Azumi, 1994, Plasma Phys. Controlled Fusion. **36**, 1385.
Yagi, M., J. P. Wang, Y. B. Kim, and M. Azumi, 1993, Phys. Fluids B **5**, 1179.
Yushmanov, P. N., J. Q. Dong, W. Horton, and X. N. Su, 1994, Phys. Plasmas **1**, 1583.
Yushmanov, P. N., T. Takizuka, K. S. Reidel, O. J. W. E. Kardoun, J. G. Corley, S. M. Kaye, and D. E. Post, 1990, Nucl. Fusion **30**, 1999.
Zakharov, V. E., V. S. L'vov, and G. Falkovich, 1992, *Kolmogorov Spectral of Turbulence* (Springer, New York).
Zakharov, V. E., and E. I. Schulman, 1988, Physica D **29**, 283.
Zeiler, A., D. Biskamp, J. F. Drake, and B. N. Rogers, 1998, Phys. Plasmas **5**, 2654.
Zhang, Y. Z., and S. M. Mahajan, 1992, Phys. Fluids B **4**, 1385.
Zhang, Y. Z., and S. M. Mahajan, 1993, Phys. Fluids B **5**, 2122.
Zhang, Y. Z., and S. M. Mahajan, 1995, Phys. Plasmas **2**, 4236.